ADVANCED MATERIALS
www.advmat.de

Frontiers in Photoelectrochemical Catalysis: A Focus on Valuable Product Synthesis

Marshet Getaye Sendeku, Tofik Ahmed Shifa, Fekadu Tsegaye Dajan, Kassa Belay Ibrahim, Binglan Wu, Ying Yang, Elisa Moretti, Alberto Vomiero, and Fengmei Wang**

Photoelectrochemical (PEC) catalysis provides the most promising avenue for producing value-added chemicals and consumables from renewable precursors. Over the last decades, PEC catalysis, including reduction of renewable feedstock, oxidation of organics, and activation and functionalization of C—C and C—H bonds, are extensively investigated, opening new opportunities for employing the technology in upgrading readily available resources. However, several challenges still remain unsolved, hindering the commercialization of the process. This review offers an overview of PEC catalysis targeted at the synthesis of high-value chemicals from sustainable precursors. First, the fundamentals of evaluating PEC reactions in the context of value-added product synthesis at both anode and cathode are recalled. Then, the common photoelectrode fabrication methods that have been employed to produce thin-film photoelectrodes are highlighted. Next, the advancements are systematically reviewed and discussed in the PEC conversion of various feedstocks to produce highly valued chemicals. Finally, the challenges and prospects in the field are presented. This review aims at facilitating further development of PEC technology for upgrading several renewable precursors to value-added products and other pharmaceuticals.

1. Introduction

Researchers have long been targeted at mitigating the ever-rising energy and environmental crisis that the extensive use of fossil fuel has posed to the globe.[1] Importantly, the continuous population growth and industrial expansion have brought heavy consumption of fossil fuels (coal, petroleum, natural gas, etc.) and concomitant generation of industrial wastes. This calls for a need to investigate an alternative strategy that could sustainably alleviate the globe's environmental and energy concerns. In pursuit of sustainable energy production and storage, eco-friendly renewable resources, such as solar energy, wind, geothermal energy, nuclear energy, and biomass, have been regarded as alternative energy sources to fossil fuel. However, the intermittency of readily available resources (such as wind and solar energy) has posed a challenge, demanding a secondary storage option to indirectly utilize these resources.[2] In this regard, the solar-driven catalytic transformation of various decentrally available feedstock to high-valued chemicals has been the subject of intense research efforts over the past few years.[1,3]

Until now, the vast majority of chemicals are manufactured using conventional thermochemical routes, which often brings the issue of both energy consumption and environmental impact. As a promising alternative to these processes, utilizing

M. G. Sendeku
Ocean Hydrogen Energy R&D Center
Research Institute of Tsinghua University in Shenzhen
Shenzhen 518057, P. R. China

M. G. Sendeku, F. Wang
State Key Laboratory of Chemical Resource Engineering
College of Chemistry
Beijing University of Chemical Technology
Beijing 100029, P. R. China
E-mail: wangfm@buct.edu.cn

The ORCID identification number(s) for the author(s) of this article can be found under https://doi.org/10.1002/adma.202308101

DOI: 10.1002/adma.202308101

T. A. Shifa, K. B. Ibrahim, E. Moretti, A. Vomiero
Department of Molecular Sciences and Nanosystems
Ca' Foscari University of Venice
Via Torino 155, Venezia Mestre 30172, Italy
E-mail: alberto.vomiero@ltu.se

F. T. Dajan, B. Wu
CAS Key Laboratory of Nanosystem and Hierarchical Fabrication
National Center for Nanoscience and Technology
Beijing 100190, P. R. China

B. Wu, Y. Yang
Shaanxi Provincial Key Laboratory of Electroanalytical Chemistry
Key Laboratory of Synthetic and Natural Functional Molecule of the Ministry of Education
College of Chemistry & Materials Science
Northwest University
Xi'an 710127, P. R. China

A. Vomiero
Department of Engineering Sciences and Mathematics
Division of Materials Science
Luleå University of Technology
Luleå 97187, Sweden

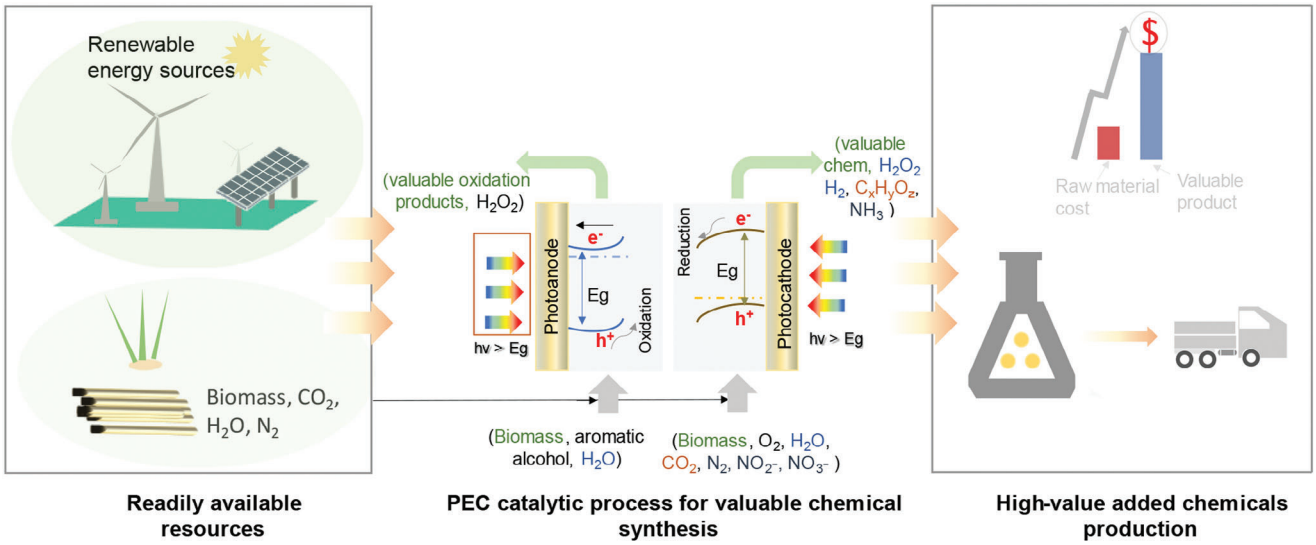

Figure 1. The conceptual illustration of PEC catalysis for value-added chemical synthesis. PEC catalysis is a greener approach to transform readily available resources to valuable chemicals. The light source with energy (hv) greater than the band gap of photoresponsive material (Eg) will be shined to generate charge carriers (e^- and h^+). The photogenerated charge carriers are separated by the applied bias, which is then involved in reducing/oxidizing the feedstocks.

electrochemical, photochemical, and photoelectrochemical techniques to efficiently upgrade various precursors such as lignocellulose,[4] and industrial wastes,[5] have been the target of several studies. While there are still some technical and marketing challenges, the electrochemical synthetic strategy has shown comparatively promising progress, thus enabling the commercial production of high-valued chemicals.[6] For instance, the manufacturing of adiponitrile, acetoin, and 2,5-dimethoxy-2,5-dihydrofuran has been realized through electrocatalytic synthesis schemes.[7] Whereas, in photocatalysis, issues related to catalyst stability, functional group tolerance, selectivity, understanding the reaction mechanism, and designing and optimizing a reactor system have made the process far behind commercial-scale production.[3b,8] Although at the early stage of development, interfacial photoelectrochemical tool has been emerged as versatile tool to derive a number of useful reactions in organic chemistry synthesis, which broaden the scope of visible light-driven catalysis for solar energy storage.[9]

At present, solar-driven PEC has garnered several research interests due to its unique potential for converting solar energy and naturally available feedstocks into value-added chemicals.[10] By and large, the fundamental mechanism for the synthesis of fuels and chemicals over a solid semiconductor via PEC catalysis can be briefly described as follows: i) upon illumination with light, a semiconductor photocatalyst can capture the light, resulting in the generation of electrons and holes at the conduction band (CB) and valance band (VB), respectively; ii) the photogenerated charge carriers are then separated and transported to the photocatalyst surface with the aid of bias; and iii) these photoexcited electrons and holes are then utilized to drive reduction and oxidation reactions. From the point of thermodynamics, the position of CB and VB is very helpful in judging the suitability of a semiconductor photocatalyst to derive a particular reaction.[11] While more rigorous study is still required to evaluate the practicality and economic benefits of employing this technology, it can be still regarded as a captivating platform to store those decentrally available resources in the form of chemicals, fuels, and consumables (**Figure 1**). The PEC synthesis of high-valued chemicals will gain impetus for at least four main reasons. First, it could be economically attractive since the process integrates sunlight, readily available resources (such as biomass, N_2, and water), and catalysts to produce highly valuable chemicals, pharmaceuticals, and consumables;[12] second, compared with the thermochemical process being employed in the manufacturing of several chemicals, it can be operated at room temperature and pressure, which can avoid the extra cost required for heating and pressurizing the reactor system; third, the PEC process can offer the "greener approach" in synthesis chemistry (it is mostly carried out in an aqueous solvent, uses sunlight, and end with limited byproducts); lastly, the PEC catalysis offers the possibility to simultaneously tune the selectivity and kinetics of a reaction via manipulating the light illumination and electrode potential. These attributes may also be exhibited by a related technique known as PV-EC, where the electrochemical systems are coupled with a photovoltaic system. However, what makes the PEC system more advantageous is that it integrates the light illumination into the catalyst, and the photogenerated carriers are directly involved in the reaction system. This configuration ensures a simple and straightforward approach to obtaining valuable chemicals.[11] Moreover, in PV-EC, the photovoltaic and electrochemical technologies need to be optimized separately, and the requirement for current–voltage matching along with the corresponding high cost has become a bottleneck.[10a] Apart from this, the potential for employing Tandem configuration and the relatively reduced energy loss in PEC catalysis are additional benefits. By virtue of the aforementioned merits, PEC catalysis offers a landscape of various applications, which could be sought as an alternative route for the thermocatalytic processes.

Considering the utmost significance of chemical synthesis via PEC catalysis, this review will cover the recent development and

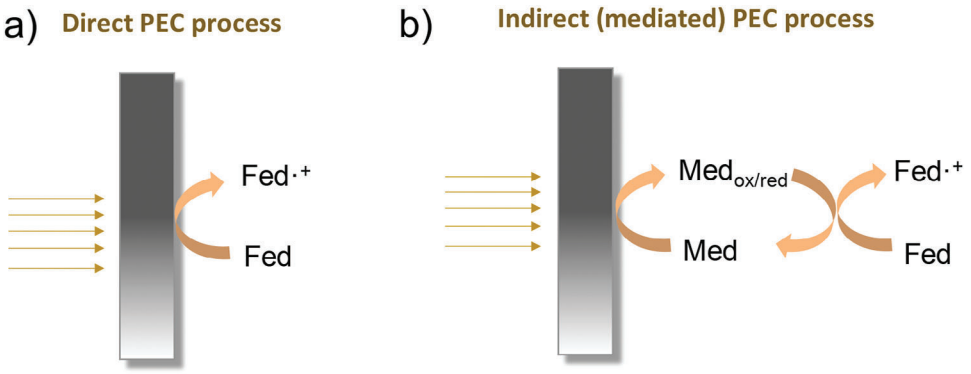

Figure 2. a) Photoelectrochemical catalysis via direct and b) indirect or mediated oxidation process. Fed and Med represent feedstock and mediator, respectively.

challenges of employing the PEC technique to achieve high-valued chemicals over rationally designed thin-film photoelectrodes. Although several reviews related to PEC catalysis have been communicated in the last few years,[13] no equivalent coverage was given to the key research findings in the library of chemical reactions, and fundamentals related to PEC catalysis were lacking. As such, a comprehensive understanding involving the design and optimization of photoelectrochemical setups, enhancement of photoelectrodes' efficiency, and development of simple electrode preparation schemes was lacking in previous reviews. Hence, it is essential and timely to review the recent progress and challenges of PEC synthesis. Given the PEC catalysis for water splitting[13b,14] and CO_2 reduction[8a,15] have already been reviewed in detail, we will not discuss them here. This review is organized as follows: i) a general background for examining photoelectrodes, quantifying the reaction products and the analytical techniques employed during the value-added product synthesis; ii) the common electrode fabrication techniques employed to achieve a high-quality photoelectrode film; iii) a timely overview of the recent progress of some selected anodic and cathodic PEC synthesis; iv) current understanding of the selective C—H and C—C bond functionalization processes for realizing high valued chemicals and pharmaceuticals; v) perspective on the future outlook for the PEC process. The target is to put a significant footprint in revolutionizing PEC catalysis for valuable product synthesis.

2. Configuration of PEC Cell and Efficiency Metrics

Several crucial factors, including the optical response of the photoelectrode, the separation/recombination of carriers, the electrolyte/electrode interfacial carrier injection, and the mass transfer (including adsorption of reactant, desorption of product, and diffusion) affect the PEC synthesis. In particular, the direct PEC synthesis on-demand, evaluated by production rate, selectivity, and Faradaic efficiency for certain chemicals, is of importance. However, the methods employed to evaluate the photoelectrochemical conversions of various feedstocks to value-added products are not well-documented. The following sections aim to offer the basic methodologies employed for evaluating photoelectrodes, PEC reactions, product identification, and quantification.

2.1. Direct versus Indirect (Mediated) PEC Processes

Generally, the PEC processes reported until now can be carried out either directly on the electrode surface or utilizing a redox mediator. In the case of the direct PEC process, the photogenerated charge carriers directly oxidize/reduce the targeted feedstocks (**Figure 2**a). In this process, the reaction selectivity could be tuned by changing the applied potential and electrolyte pH.[16] On the other hand, an indirect (mediated) process involves redox mediators in which these mediators are first oxidized or reduced to give an active intermediate. The as-formed species would be then utilized to oxidize/reduce the targeted feedstocks to give the desired product (Figure 2b).

In the indirect PEC process, organic/inorganic compounds, molecules, or ions that own a specific property of being oxidized or reduced reversibly under certain conditions can be used as redox mediators (**Table 1**). Unlike the direct PEC process where the reaction takes place at the electrolyte–electrode interface, an indirect PEC process could extend the phenomenon in the bulk electrolyte, further expanding the space for the photoelectrochemical conversion.[17] Before choosing the redox mediator, its electrochemical behavior should be studied under the working conditions of the target reaction. When PEC catalysis is carried out in an aqueous electrolyte, the redox mediator may play several key roles. For instance, it could partly alleviate the problem associated with photoelectrode instability and minimize the possible competing/side reactions.

While the use of redox mediators in electrocatalytic and PEC synthesis of valuable chemicals is still ongoing research, several key factors are sought to influence the performances.[21] First, the alignment of the thermodynamic redox potential of the mediator with respect to the energy level of the semiconductor photoelectrode is essential, since it determines the possibility of the photogenerated electrons to be directly transferred to the mediator. Apart from this, the electrolyte pH, solubility of the mediator in the given electrolyte, and the reversibility of the mediator are very crucial factors that should be considered in choosing mediators. For further understanding of the nature and properties of common redox mediators, we direct the readers to refer to previously communicated reviews.[21] The PEC processes compiled in this review focus on the reduction or oxidation of several kinds of feedstocks involving both direct and indirect PEC processes.

Table 1. Key redox mediators commonly used in PEC transformation of organic chemicals.

Redox mediators	Redox couple	Target conversions	Typical activity	Ref
2,2,6,6-Tetramethylpiperidine-1-oxyl (TEMPO)	TEMPO/TEMPO$^+$	Alcohol oxidation	Electron transfer	[4j]
Phthalimide *N*-oxyl (PINO)/*N*-hydroxyphthalimide (NHPI)	*N*-NHPI/PINO$^\bullet$	C—H bond activation		[18]
Tetrabutylammonium nitrate (Bu_4NNO_3)		Alcohol oxidation	Abstraction of proton	[19]
Halide redox mediators	Br^-/BrO^-	Alkene epoxidation	Electron transfer	[17a]
N-hydroxysuccinimide in the presence of pyridine[a)]	$NHS^-/NHS^\bullet$	Alcohol oxidation, cyclohexene to cyclohexanone, tetralin to tetralone	Hole transfer	[20]

[a)] Pyridine is added to abstract proton from *N*-hydroxysuccinimide.

2.2. Geometry of Light Illumination

Prior to any photoelectrochemical measurement, identifying which side of the photoelectrode could deliver higher photocurrent density is crucial.[22] Considering an n-type semiconductor photoelectrode as an example, the impact of the geometry of light illumination on the carrier migration can be briefly described as follows. When the electrode is illuminated from the front side (surface of catalyst), the light absorption occurs near the electrode surface, and less light reaches the back of the electrode since the light is absorbed through the thickness of the electrode film. As a result, a greater density of photogenerated charge carriers is formed near the surface of the electrode than on the backside. As clearly shown in **Figure 3a**, the photogenerated holes are closer to the semiconductor–electrolyte interface, and hence, the diffusion length for the holes does not need to be high. Instead, the photogenerated electrons created near the surface need to diffuse through the film to the back contact, where they are extracted and transported to the counter electrode for the corresponding reduction reaction. Hence, the electron diffusion length is greater than or equal to the film thickness in the case of front-side illumination. On the contrary, when light is shined from the backside, a higher density of photogenerated charge carriers will be created closer to the back contact (Figure 3b). As a result, the electrons need to travel only a short distance while the holes are required to diffuse through the bulk electrode to reach the electrode surface. Hence, it is very useful to identify the glass substrate side that can give better photocurrent density prior to further performance evaluation. For example, Mazzaro et al. showed that the direction of photoelectrode illumination could significantly affect the photocurrent behavior of Ti-doped hematite electrodes.[23] Owing to the inefficient hole transport process across the semiconductor, the undoped sample displayed a drop in its photocurrent when illuminated from the backside.

PEC reactions in flow cell reactors usually fall on the option of using only back-side light illuminations. Hence, the photoelectrode design requires a proper optimization of electrode thickness. In a recent example by Gong et al., a Si photoanode passivated by amorphous Si was utilized to achieve an ultra-long minority carrier diffusion length and facilitate the separation of the light absorption region from the catalytic sites.[24] Such a decoupled structure allows the light to be illuminated on the photoelectrode from the anode side, which finally results in a high performance (38 mA cm^{-2}) for CO_2 reduction.

Moreover, the direction of light illumination on the photoelectrode may make a difference in the quantum efficiency (QE). To quantify the QE of different illumination on photoelectrode, some theoretical models are established:

i) For a photoelectrode illuminated with light from the front side, a simplified Gärtner–Butler expression can be applied

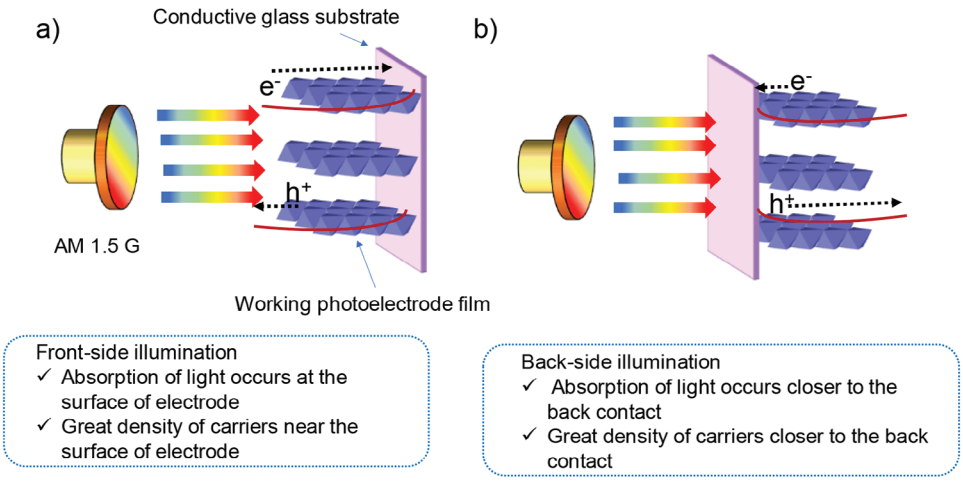

Figure 3. Schematics illustration of semiconductor photoelectrode under simulated solar light Air Mass 1.5 Global (AM 1.5 G) illumination. a) Front side illumination. b) Back side illumination.

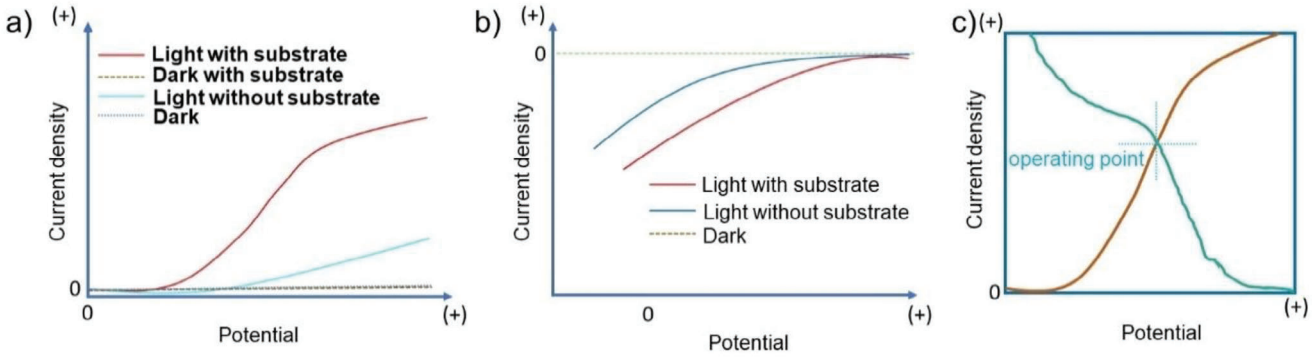

Figure 4. a,b) Comparison of *J–V* curves for a typical PEC oxidation and reduction of a target feedstocks with competing HER/OER in an aqueous solution. c) Operating current selection in an integrated photo-electrochemical cell from the intersection of the LSV curves of the photoanode and photocathode.

to estimate the quantum efficiency as follows:[25]

$$QE_{FS} = 1 - \frac{1}{1+\alpha L_p} e^{(-\alpha w)} \quad (1)$$

where QE_{FS} is quantum efficiency up on light illumination from the front side, α is the optical absorption coefficient, L_p is the minority carrier diffusion length (electron in p-doped semiconductors and holes in n-doped semiconductors), and w is the width of the depletion layer in the p-n junction. The value of w can also be calculated from the following equation:

$$W = \left(\frac{2\varepsilon\varepsilon_o}{eN_D}\right)^{\frac{1}{2}} \left(U - U_{FB}\right)^{\frac{1}{2}} = W_o \left(U - U_{FB}\right)^{\frac{1}{2}} \quad (2)$$

where ε is the relative dielectric constant, ε_o is the permittivity of free space, N_D is the donor concentration, and e is the elementary charge. In this equation, the difference between the electrode potential (U) and the flat band potential (U_{FB}) corresponds to band bending.

For a small value of optical absorption coefficient (α), Equation (1) can be simplified based on Taylor series expansion as follows:

$$\frac{1}{QE_{FS}} = \frac{1}{L_p + W}\left(\frac{1}{\alpha} + L_p\right) \quad (3)$$

ii) For the back-side illuminated electrode, the expression for estimating QE is given below.

$$QE_{BS} = \frac{1}{1-\alpha L_p} e^{[-\alpha(d-w)]} - e^{[-\alpha d]} \quad (4)$$

where QE_{BS} is quantum efficiency upon back-side illumination, and d is the thickness of the semiconductor.

Moreover, it is very useful to measure the photocurrent as a function of the thickness of the photoelectrode film, which could be helpful to determine the minority-carrier diffusion length both theoretically and experimentally.[26] For a typical n-type semiconductor photoelectrode strongly illuminated from the back-side, the quasi-neutral region thickness of $W >$ diffusion length, L_p, the photocurrent can be given by:

$$|J/e| \approx 2(1-R)\varphi \left(1 + \frac{S}{\alpha L_p}\right)(1+S)^{-1} e^{-\frac{w}{L_p}} \quad (5)$$

where R is the reflectivity of the surface, e is the charge on an electron ($1.6021892 \times 10^{-19}$ C), φ is the incident light flux, α is the absorption coefficient, and S is a dimensionless parameter (sL_p/D_p) which describes the surface recombination velocity (s) at the backside of the PEC device relative to the minority-carrier diffusion coefficient (D_p). Equation (5) is useful to examine the characteristics of photocurrent as a function of electrode thickness. Accordingly, a reduced photocurrent will be achieved as a result of a high rate of surface electron–hole recombination at the photoelectrode's backside. Given that the efficiency of a photoelectrode can be affected by the geometry of photoelectrode illumination, it appears to deserve more comprehensive theoretical and experimental work to uncover the relationship between the semiconductor electrode and the carrier transport.

2.3. Evaluation of a Photoelectrode and Efficiency Metrics for PEC Synthesis of Valuable Chemicals

The capability of the photoelectrode to obtain the targeted reaction can be evaluated based on its current density-potential profile, namely *J–V* curve, in the presence and absence of the reactant under light illumination. For a typical PEC reaction in aqueous media, the possibility of oxidizing/reducing the targeted feedstocks can be evaluated from the onset potential linear sweep voltammetry (LSV), which should be different from the competitive reduction or oxidation of water. For an oxidation process, the photocurrent density shows a drastic enhancement upon the introduction of the reactant to be oxidized (**Figure** 4a,b). When recorded under aqueous conditions, a careful analysis of the LSV curve is required to compare the competitive water oxidation with the targeted oxidation reaction. The linear sweep voltammograms for the water oxidation and feedstocks oxidations must be evaluated to identify the proper potential window. Recently, many innovative PEC processes have been made available, in which the

concurrent oxidation and reduction of the targeted feedstocks is carried out at a time. For such a process, the operating current could be obtained from the intersection of the LSV of the two half-reactions (Figure 4c).

Apart from the simple assessments of the electrode on LSV, several efficiency metrics, including solar-to-fuel conversion (STF), incident photon-to-current conversion efficiency (IPCE), Faradaic efficiency (FE), external quantum efficiency (QE), applied bias photon-to-current efficiency (APCE), and absorbed photon-to-current efficiency (ABPE), have been used to evaluate the overall performance and stability of a particular photoelectrode. It should be noted that the FE and STF are two important factors that indicate the performance of the PEC chemical synthesis process, while the efficiencies metrics such as IPCE, APCE, and ABPE mainly provide an overall efficiency of the photoelectrode and they do not offer very crucial information on how well the photoelectrode reduce or oxidize the targeted feedstock.[27] Here, we summarize available efficiency metrics frequently used in PEC catalysis.

2.3.1. Solar-to-Fuel Conversion Efficiency

The solar-to-fuel (STF) conversion efficiency is quantified as the ratio of "chemical energy produced" to the "solar energy input." It is the most important of all efficiency measurements as it provides a comprehensive description of the overall efficiency of the PEC device when subjected to broadband solar illumination at Air Mass 1.5 Global (AM 1.5 G) conditions, without any external bias applied. In a given PEC reaction, STF can be calculated from the rate of fuel production (r_{fuel}) and the Gibbs free energy change (ΔG) associated with that particular reaction (conversion).[10]

$$\mathrm{STF} = \frac{r_{\mathrm{fuel}}\,(\mathrm{mmol\ of\ fuel}) \times \Delta G^{\circ}\,(\mathrm{kJ\ mol^{-1}})}{P_{\mathrm{solar}}\,(\mathrm{mW\ cm^{-2}}) \times \mathrm{Area\ (cm^{2})}} \tag{6}$$

where P_{solar} is the intensity of solar light.

2.3.2. Incident Photon-to-Current Conversion Efficiency (IPCE)

IPCE can be used to determine the contribution to the photocurrent of photons with different energies.[28] IPCE is usually obtained from a chronoamperometry measurement. In this system, a bias can be applied between the substrate (i.e., working electrode) versus a counter electrode (in the case of 2-electrode system) or a reference electrode (in the case of 3-electrode system) while measuring the current that arises as a result of illuminating monochromatic light at various wavelengths. It corresponds to the external quantum efficiency (EQE). In order to obtain IPCE as a function of wavelength, λ(nm), a calibrated monochromated light should be used. For a direct PEC catalytic process, the IPCE can clearly define how efficient the incoming radiation is in producing the target product. This implies that all electrons/holes are utilized to facilitate the targeted conversion (either via reduction or oxidation) instead of corroding the catalyst itself or deriving other side reactions. It can be calculated based on the following equation:[27]

$$\mathrm{IPCE} = \frac{hc}{e}\frac{J_{\mathrm{ph}}}{P_{\mathrm{mono}} \cdot \lambda} \tag{7}$$

$$= \frac{J_{\mathrm{ph}}\,(\mathrm{mA\,cm^{-2}}) \times [1239.8\,(\mathrm{V \times nm})]}{P_{\mathrm{mono}}\,(\mathrm{mW\,cm^{-2}}) \times \lambda\,(\mathrm{nm})} \tag{8}$$

where J_{ph} is the photocurrent density, (1239.8 (V × nm)) represents the result of the multiplication of Planck's constant (h) by the speed of light (c), P_{mono} is the intensity of incident monochromatic light, and λ is the wavelength at which this illumination power is measured.

2.3.3. Faradaic Efficiency (FE)

The amount of product generated via PEC catalysis could be related to the charge passed during the galvanostatic or potentiostatic measurement. The FE is one of the most crucial parameters used to quantify the efficiency of a PEC system which can be evaluated as follows.[10a]

$$\mathrm{FE} = \frac{\mathrm{Number\ of\ holes/electrons\ to\ oxidize/reduce\ the\ substrate}}{\mathrm{Number\ of\ all\ photogenerated\ holes/electrons}} \tag{9}$$

For a particular reaction involving the electron/hole transfer process, the FE for target product can be calculated as:

$$= \frac{e_{\mathrm{target\ product}} \times n_{\mathrm{target\ product}} \times N}{Q/e} \times 100\% \tag{10}$$

where $e_{target\ product}$ is the number of electrons or holes involved in the transformation of 1 mole of reactant to target product, N is Avogadro number, $n_{target\ product}$ is the yield of the target product, Q is electric charge, and e is elementary charge.

2.3.4. External Quantum Efficiency (QE)

The external quantum efficiency of the targeted product can be directly calculated from FE and IPCE as follows:

$$\mathrm{QE} = \frac{\mathrm{Number\ of\ electrones/holes\ to\ convert\ the\ substrate\ to\ product}}{\mathrm{Number\ of\ incident\ photon}} \times 100\%$$

$$= \mathrm{IPCE} \times \mathrm{Faradaic\ efficiency} \times 100\% \tag{11}$$

2.3.5. Applied Bias Photon-to-Current Efficiency (ABPE)

When a bias is applied between the working and counter electrodes, the current drawn from the PEC device will increase. One should be mindful of the thermodynamic redox potential (ΔE°) of the PEC reactions under consideration: if an applied bias is higher than the thermodynamic potential, it might be difficult to conclude if the PEC process offers an advantage over dark electrolysis. This parameter can be calculated from FE and J as follows:[10b]

$$\mathrm{ABPE} = \frac{J_{\mathrm{ph}}\,(\mathrm{mA\,cm^{-2}}) \times \left[\Delta E^{\circ}\,(\mathrm{V}) - V_{\mathrm{bias}}\,(\mathrm{V})\right] \times \mathrm{FE}}{P_{\mathrm{solar}}\,(\mathrm{mW\,cm^{-2}})} \tag{12}$$

Table 2. Summary of the analytical techniques employed for qualitative identification and quantitative determination of products.

Reaction	Valuable products	Quantification techniques	Ref.
Glycerol oxidation	DHA, GA, FA	HPLC, NMR	[31]
HMF oxidation	DFF, HMFCA, FDCA	HPLC, NMR	[4j,29b]
NRR, Nitrate reduction	NH_3	UV–vis spectrophotometer, NMR	[32]
ORR	H_2O_2	UV–vis spectrophotometer, permanganate titration	[33]
Benzyl alcohol oxidation	Benzaldehyde, benzoic acid	HPLC	[34]
HMF reduction	BHMF	HPLC, NMR	[35]
Glucose oxidation	GLA, GLU	HPLC	[12]
Conversion of lignin models	Phenol, benzaldehyde	HPLC, GC-MS, NMR, UV–vis spectrophotometer	
Methane oxidation	Ethylene glycol	NMR	[36]

2.3.6. Absorbed Photon-to-Current Efficiency (APCE)

The losses of photons resulting from both reflection and transmission are not excluded in IPCE and STF evaluations. Hence, the characterization of the inherent performances of the material should consider the subtraction of these losses. The APCE shows how efficiently the absorbed photons are converted into current. Therefore, it corresponds to the internal quantum efficiency (IQE). The APCE of a PEC system can be calculated from the ratio of IPCE to absorptance ($\eta_{e-/h+}$).[10b]

$$\mathrm{APCE} = \frac{\mathrm{IPCE}}{\eta_{e^-/h^+}} = \eta_{\mathrm{transport}}\,\eta_{\mathrm{interface}} \tag{13}$$

where $\eta_{\mathrm{transport}}$ and $\eta_{\mathrm{interface}}$ are efficiencies corresponding to the charge transport to the solid–liquid interface and interfacial charge transfer, respectively. The value of absorptance, $\eta_{e-/h+}$, determines the fraction of electron–hole pairs obtained per incident photon flux. Note that the APCE value offer a versatile platform for understanding the property of a thin film electrode via optimizing the maximum photon absorption path length along with minimum effective e^-/h^+ transport distance.

2.4. Product Analysis and Quantification

As for the analysis of the products, one or more analytical techniques are usually employed. UV–vis spectrophotometry, gas chromatography (GC), high-performance liquid chromatography (HPLC), gas chromatography-mass spectrometer (GC-MS), and nuclear magnetic resonance (NMR) are the most common analytical techniques utilized to quantify the amount of product formed during or at the end of the reaction. Based on the typical PEC synthesis, the analytical techniques employed for qualitative and quantitative analysis of products are summarized in **Table 2**. For a more precise quantitative estimation of some products, two or more techniques can be utilized. For instance, the amount of NH_3 produced from PEC catalysis of N_2 and NO_3^- precursors can be obtained from UV–vis spectrophotometry and NMR analysis. A detailed procedure for quantifying the reaction products described in this review can be found in previous reports elsewhere.[29] Meanwhile, more than one product may be detected during PEC synthesis, and some factors of conversion efficiency, production rate, and selectivity are very important to evaluate the process. For instance, the conversion of glycerol may yield several products such as 1,3-dihydroxyacetone (DHA), glyceric acid (GA), formic acid (FA), glycolic acid (GLA), and lactic acid (LA). Accordingly, the selectivity and production rate of the targeted product DHA can be calculated as follows;[10a,30]

$$\mathrm{Selectivity}_{\mathrm{target\ product}} = \frac{n_{\mathrm{target\ product}}}{n_{\mathrm{all}}} \times 100\% = \frac{n_{\mathrm{target\ product}}}{n_1 + n_2 + n_3 + n_4} \times 100\% \tag{14}$$

$$= \frac{C_{\mathrm{target\ product}}}{C_1 + C_2 + C_3 + C_4} \times 100\% \tag{15}$$

where $n_{\mathrm{target\ product}}$ is the yield of target product, n_1, n_2, n_3, and n_4 are the yield of side products. $C_{\mathrm{target\ product}}$, C_1, C_2, C_3, and C_4 are the target and side products concentrations in mol L^{-1}, respectively.

Similarly, the production rate of the target product can be calculated from the following equation:

$$\mathrm{Production\ rate}\left(\mathrm{target\ product}\right) = \frac{C_{\mathrm{target\ product}} \times V}{t} \times 100\% \tag{16}$$

$$\mathrm{Production\ rate\ per\ unit\ area}\left(\mathrm{target\ product}\right) = \frac{C_{\mathrm{target\ product}} \times V}{t \times A} \times 100\% \tag{17}$$

where V is the volume of the reaction solution in L, t is the reaction time in hour, and A is the area of photoelectrode in cm^2.

3. Methods of Photoelectrode Fabrication

The electrode fabrication process has serious implications for the overall performance and stability of photoelectrodes.[37] Besides, it can be regarded as one important factor as it may determine the cost of a PEC device. For instance, a photoelectrode prepared under a complex procedure, harsh experimental conditions, and expensive inputs will increase the PEC device's overall cost, questioning the practicality of large-scale production. Hence, a simple and inexpensive electrode fabrication strategy is needed. To date, photoelectrodes can be either directly grown on the substrates of

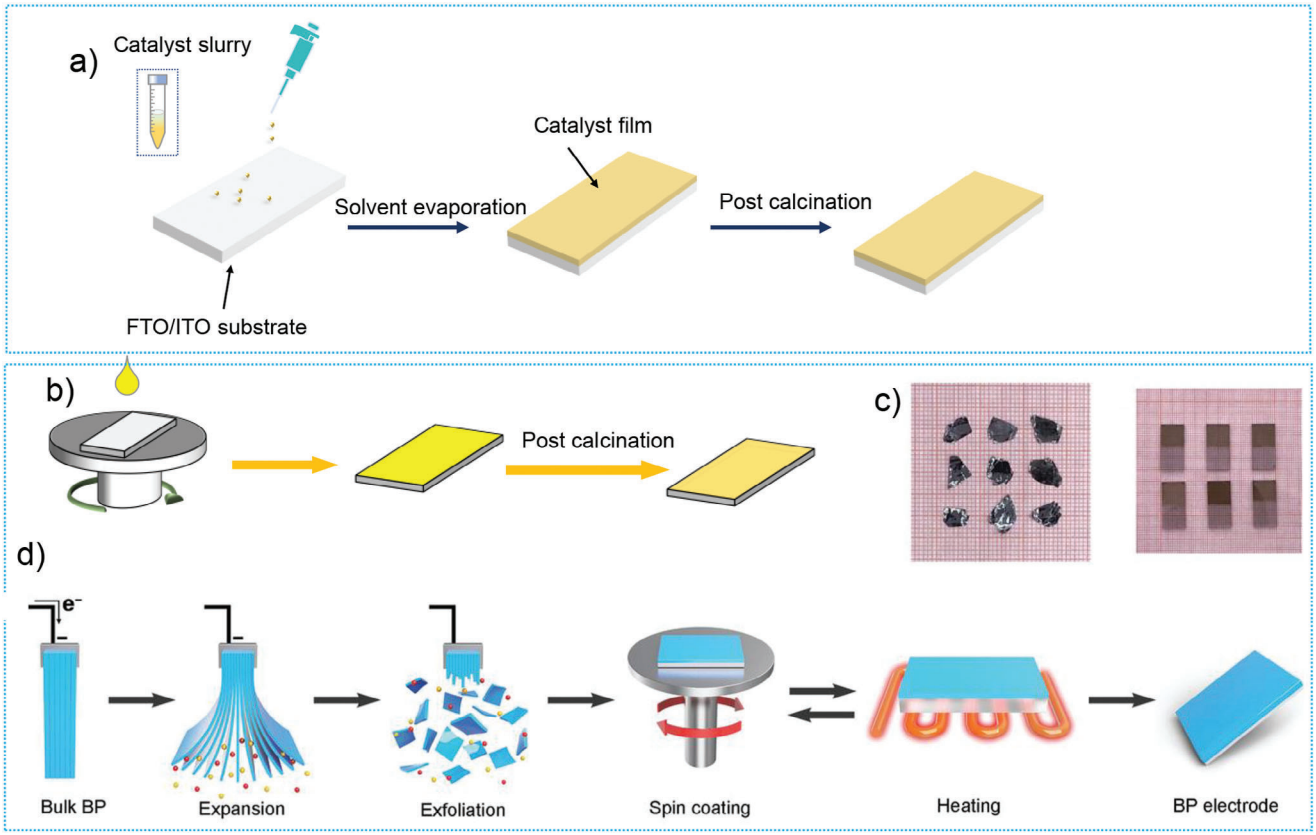

Figure 5. Drop casting and spin coating electrode fabrication methods. Schematic illustration of electrode preparation by a) drop-casting and b) spin coating methods. The catalyst slurry is directly cast on fluorine-doped tin oxide (FTO) or indium tin oxide (ITO) substrates. c) The digital image of black phosphorus (BP) and its photoelectrode film. d) Illustration of the electrochemical synthesis method for black phosphorus nanosheets and the spin coating method employed for BP electrode fabrication. Reproduced with permission.[40] Copyright 2020, Wiley VCH Weinheim.

interest (in situ preparation method) or cast on a piece of substrate once the catalyst is prepared (ex situ preparation method). In this section, we provide a brief introduction to the existing photoelectrode fabrication strategies that have been employed in PEC cells. The methods described in Section 3.1 mainly focus on the ex situ preparation techniques where the semiconductor material is initially synthesized and cast over the substrate via different means. In fact, spin coating and spray pyrolysis are categorized as ex situ photoelectrode fabrication methods when only the final catalyst slurry is directly deposited on the specific substrate. However, when a precursor of the final product is coated via the above techniques to yield the final electrode, both fabrication methods would be considered as an in situ preparation technique. While the ex situ preparation techniques afford several advantages, the poor attachment of the catalyst on the substrate is considered a major limitation that affects the PEC system's performance. The methods categorized under in situ techniques, which are discussed in Section 3.2, can practically overcome these problems since the catalyst with the desired morphology can directly grow on the substrate of interest. In fact, both methods have their own merits and demerits, and a careful selection of electrode fabrication methods is required in the context of the type of semiconductor material to be prepared.

3.1. Ex Situ Electrode Preparation Process

3.1.1. Drop Casting and Spin Coating

Drop casting and spin coating are the most straightforward techniques for fabricating photoelectrodes from the catalyst powder. In a typical fabrication procedure, a semiconductor suspension is prepared via dissolving an appropriate amount of the catalyst in a suitable solvent, followed by ultrasonication of the solution to get a uniform suspension.[38] In the case of drop-casting, this suspension is directly transferred to a substrate, commonly indium tin oxide (ITO) or fluorine-doped tin oxide (FTO) dropwise, and the solvent is allowed to evaporate, resulting in the formation of the semiconductor film (**Figure 5**a). As for the spin-coating, the prepared suspension is added on a suitable substrate already attached to a spin-coater (Figure 5b). The solvent will be removed from the substrate during the spinning process, resulting in a homogeneously prepared thin film.[38b] After this process, post-calcination is needed to improve the adhesion of semiconductor particles on the substrate surface. Taking advantage of the centrifugal force during the spin-coating process, the method offers a comparatively uniform film thickness, which could be controlled by manipulating the rotating speed, the concentration of the

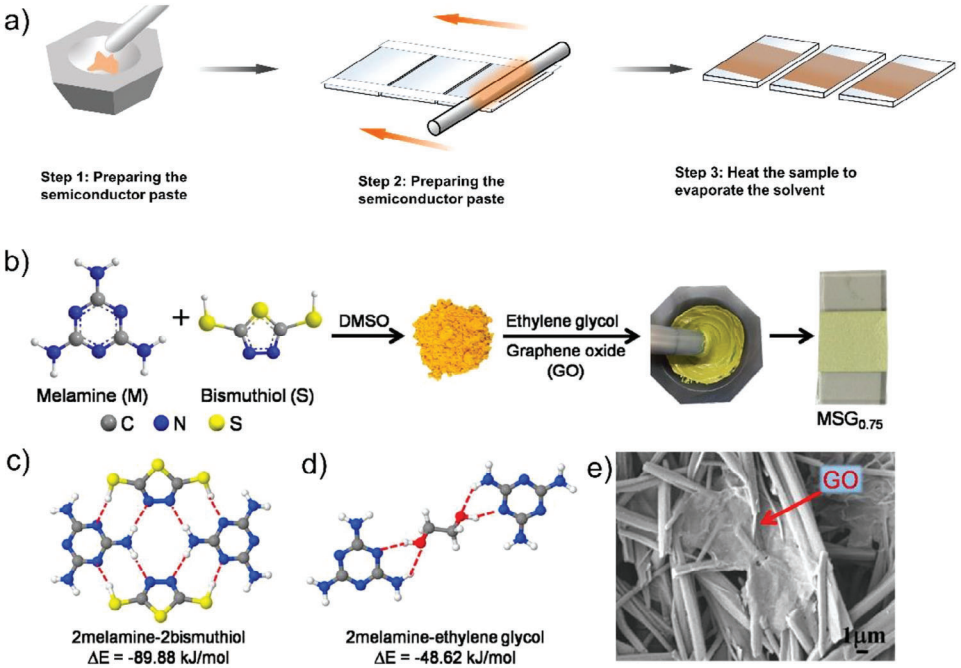

Figure 6. a) Schematic illustration of the doctor blade electrode fabrication method. b) Facile electrode fabrication scheme for carbon nitride photoelectrode. A supramolecular complex containing melamine and bismuthiol was formed and finely ground. This mixture was blended into a paste along with ethylene glycol and graphene oxide (GO), and doctor-bladed onto an FTO substrate to get the photoelectrode films. c,d) DFT calculation depicting the interaction energy between melamine–bismuthiol and ethylene glycol (EG) and the melamine–bismuthiol supramolecular assemblies, respectively. e) Scanning electron microscopy (SEM) image of melamine–bismuthiol–graphene oxide$_{0.75}$ (MSG$_{0.75}$) films on FTO prior to calcination. Reproduced with permission.[42a] Copyright 2020, American Chemical Society.

catalyst slurry, and its viscosity. However, the combination of gas flow by spinning substrate and the centrifugal force could also result in a much faster drying kinetics compared with other conventional industrial coating procedures. In this context, the spin coating procedure appears difficult to facilitate a large-scale fabrication of PEC devices.[39] Yu et al. reported that an electrochemically exfoliated black phosphorous (BP) spin-coated on an indium tin oxide (ITO) substrate efficiently catalyzed the PEC nitrogen reduction reaction (Figure 5c,d).[40] During the electrochemical exfoliation, tetra-n-butylphosphonium was used instead of quaternary ammonium salt, which reduces interferences during ammonia detection.

3.1.2. Doctor Blade

The doctor blade is also a simple and common method for preparing semiconductor film on a relatively large surface area.[41] This method is widely employed for preparing photoelectrodes in dye-synthesized solar cells or chemoresistive gas sensors. A homogeneous catalyst ink/paste is first prepared in a typical fabrication procedure by dissolving the semiconductor in a suitable solvent. Once the required ink/paste is prepared, it is applied on the conductive surface of the substrate, followed by thermal treatment under an air or argon atmosphere. As shown in **Figure 6**a, scotch tape is usually applied at the sides of the substrate, which acts as a spacer to maintain a relatively uniform film thickness. A very smooth and homogeneous layer can be achieved via blending the catalyst ink with additives such as glycerol or ethylene glycol.[42]

The Shalom group utilized the doctor blade technique to rationally fabricate a carbon nitride photoanode that exhibits excellent electron diffusion length and hole extraction properties. Typically, a supramolecular film was first prepared from melamine and bismuthiol precursors. Then, the mixture was blended with ethylene glycol (Figure 6b). From density functional theory (DFT) calculations, it was speculated that the ethylene glycol additive interacts preferentially with melamine (E_{int}, −48.62 kJ mol^{-1}) than bismuthiol (E_{int}, −44.41 kJ mol^{-1}), as shown in Figure 6c,d. Besides, the relatively higher E_{int} of 89.88 kJ mol^{-1} in a finely grounded mixture of melamine and bismuthiol suggests the probability of forming supramolecular structure. Finally, carbon nitride films were achieved after calcinating the as-prepared supramolecular films at 550 °C under N_2 atmosphere. Interestingly, graphene oxide was also blended in a similar fashion, drastically boosting the overall performance of the photoanode (Figure 6e). This method also affords additional possibilities for manipulating film thickness by adjusting the number (amount) of scotch tape.[42a]

3.1.3. Finger Rubbing and Particle Transfer

The finger-rubbing method is widely employed for fabricating faceted semiconductor photoelectrodes since it can directly use catalyst powder without dissolving it in a solvent.[43] In a typical fabrication procedure, the semiconductor catalyst powder is manually rubbed on the surface of a planar substrate with the ease of a finger.[44] Before the rubbing procedure, a polyethylenimine (PEI) solution in alcohol is usually spin-coated over the

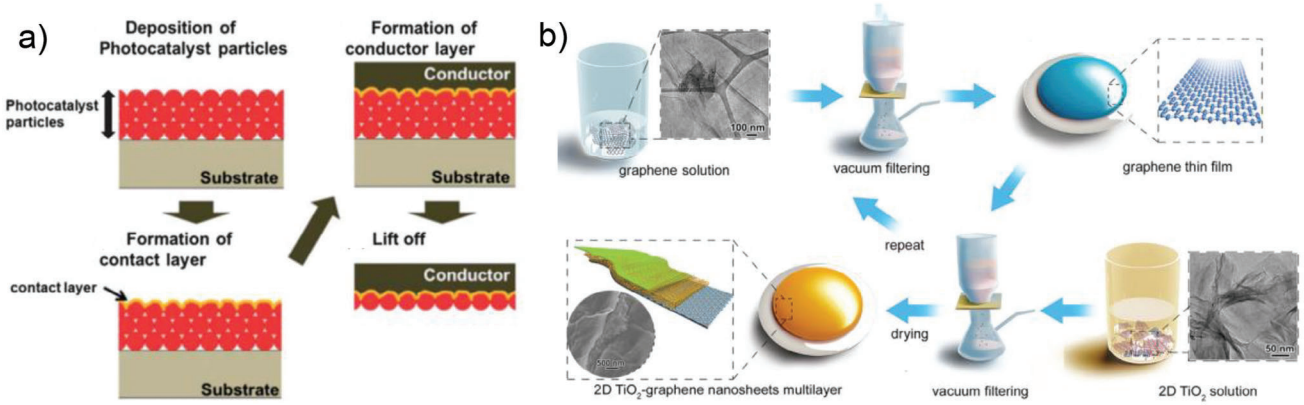

Figure 7. a) Schematic illustration of particle transfer method of electrode fabrication. Reproduced with permission.[45] Copyright 2013, Royal Society of Chemistry. b) Vacuum filter transfer method. Reproduced with permission.[46] Copyright 2019, Wiley VCH Weinheim.

substrate as the hydrogen-bonding mediator. For a similar purpose mentioned in the previous procedures, calcination is usually required to make a high-quality film. Two important factors likely govern the facile attachment of catalysts on substrates for this fabrication method. i) The "pressing" of the semiconductor against the substrate and ii) the forced surface migration of the crystals during the rubbing process.

In the case of the particle transfer method, the catalyst particles are first transferred onto a glass substrate using a suspension of photocatalyst powder in a suitable solvent (**Figure 7a**).[45] The resulting coated substrate is then dried under ambient conditions. Next, a contact layer is deposited on the resultant electrode (for instance using magneton sputtering or other thin film deposition methods), followed by forming a mechanically strong conductive layer over the contact layer. These layers are attached to a second glass plate using an epoxy resin, and then the primary glass plate is peeled off. The excess particles are finally removed by ultrasonication in water to obtain the desired electrode.

3.1.4. Vacuum Filter Transfer

Vacuum filter transfer is another alternative for fabricating photoelectrode film: i) the catalyst is dispersed in a suitable solvent to create a uniform slurry; ii) the slurry is subjected to vacuum filtration using a cellulose membrane, followed by transferring the film to a suitable conductive substrate; iii) a calcination or etching procedure is usually required to remove the cellulosic membrane prior to performance evaluation. This fabrication method appears simple, yet the poor adhesion of the as-obtained film with the substrate is the biggest limitation. As described in the aforementioned fabrication procedures, a post-calcination step is required to ensure proper attachment of the film and enhance the charge transfer of the semiconductor film and conductive substrate. In 2019, Sun and co-workers[46] successfully demonstrated seashell-inspired nanomaterials via assembling graphene and atomically thin 2D TiO_2 nanosheets layer-by-layer (Figure 7b). In a typical vacuum filter graphene or graphene oxide was firstly dispersed in *N*, *N*-dimethylformamide (DMF), or in water, respectively, and vacuum filtration was carried out to form a substrate layer. Next, the dilute 2D TiO_2 nanosheets' aqueous solution was slowly added into the filtering container to form a dense inorganic layer on the graphene substrate layer.

3.1.5. Spray Pyrolysis

The spray pyrolysis method has also been adopted to fabricate semiconductor or composite photoelectrodes.[47] In this technique, a precursor solution is first prepared and sprayed on a heated substrate where the constituents in the precursor solution react to form the desired product. This method affords several advantages, including its suitability to introduce dopant and composite structures in the target semiconductor, ease of operation, simplicity, and low cost. In 2017, Berglund and co-workers reported the facile fabrication of dense and homogeneous $CuBi_2O_4$ photocathodes.[48] A precursor solution containing Bi^{3+} and Cu^{2+} in a mixture of acetic acid and ethanol was used as a spraying solution. The authors noted the rapid precipitation of the precursor solution, which was likely caused by the hydrolysis of Bi^{3+} in water. Hence, additives, namely 5% triethyl orthoformate (TEOF) and 1% polyethylene glycol (PEG), were added to improve the stability of the precursor and the spreading behavior of the droplet, respectively. This method has widely been used to deposit electron transport layers, such as the dense blocking layer of TiO_2, applicable to many PEC cells. Owing to the controllability of various process parameters such as substrate heating temperature, distance from the atomizer to the substrate, the concentration and content of precursor, and spray time and speed, this process allows the fabrication of diverse and large area semiconductor photoelectrode films.

The ex situ electrode preparations described above have their own advantages and limitations (**Table 3**). Hence, choosing the most suitable method requires understanding their merits.

3.2. In Situ Electrode Preparation Methods

In this section, we highlight the general in situ electrode fabrication techniques that are commonly employed to prepare photoelectrodes.

Table 3. Summary of pros and cons of various ex situ photoelectrode fabrication methods.

Method of electrode preparation	Advantages	Disadvantages
Drop casting and spin coating	Easy, cheap, and scalable	Difficult to control film thickness and uniformity, a time-consuming process
Vacuum filter transfer	Simple	Poor contact between the semiconductor film and the substrate
Doctor blade and screen printing	Possibility of scale-up	Difficult to control film thickness below 1 µm for a short charge diffusion length
Finger rubbing	Does not require solvents, reactors, or other equipment	Not good at making ultra-thin films using particles with a thickness lower than 200 nm
Particle transfer	No high-temperature post-calcination	Higher fabrication cost due to the equipment and metal targets applied in the radio frequency (RF) magnetron sputtering
Spray pyrolysis	Simple, low-cost, and flexible	Leading to oxidation in sulfide and oxysulfide-based semiconductors

3.2.1. Electrochemical Fabrication Method

The electrochemical deposition method is among the most widely used electrode fabrication techniques which allows the synthesis of various semiconductor electrodes on the desired substrate. The electrodeposition can be carried out via manipulating the current (potentiostatic deposition) or potential (galvanostatic deposition) while keeping the other parameter constant. Under the conditions set for electrodeposition, the substrate should be electrochemically inert to avoid possible parasitic reactions. Hence, understanding the electrochemical behavior of the substrate is very useful, which is usually extracted from its CV curve. An influential example of this technique is the anodic deposition of $BiVO_4$ film, which was reported by the Choi group in 2012 for the first time.[49] By utilizing $Bi(NO_3)_3$ and $VOSO_4$ as Bi and V precursors, respectively, the authors successfully synthesized the $BiVO_4$ photoelectrocatalyst. Later, this electrochemical deposition method was also adopted to dope Mo in $BiVO_4$ via simply introducing peroxomolybdates in the plating solution as a Mo precursor, indicating the versatility of the method.[50] Until now, the electrochemical deposition method has been widely employed to synthesize many binary and ternary photoelectrodes on different substrates.[51]

One feature of the electrochemical method is the facile deposition processes for target layers and protective layers on semiconductor photoelectrodes. When depositing a protective layer on synthesized photoelectrode, one should give attention to the stability of the photoelectrode in the plating solution. A careful examination of the chemical stability of the photoelectrode in the plating solution is always required before the deposition process. The LSV curve can be collected in the plating solution without the electrochemically active species, and a proper potential window where the photoelectrode is electrochemically inert should be identified for the electrodeposition process. To date, this method is well-acknowledged for depositing several kinds of protecting layers, including metal oxides, layered double hydroxides,[52] oxyhydroxides, etc. For a detailed understanding of the electrochemical deposition strategy, we direct the reader to refer to some seminal reviews communicated earlier,[51] which briefly discuss the selection and preparation of electrodes, plating solution, working parameters, deposition modes, etc., in the context of several kinds of photoelectrodes.

3.2.2. Hydrothermal/Solvothermal Method

The hydrothermal/solvothermal method is commonly defined as the synthesis or growth of crystals at an elevated temperature and pressure in a particular solvent.[53] It is especially used for substances that are not soluble under normal temperature and pressure conditions. The specific attributes can be modified by adjusting various experimental factors such as reaction temperature, reaction time, solvent type, surfactant type, precursor type, etc. This method is one of the most common and facile electrode preparation techniques employed to directly grow the catalyst on the substrate surface.[54] Until now, it has widely been adopted to design several traditional metal oxide catalysts, including $BiVO_4$, WO_3, ZnO, etc.[43b,55] It is worth noting that the compatibility of the resulting semiconductor catalyst with the target substrate is very crucial. For instance, semiconductors such as TiO_2,[56] and Fe_2O_3[57] can be directly grown on FTO while oxides of Zn[58] and W[59] require a seed layer to facilitate the facile nucleation and thereby deposition of the oxide on the substrate.

In earlier pioneer work by Liu and Aydil,[60] a facile hydrothermal method was employed to directly grow oriented TiO_2 nanorod single crystals on a planner FTO substrate. The authors carefully studied the effects of titanium precursors, reaction time, additives, initial precursor concentration, and growth temperature on the length, diameter, and density of the as-obtained TiO_2 nanorods. It was noticed that a temperature less than 100 °C cannot facilitate the growth of TiO_2 nanorods on the FTO substrates, while the growth rate can be increased by a factor of 5 when tuning the temperature from 150 to 200 °C. Moreover, the diameter of TiO_2 nanorod grows faster when $TiCl_4$ precursor is used. Whereas utilizing titanium isopropoxide and titanium butoxide resulted in almost similar morphology under the same growth conditions. In another study, Feng and co-workers vertically grew tetragonal TiO_2 nanosheets with (001) exposed facets on the FTO substrates.[61] It was found that the addition of $(NH_4)_2TiF_6$, the ratio of H_2O to HCl, the reaction temperature, and reaction time play significant roles in facilitating the growth of TiO_2 with (001) facet. The authors realized that lower growth temperature (<150 °C) and the absence of HCl cannot completely grow TiO_2. Therefore, the hydrothermal/solvothermal method is the facile method for fabricating photoelectrodes enabling accurate control of size, shape/facet, crystalline structure, etc.

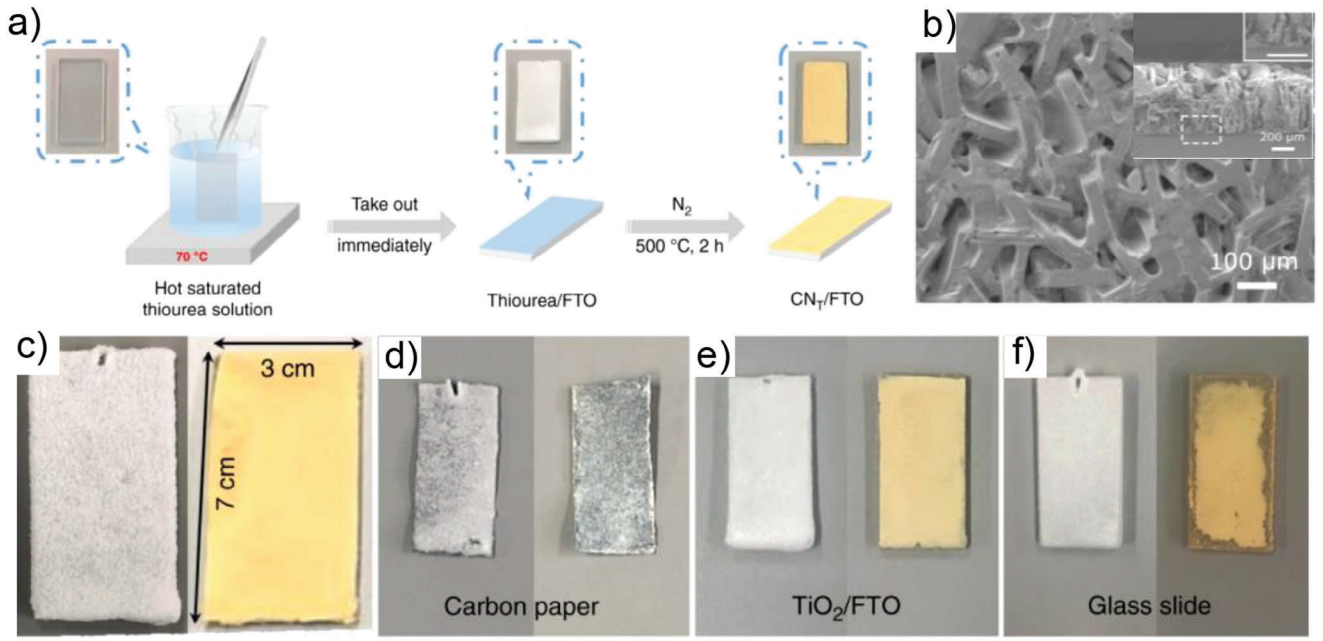

Figure 8. a) Schematic illustration for the synthesis process of carbon nitride film based on thiourea (CN_T) on FTO substrate. b) SEM image of thiourea on FTO substrate (inset: a cross-sectional image of three-layer thiourea film). c–f) Digital images of thiourea and CN_T films on a different substrate. The images at the left correspond to thiourea, and CN_T films at the right. Reproduced with permission.[66] Copyright 2020, Springer Nature.

3.2.3. Chemical Vapor Deposition

The chemical vapor deposition (CVD) is a synthesis process in which the chemical constituents react in the vapor phase near or on a heated substrate to form a solid deposit.[62] It is among the most widely employed electrode fabrication methods utilized for depositing thin film on different kinds of substrates. In general, the CVD process involves several key steps: the first step comprises the thermal evaporation and transportation of precursors/reactants and subsequent gas phase reaction. Next, the reactants will diffuse toward the substrate surface. After that, they adsorb and undergo surface diffusion toward the growth site where nucleation and surface chemical reactions take place. Finally, the desorption of fragmented products will take place. During the CVD growth process, an inert carrier gas is continuously fed into the heating chamber to facilitate the volatilization/transportation of the precursors. The CVD method has been employed to grow several kinds of metal oxide semiconductor photoelectrodes and their related heterostructures.[63] In previous work by Ariffin et al., an inert carrier gas (gaseous ethanol) was utilized to facilitate the ZnO precursor solution atomization into fine droplets.[64] After the small droplets are transported to the heating chamber, their facile deposition takes place directly onto an FTO substrate. Apart from oxide-based semiconductors, sulfides of transition and post-transition metals can be also fabricated by this method.[65] Hu and co-workers utilize the CVD method to realize wafer-scale vertically oriented SnS_2 nanosheets on conductive FTO substrate.[65a] According to the authors, the loading of the SnS_2 nanosheets can be manipulated by controlling the growth temperature. In general, the most governing parameters to control the fabrication of photoelectrodes in this technique are the temperature at various zones, flow rates of gases, pressure, type of precursors, type of substrate, substrate-precursor distance, etc.

Moving beyond the above two methods, the direct fabrication of a photoelectrode film on different substrates offers fair attachment between the catalyst and substrate, as well as ease of controlling morphology. For instance, the Shalom group utilized a facile route to synthesize carbon nitride (CN) film on an FTO glass substrate.[66] First, a film layer of thiourea was obtained by immersing a clean FTO substrate into a hot saturated thiourea solution; then, the obtained film layer was dried and calcined at 500 °C under N_2 atmosphere to get the carbon nitride film (**Figure 8**a,b). This method could be used to fabricate CN film on various substrates (carbon paper, glass slide, etc.), and the thickness of the film was controlled via a sequential dip-dry cycle.

4. Synthesis of Valuable Chemicals via Photoelectrocatalysis

This section discusses the recent development of photoelectrochemical strategies for the production of high-value chemicals. In particular, the photoelectrochemical processes involving the oxidation, reduction, bond activation, and functionalization of various organic and inorganic feedstocks, such as glycerol, HMF, benzyl alcohol, oxygen, nitrogen, N_2, water (to H_2O_2), nitrate, nitrite, etc. to high-valued chemicals are highlighted. Given the numerous reviews on PEC hydrogen evolution reaction[67] and CO_2 reduction,[15a,b,68] we do not include these two reactions in the present review.

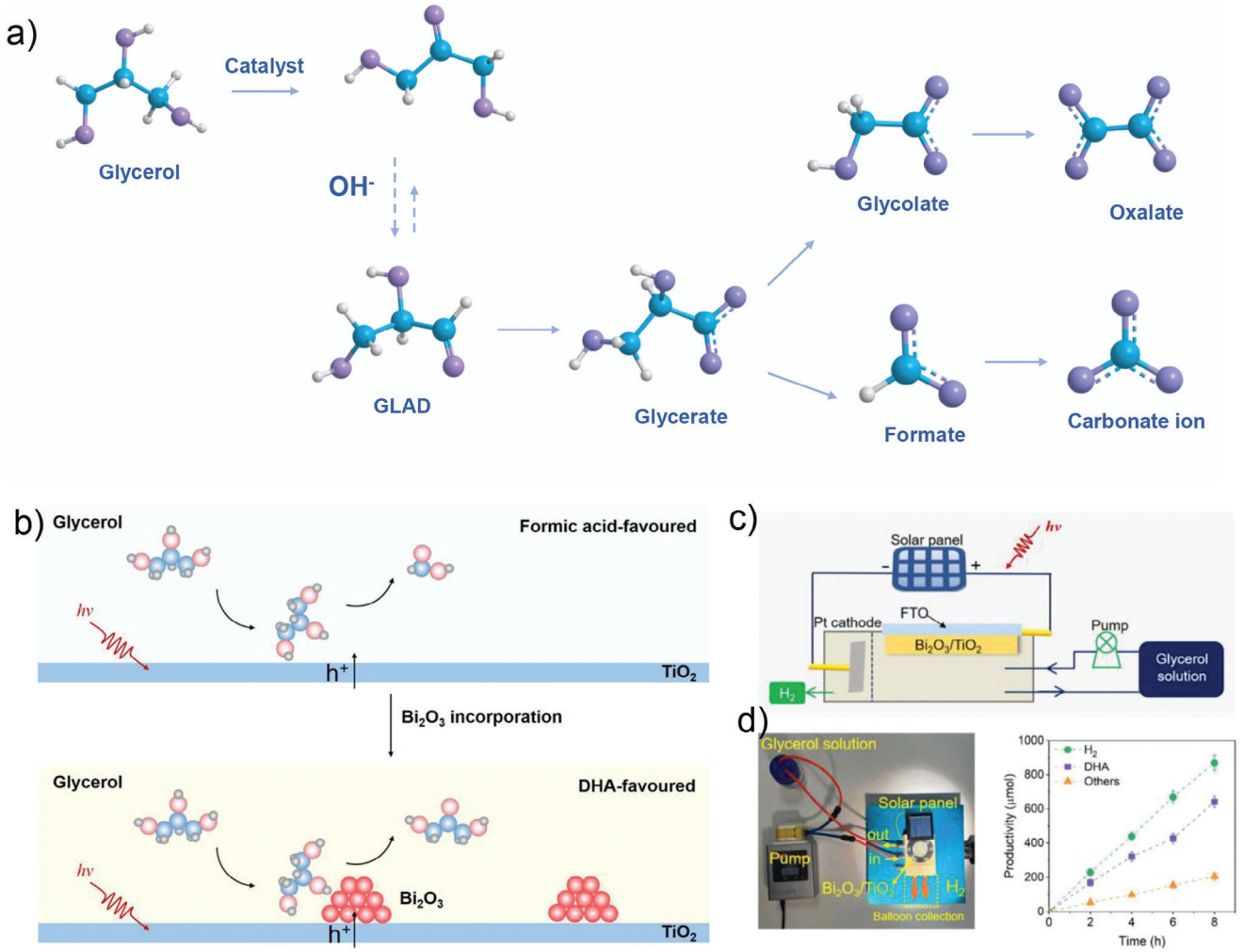

Figure 9. a) Catalytic oxidation pathway for glycerol. b) Schematic depicting the role of Bi_2O_3 in Bi_2O_3/TiO_2 nanorod array for preferential adsorption of the middle hydroxyl group of glycerol to facilitate its oxidation into 1,3-dihydroxyacetone (DHA). c) Schematic illustration and d) digital image depicting the construction of a practical PEC device for glycerol valorization. Time-dependent DHA and H_2 production in a paired electrochemical system. The PEC process is carried out under simulated solar light illumination of Bi_2O_3/TiO_2 photoanode in 0.5 M Na_2SO_4 electrolyte (pH = 2) and 0.1 M glycerol concentration. The Pt cathode is used to generate H_2 gas on the counter. Reproduced with permission.[80] Copyright 2022, American Chemical Society.

4.1. PEC Synthesis at Anode

4.1.1. Oxidation of Glycerol

Glycerol is one of the main by-products of biodiesel production, and its purification process in wastewater is complex due to its viscosity. Glycerol has several oxidation products with industrial and economic importance in polymer synthesis and cosmetics, including 1,3-dihydroxyacetone (DHA, 150US$ per kg), glyceraldehyde (GLD, 40 US$ per kg), formic acid (0.4US$ per kg), glycolic acid (3.1US$ per kg), and lactic acid(1.7US$ per kg).[69] In 2020, the annual production of glycerol has reached 3–4 Mt[70] and is projected to grow up to 6 Mt yr^{-1} by 2025.[71] Owing to its lower thermodynamic oxidation potential (<0.3 V vs RHE) than OER (1.23 V vs RHE),[72] glycerol oxidation has received a lot of interest mainly aimed at replacing the less industrially important and kinetically sluggish OER at the anode.[34b,73] For example, a recent report from the Yang research group showed that Si photoanode can achieve a low onset potential (−0.05 V vs RHE) and high photocurrent density of 10 mA cm^{-2} at 0.5 V versus RHE bias during glycerol oxidation.[74] However, the selectivity toward a specific oxidation product is still a great challenge, and this emanates from the presence of two primary and one secondary hydroxyl functional group leading to complex oxidation paths (**Figure 9**a). As such, catalyst design strategies that favor the oxidation of glycerol toward the selective production of more valuable chemicals has become the focus of many researchers in this field.

The PEC transformation of glycerol over a semiconductor photoanode largely depends on several factors, including exposed facet,[75] morphology,[76] surface and interface of the catalyst,[77] and some other extrinsic factors like pH[31,70,78] and nature of electrolyte.[31] Until recently, several strategies involving the manipulation of photoelectrode or electrolyte composition have been tried to activate the middle hydroxyl functional group, thereby enhancing its selectivity toward DHA production.

Earlier work from Liu's group utilized nanoporous $BiVO_4$ photoanode to selectively oxidize glycerol in acidic media.[30] The oxidation product formation rate shows dependency on the applied potential and the selectivity toward DHA formation reached 63.6% at pH ≈2, while the overall FE in the liquid products was near ≈50%. Further, DFT calculations enabled the understanding of possible reaction pathways, in which the strong electrostatic force between Bi^{3+} and oxygen at the terminal and middle hydroxyl group was predicted to favor the adsorption of glycerol on Bi^{3+}. Compared with the terminal radicals, the tertiary radicals on the middle carbon were found stable, which supports the observed higher selectivity toward DHA production. Following this seminal report, a remarkable improvement in FE of DHA was achieved by tuning the acidity and composition of the electrolyte. For this purpose, Sayama and co-workers constructed Ta doped $BiVO_4/WO_3$ composite photoanode as an acid resistant material, which was capable of oxidizing glycerol in an electrolyte containing 100 mM H_2SO_4 and acetone to yield 96% FE.[70] In another recent study, Huang's group designed a metal-organic framework (MOF) derived N-doped carbon $TiO_2/CsPbBr_3/TiO_2$ photoanode for PEC glycerol oxidation.[79] In this work, the N-doped carbon serves as a carrier transport channel to significantly enhance the charge transfer property of the electrode. The designed system showed promising performance and stability toward glyceraldehyde and DHA production under the optimized electrolyte composition and glycerol concentration. While these reports mainly focused on controlling the pH and content of the electrolyte, manipulation of the photocatalyst itself is found to trigger the adsorption of specific OH site. Very recently, Duans group highlighted that the selectivity of glycerol oxidation product can be switched from formic acid to DHA by incorporating Bi_2O_3 on TiO_2 surface (Figure 9b).[80] On accounts of enhanced adsorption of the middle hydroxyl group of glycerol on Bi_2O_3, the designed Bi_2O_3/TiO_2 photoanode exhibited excellent selectivity (75.4% at 1.0 V vs RHE) compared with its TiO_2 counterpart (22.3%). Furthermore, a self-powered system constructed using Bi_2O_3/TiO_2 anode and Pt cathode enables the concurrent production of DHA and H_2 gas with a productivity of 11.5 μmol cm^{-2} h^{-1} and 0.32 mL cm^{-2} h^{-1}, respectively (Figure 9c,d).

Along with the development of photoelectrodes for the transformation of glycerol, various efforts have been devoted to improving the performance and selectivity of its oxidation products.[77b,81] For instance, Qu et al. have successfully developed a microfluidic structured WO_3/TiO_2 photoelectrode constructed from rationally engineered defective WO_3/TiO_2 heterostructures (**Figure 10**a,b).[77a] The designed architecture displayed a threefold improvement in the yield of glyceraldehyde and DHA during glycerol oxidation compared with H-WO_3 (Figure 9c). Evidence collected from the Kelvin probe force microscopy (KPFM) and photoluminescent (PL) imaging reflected the accumulation of charge at the interface within the defective heterostructure. Along with the positive surface photovoltage (SPV) signals of 140 and 40 mV for TiO_2 and H-WO_3, respectively, the 0 mV SPV at the defective heterointerface has indicated the migration of electrons from TiO_2 to WO_3 and the holes from WO_3 to TiO_2 (Figure 10d,e). In contrast, the SPV value at the heterointerface of the defect-free WO_3/TiO_2 (Figure 10f) was much higher (60 mV), indicating the slow charge separation process. The PL measurements further support the inhibition of carrier recombination at the interface of a defective heterostructure (Figure 10g,h). The negligible fluorescence on the defective WO_3 surface has indicated the possible suppression of carrier recombination on the defective heterointerface. The intra-band state introduced due to this defective surface permits the reservoir of charge, facilitating the oxidation of glycerol (Figure 9i). Besides, the exposed facet of the photoelectrocatalyst also contributes to the PEC performance. Chiang and co-workers[82] unveiled the PEC transformation of glycerol promoted by monoclinic phase $BiVO_4$ photoanode with (010) dominated crystal facet. The authors rationally designed $BiVO_4$ with (010) and (121) exposed facets and investigated their relative performances toward the oxidation of glycerol. Owing to the preferential adsorption of glycerol on its surface, the (010) facet dominated $BiVO_4$ exhibited a higher yield of products when compared to $BiVO_4$ with the (121) dominated facet. Indeed, this study offers an insight on facet dependent glycerol oxidation, which could open new avenues for further study on numerous organic reactions.

Moving beyond crystal facet control and defect engineering strategies, existing modification techniques have also been employed to enhance glycerol oxidation in different media. Typically, the electrodeposition of layered double hydroxides on semiconductor photoelectrodes showed a positive influence during the oxidation of glycerol. Wang and co-workers electrochemically deposited trimetallic CoNiFe-layered double hydroxides (CoNiFe-LDHs) nanosheets on Ta_3N_5, which permits the enhancement of performance and stability of the semiconductor. The obtained photoelectrode exhibited 100% Faradaic efficiency for concurrent formate production from anodic glycerol oxidation and hydrogen production at the cathode along with marked improvement in solar energy conversion efficiency (0.56%). A similar benefit was also obtained through depositing $NiO_x(OH)_y$ co-catalyst on W:$BiVO_4$ photoelectrode via atomic layer deposition (ALD). The product distribution resulting from glycerol oxidation utilizing $NiO_x(OH)_y$ modified W:$BiVO_4$ photoelectrode is controlled by $NiO_x(OH)_y$ co-catalyst and electrolyte pH.[78a] Another study by Wang and collaborators highlighted the synergistic effect of Au and C_3N_4 for the selective oxidation of glycerol to DHA.[83] By combining the theoretical and experimental results, the altered electronic structure of Au due to the strong electronic interaction with C_3N_4 endows the Au site to preferentially adsorb and selectively oxidize the middle OH. Recently, a rationally designed ternary photoelectrode constructed from Ag, CoAl-LDH, and TiO_2 which enable DHA production from glycerol oxidation in neutral media is reported.[84] The hydroxyl radicals generated from the PEC water oxidation account for the observed selectivity. In this report, the LDH and Ag were found to play different roles: the LDH facilitated the selective adsorption and activation of the targeted OH in glycerol molecule and Ag accelerated the secondary OH oxidation, and their synergy resulted in higher selectivity toward DHA (72%).

4.1.2. Oxidation of Furan Based Feedstocks

Furfural and 5-hydroxymethylfurfural (HMF) are striking members of furanic compounds, which could be obtained via acid-catalyzed dehydration of pentose and hexose sugars, respectively.[85] The catalytic oxidation of furfural and HMF

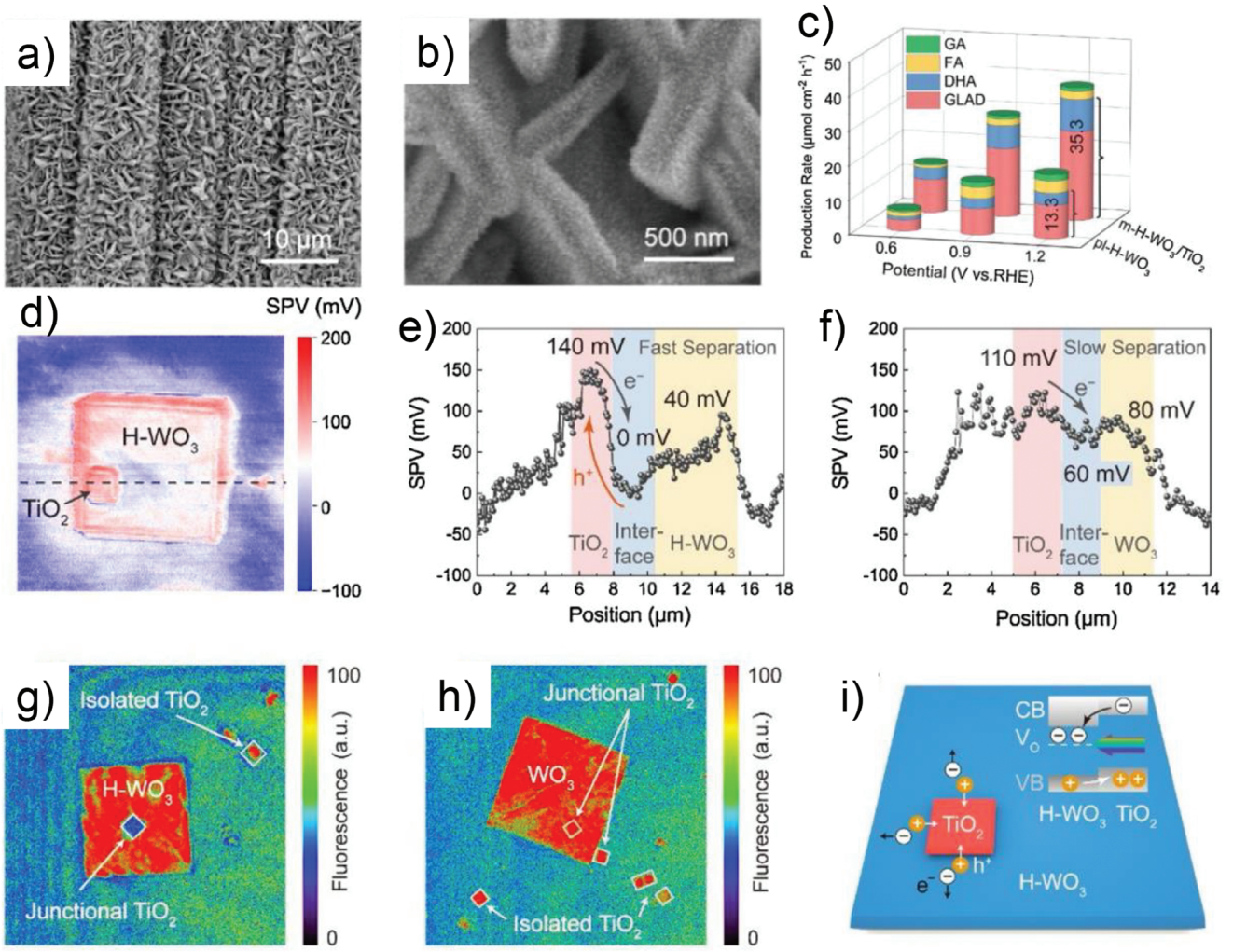

Figure 10. a,b) SEM images of m-H-WO_3/TiO_2 photoanode. c) Comparison of the PEC production rates over m-H-WO_3/TiO_2 and pl-H-WO_3 during glycerol oxidation. d) The surface photovoltage (SPV) image of defective H-WO_3/TiO_2. The representative cross-sectional SPV profiles of e) defective and f) defect-free WO_3/TiO_2 heterostructures, respectively. Spatially resolved PL images of g) defective and h) defect-free WO_3/TiO_2 heterostructure. i) Schematic diagram depicting the charge separation across the defective WO_3/TiO_2 nanointerface. Reproduced with permission.[77a] Copyright 2021, Elsevier BV.

results in the generation of industrially important chemicals, namely furanic acid (FA) and 2,5-furandicarboxylic acid (FDCA), respectively. While the previous studies largely focused on aerobic oxidation through heterogeneous catalysis, the extreme reaction conditions such as alkaline solution (pH ≥ 13), the need for highly pressurized O_2 or air as oxidant (3–20 bar), elevated temperatures (30–130 °C), and use of precious metals seriously affect the feasibility of the process. This derives the quest for an alternative technology that could produce chemicals and consumables from such bio-based refineries. In recent years, various scholars focused on converting biomass-based furanic compounds into useful chemicals and fuels through different strategies, including electrocatalytic,[4l] photo, and photoelectrocatalytic[86] transformations. Here, we briefly summarize the recent trends in the oxidation of the aforementioned furanic compounds via photoelectrocatalytic routes.

In 2017, the Choi group pioneered the 2,2,6,6-tetramethylpiperidine-1-oxyl (TEMPO) mediated photoelectrochemical upgrading of HMF to FDCA using $BiVO_4$ photoanode (**Figure 11a–d**), with nearly complete conversion of HMF (about 99%) into FDCA.[4j] The mechanistic studies have suggested that the PEC oxidation of HMF followed initial alcohol oxidation forming 2,5-diformylfuran (DFF) as an intermediate (Figure 11a). Moreover, the oxidation of 5-formyl-furan carboxylic acid (FFCA) to 2,5-furandicarboxylic acid (FDCA) is found to be the rate-limiting step during TEMPO-assisted oxidation of HMF. Following this inspiring work, the Li group reported a similar study employing TEMPO as a redox mediator.[87] They developed a heterostructured film composed of $BiVO_4$ and cobalt phosphate (CoPi) and demonstrated that the presence of CoPi can reduce the potential needed to oxidize TEMPO by 0.5 V. The as-deposited CoPi plays a crucial role in suppressing

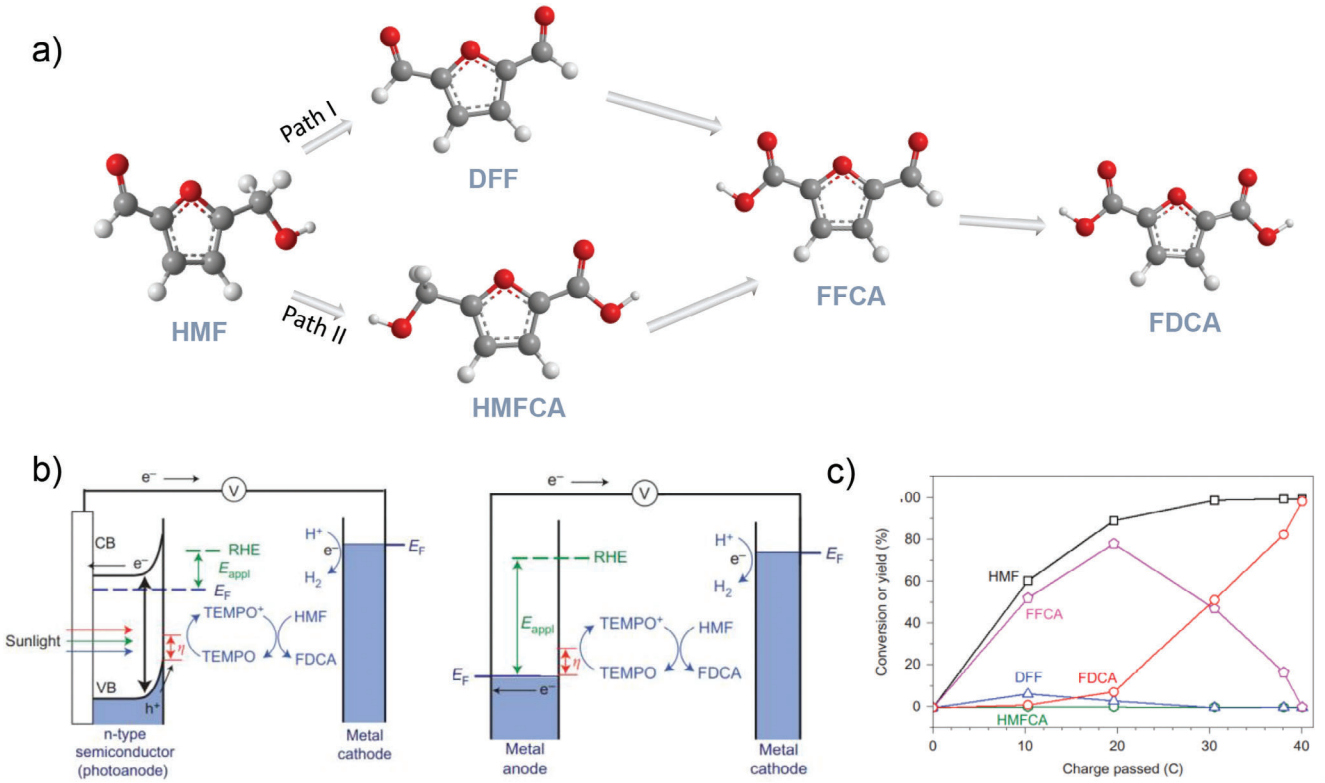

Figure 11. a) Schematic depicting the reaction pathway for oxidation of HMF to FDCA. b) Photoelectrochemical and electrochemical TEMPO-assisted HMF oxidation. CB, conduction band; VB, valence band; EF, Fermi energy. c) Yield (%) of HMF oxidation products and their conversion change during TEMPO-mediated PEC oxidation. The applied potential was 1.04 V versus RHE in a 0.5 M borate buffer solution containing 5 mM HMF and 7.5 mM TEMPO. The photoelectrode was illuminated from the front side under AM 1.5 G illumination (100 mW cm^{-2}). Reproduced with permission.[4j] Copyright 2015, Springer Nature.

the recombination loss that could result from the reduction of $TEMPO^+$ to TEMPO, resulting in an overall improvement in the performance. The designed heterostructure was able to offer a nearly 88% yield of FDCA utilizing TEMPO as a redox mediator. While the redox mediator (TEMPO) used in the aforementioned studies has a crucial role in oxidizing the organic feedstocks, the overall PEC process still suffers from some limitations, such as the difficulty of separating the final product and stability of TEMPO itself during the catalytic process. Lhermitte and co-workers attempted the PEC oxidation of HMF in absence of such redox mediators utilizing WO_3 as photoanodes in acidic media (pH 4).[88] However, the yield of FDCA in this study was far too low (1%). Considering the industrial importance of HMF oxidation products, further study may be required to fully utilize bio-based resources and sunlight to produce value-added chemicals.

Apart from HMF, the oxidation of furan and its derivatives has recently gained enormous research interest due to the importance of their oxidation products in pharmaceuticals, agriculture, and other biorefineries.[89] In 2017, the Sayama group reported the PEC dimethoxylation of furan using a bromide redox mediator and $BiVO_4/WO_3$ photoanode.[18] As high as 99% faradaic efficiency was achieved at an applied bias of 0.1 V versus SHE employing Et_4NBr as Br^- source. Further, the effect of co-supporting electrolytes (50 mM Et_4NX (X = Br^-, BF_4^-, OTf^-, and ClO_4^-) in MeCN/MeOH (9/1)) was examined for PEC dimethoxylation of furan. On accounts of anions effect toward stabilizing the cation (electron-donating ability) the faradaic efficiencies follow the order: BF_4^- (73%) > OTf^- (55%) > Br^- (48%) > ClO_4^- (41%).

In a recent work by Wang and co-workers,[90] methylammonium lead bromide single crystal thin film ($MAPbBr_3$ SCTF) was used as a photoanode for the dimethoxydihydrofuran evolution from furan (**Figure 12**a–d). Like most photoanodes, the as-synthesized crystal faced a major challenge in its stability. Interestingly, by using an ultrathin Al_2O_3 as a passivation layer, the trap-assisted nonradiative charge recombination was effectively suppressed, resulting in a twofold improvement of its surface charge carrier lifetime. Compared with the pristine $MAPbBr_3$ SCTF, the sample with the Al_2O_3 passivating layer exhibited a nearly twofold enhancement of the SPV value (Figure 12e–h), affirming the crucial role of Al_2O_3 in causing the accumulation of holes at the surface for further oxidation. Furthermore, the $MAPbBr_3$ SCTF photoelectrodes stability and performance toward oxidation of furan was improved via Ti layer deposition. The deposited Ti plays two basic roles: i) it isolates the halide perovskite from the electrolyte solution, which contributed to the robust stability; ii) it facilitates the desired oxidation reaction since the Ti^{3+} can serve as a catalytically active site. Consequently, the photoanode exhibited excellent photoelectrochemical

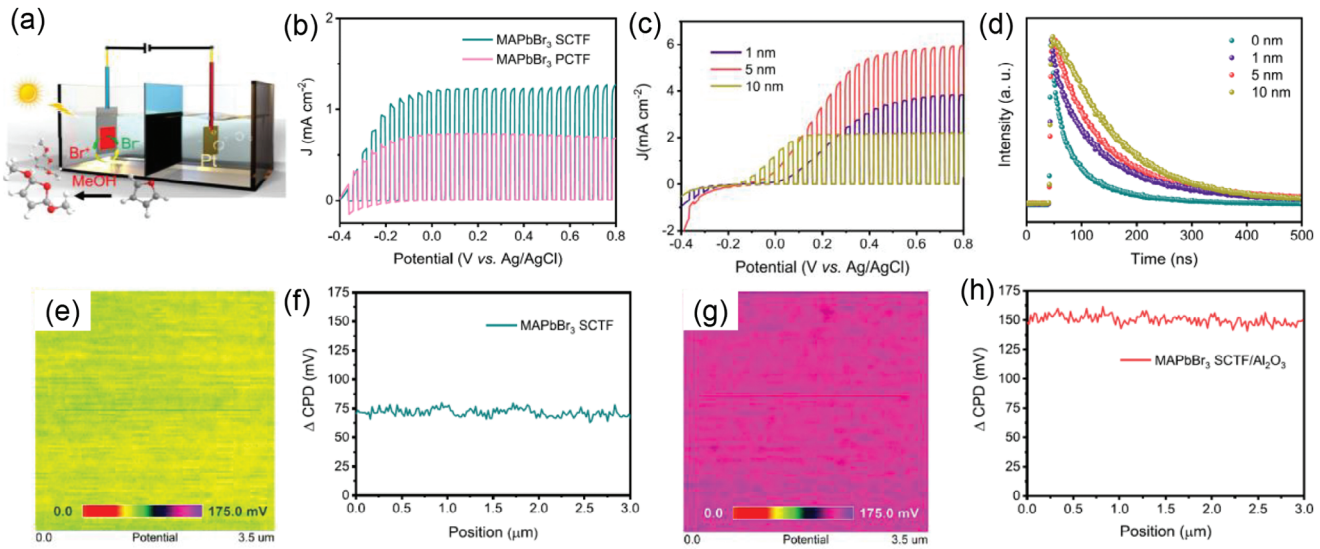

Figure 12. a) Schematic illustration of methylammonium lead bromide single crystal thin film ($MAPbBr_3$) PEC device configuration. b) Linear sweep voltammetry (LSV) of $MAPbBr_3$ single crystal thin film (SCTF-based) and polycrystalline thin film (PCTF-based) photoelectrodes. c) PEC behavior of $MAPbBr_3$ SCTF/Al_2O_3-based photoelectrodes as a function of Al_2O_3 deposition thickness. d) Time-resolved PL decay curves of $MAPbBr_3$ with varying Al_2O_3 layer thickness (0–10 nm). Kelvin probe force microscopy (KPFM) images (e,g) and ΔCPD profiles (f,h) of pristine, $MAPbBr_3$ SC film and $MAPbBr_3$ SCTF/Al_2O_3. Reproduced with permission.[90] Copyright 2021, Springer Nature.

performance and stability, demonstrating 93% faradaic efficiency and robust stability for 6 h continuous operation.

4.1.3. Oxidation of Benzyl Alcohol

Akin to the valorization of biomass model compounds, PEC catalysis has also been used to derive the selective transformation of various aromatic-based compounds, including complex molecular structures.[20,23,91] For instance, selective oxidation of benzyl alcohol (BA) to benzaldehyde (BAD) has been realized through PEC catalysis.[20,91a] BAD, which is industrially produced via direct oxidation of toluene, has several applications, including in the production of dyes (like acridine and aniline), pharmaceuticals, antibacterial and antifungal preservatives, etc. In addition, it can be used as an intermediate for the synthesis of several organic compounds. While optimizing the catalyst surface and reaction parameters is still required to suppress the competitive and industrially less important OER, alcohol oxidation can be regarded as a good alternative anodic reaction for a complete PEC fuel production system.[92] In a very recent example by Zhao and co-workers, a photoelectrode based on a Bi_2MoO_6 nanoparticle and a TiO_2 nanotube array was utilized to promote the anodic BA oxidation of BAD. The authors realized concurrent benzyl alcohol oxidation and H_2 production with the % conversion of BA and FE for H_2 reaching 100% and 85%, respectively.[91a]

The search for an alternative photoelectrochemical system to derive alcohol oxidation continues to grow rapidly. Recently, Zhang's group utilized $BiVO_4$ photoanode coated with 2,2′-bipyridine-based covalent organic framework containing single Ni sites (Ni-TpBpy/$BiVO_4$) to transform BA to BAD.[93] A radical-mediated reaction pathway followed in this system enables an efficient BAD conversion rate with the coated sample (Ni-TpBpy/$BiVO_4$) showing sevenfold improvement compared with pristine $BiVO_4$ photoanode (11.49 vs 80.63 μmol h^{-1}). In-depth experimental exploration elucidates that the surface-bound ·OH radicals formed by the Ni-TpBpy served as the main reactive oxygen species (ROS) to efficiently catalyze BA oxidation. Moreover, Odobel and collaborators demonstrated a dye-synthesized photoelectrosynthesis system for upconverting para-methoxy BA to the corresponding aldehyde.[94] The authors fabricated TiO_2-based dye-synthesized PEC cells that employ zinc porphyrin and TEMPO as sensitizers and organocatalysts, respectively. Such a PEC system showed a maximum of 82% FE for aldehyde formation using a borate buffer electrolyte (pH = 8). However, the catalyst performance decreased when acetonitrile was used as an electrolyte. The authors attributed the marked performance loss to emanate from the leaching of the photocatalyst from the TiO_2 electrode. Another recent study from the Reek group used dye-sensitized PEC (DSPEC) cells to compare the homogeneous and heterogeneous catalytic processes during the oxidation of BA to BAD.[91d] In this study, the authors fabricated a DSPEC that contains a photoanode of TiO_2 film sensitized with thienopyrroledione-based dye. For the sake of comparison, the authors immobilized TEMPO on the photoanode (denoted as a heterogeneous system) and directly added TEMPO to the DSPEC anolyte (in the case of the homogeneous system). They noted a marked decline in the photocurrent density when TEMPO was immobilized on the photoanode.

Utilizing nitrate salts as a mediator for the light-assisted oxidation of alcohols was found a crucial role in facilitating the rate of alcohol oxidation and improving its product yield.[19,95] In 2020, Bartlett and co-workers developed an indirect BA oxidation scheme employing tetrabutylammonium nitrate (Bu_4NNO_3) as a mediator over $BiVO_4$ photoanode in acetonitrile solvent.[19] The nitrate ion (NO_3^-) oxidation produces a reactive nitrate radical (NO_3•) that can directly react with BA through the abstraction of a hydrogen atom. Shortly thereafter, the same group studied

the base-assisted NO_3^- mediated oxidation of BA to BAD.[95b] In this study, a nearly 80% FE for BAD production was achieved using 0.25 M BA as the initial feedstocks. Kinetic experiments have shown that the electrochemical oxidation of NO_3^- is the rate-determining step that follows first-order reaction kinetics, whereas it is zero-order with respect to alcohol. In this work, the formation of oligomers derived from acetonitrile and the removal of ancillary C—H bond was pointed as grand challenges during NO_3^- mediated PEC alcohol oxidation, which requires further effort. A more experimental effort has also been made by the Santiago group, which aimed to examine the effect of light and atmosphere on the PEC oxidation of BA to BAD.[96] The authors unveiled the role of UV light-induced singlet oxygen in BAD production during PEC catalysis. Moreover, they noted that non-electrochemical oxidation of BA over $BiVO_4$ photoelectrode could be possible through singlet oxygen sourced from UV light and oxygen. The examples above show that alcohol oxidation, which is a 2-electron transfer process, is still the ideal anodic reaction for developing a complete PEC fuel cell. However, further work is still required to improve the selectivity and yield of this reaction.

4.1.4. Miscellaneous PEC Reactions at the Anode

Apart from the oxidation of furan-based biomass precursors, glycerol, and others, the PEC technique has also been applied to derive a number of organic reactions ranging from simple to complex molecules.[97] In this section, we summarize the oxidation reactions, which are not highlighted in the aforementioned topics.

The conversion of methane to oxygenated products is economically attractive since methane is one of the most abundant and stable hydrocarbons found in different sources such as landfills, enteric fermentation, natural gas, and petroleum.[98] Albeit significant research effort has already been made for upgrading this resource, it has remained a challenge to design a highly selective catalyst for methane conversion to C_{2+} products, and the over-oxidation of methane is still one of the issues in CH_4 catalysis. Moreover, the activation of a strong C—H bond (bond energy = 434 kJ mol^{-1}) and its subsequent oxidation require high pressure and temperature (>700 °C).[99] In 2018, Wangs' lab reported the selective oxidation of CH_4 to CO using ALD-grown TiO_2 photoanode, and nearly 81.9% production yield was achieved.[100] The authors compared this result with those obtained with the commercial TiO_2 and found a significant difference. Experimental evidence revealed that such a difference in performance arose due to a higher concentration of Ti^{3+} sites in ALD-grown TiO_2 photoanode. In another study, Amano and co-workers successfully demonstrated the gas phase PEC system to realize homo-coupling of methane under blue light illumination and achieved C_2H_6 and H_2 at room temperature. However, the CH_4% conversion (nearly 0.1%) and the selectivity of C_2H_6 (54%, C-based) were not high, which shows the need of further improvement.[101]

In an attempt to realize efficient ethylene glycol production from methane, the Xiaong group reported a facet-engineered WO_3 photoanode, which provides an optimized reactivity of hydroxyl radicals and efficient CH_4 conversion.[36] Hydrothermally synthesized WO_3 nanoplate arrays (WO_3NP), WO_3 nanobar arrays (WO_3NB), and WO_3 nanoflake arrays (WO_3NF) possessing {010} exposed facets at their sides were employed as a photoanode for CH_4 PEC catalysis (**Figure 13a**). An obvious onset potential shift was observed for all obtained samples upon CH_4 gas introduction to the reaction system, indicating the preferential oxidation of CH_4 over the competitive water oxidation reaction. It was revealed that the {010} exposed facet in WO_3 played an important role. Accordingly, the WO_3NP with the highest ratio of {010} exposed facet showed maximum PEC CH_4 conversion to ethylene glycol with the production rate and selectivity reaching 0.47 mmol cm^{-2} h^{-1} and 66%, respectively (Figure 13b,c). From an in situ diffuse reflectance infrared Fourier-transform spectroscopy (DRIFTS) study, a PEC duration-dependent peak corresponding to methylene (CH_2) symmetric stretching had gradually appeared at an applied potential of 1.3 V versus RHE, suggesting the production of EG (Figure 13d). Combining their experimental evidence, the authors proposed the mechanism as follows: Firstly, the •OH attached to the {010} facets abstract H from the C—H bond of CH_4, resulting •CH_3 production. In the next step, the as-formed •CH_3 either combine with •OH or is coupled with •CH_3 to form CH_3OH or C_2H_6. The EG was formed through the preferential attack of CH_3OH by •OH on {010} facets of WO_3NB (Figure 13d,e).

Moreover, it has been well-established that using a redox mediator in PEC catalytic oxidation of feedstocks could potentially suppress the competing oxygen evolution reaction and improve the selectivity toward the targeted product.[4j,18,20] Inspired by such seminal studies, the Sayama group used phthalimide *N*-oxyl (PINO)/*N*-hydroxyphthalimide (NHPI) mediator to achieve an indirect PEC oxidation of cycloalkenes to cycloalkenones, realizing above 99% Faradaic efficiency. In this PEC system, photogenerated holes oxidize NHPI to PINO radical on the surface of the photoanode ($WO_3/BiVO_4$). Subsequently, the PINO radical was directly involved in the process of C—H bond activation, facilitating the next bond functionalization process. The applicability of this PEC system was further investigated using a variety of *N*-oxyl radical mediators and showed moderate to excellent faradaic efficiency for the oxidation of cycloalkenes.[102]

The visible-light-driven PEC catalysis of lignin compounds has also been regarded as a potential strategy to provide economically competitive and valuable aromatic compounds, including phenol, benzaldehyde, and other feedstocks.[103] The Leems' group[104] designed dye-sensitized photoelectrochemical cells and investigated the selective transformation of benzylic alcohol moieties in different lignin model compounds. In this study, the PEC system was established using a TiO_2-based photoanode surface decorated with Ru(II)-based photocatalyst as photoanode and hydrogen atom transfer (HAT) co-catalyst was involved in the electrolyte solution to derive the reaction. The designed photoelectrode displayed nearly 90% conversion efficiency (**Figure 14a**) and robust stability for nearly 80 h operation (Figure 14b). The authors noted a slight decrease in the conversion efficiency of the lignin model, which was attributed to the desorption or oxidative decomposition of RuC on the TiO_2 catalyst surface. Overall, experimental works have suggested that employing a mediator in the PEC system could have the following advantages: 1) mediators can efficiently minimize the influence of competitive water oxidation since the selected mediators can be easily oxidized compared to water oxidation. 2) As

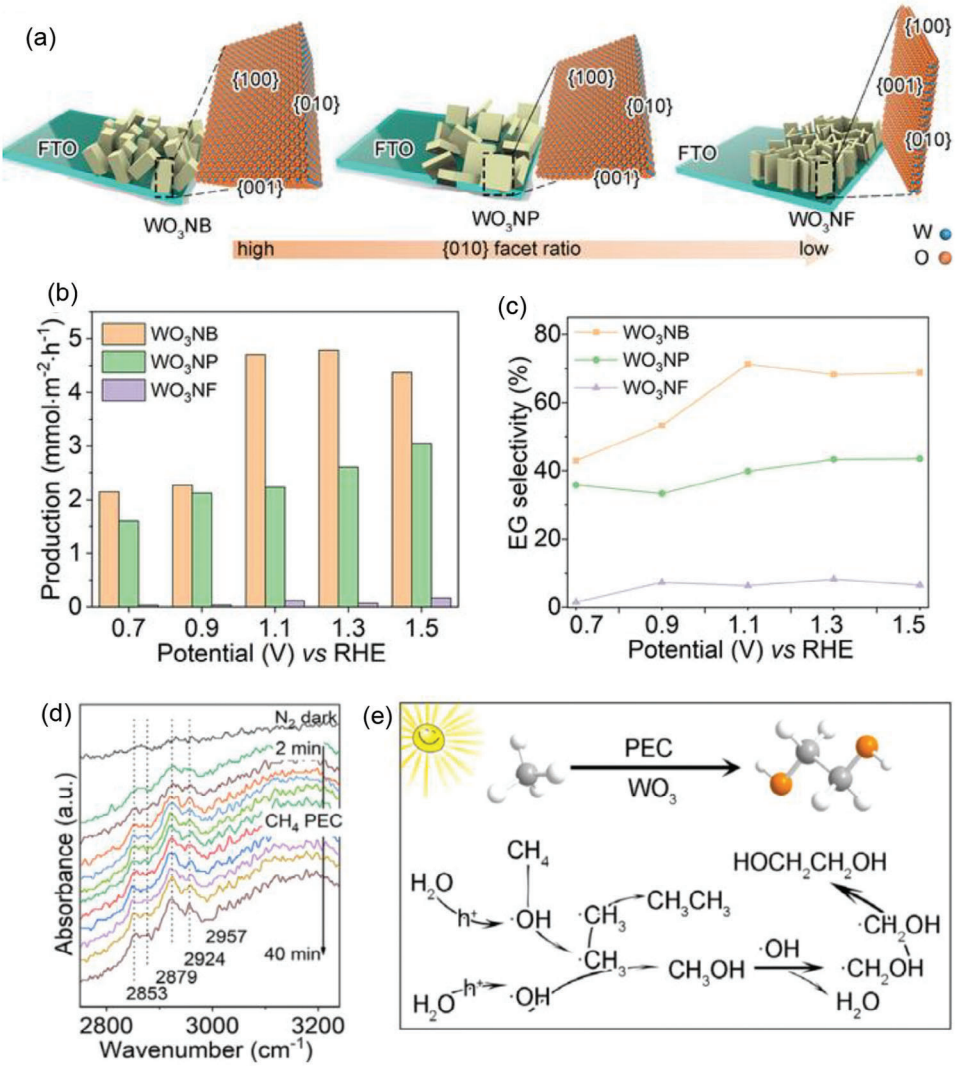

Figure 13. a) Schematic illustration depicting the hydrothermally grown monoclinic WO_3 nanostructures with different {010} facet ratios on FTO substrate. b) Potential dependent production of ethylene glycol (EG) over WO_3 photoanode with different {010} facet ratio. c) Potential dependent selectivity of EG produced during PEC CH_4 catalysis over WO_3 photoanodes with different {010} facet ratios. The photoelectrocatalysis was carried out under 1 sun (100 mW cm^{-2}) illumination. d) In situ diffuse reflectance infrared Fourier-transform spectroscopy for PEC CH_4 conversion on WO_3NB. e) Schematic illustration of the proposed reaction mechanism for PEC CH_4 conversion into EG. Reproduced with permission.[36] Copyright 2021, Wiley VCH Weinheim.

a consequence of (1), the Faradaic efficiency could increase. 3) The radicals formed as a result of mediator oxidation facilitate the formation of carbon radicals, allowing their selective oxidation. In spite of all these, the product separation and the additional cost incurred to design the PEC system with a mediator may pose a problem, which could limit its practical application in the future. In another study, the Park group attempted lignin valorization under visible light using an unassisted PEC cell.[105] They used a PEC cell that consisted of three main components: a $BiVO_4$ photoanode, a triple-cation perovskite photovoltaic (PV) cell, and a carbon cloth cathode (Figure 14d). Here, the carbon cloth cathode was used to trigger the reduction of nicotinamide adenine dinucleotide (NAD^+) to NADH in the enzymatic redox process, which aids the reduction of CO_2 at the cathode. The lignin-fueled system presented a nearly threefold enhancement in formate synthesis rate compared with the reaction with water oxidation. Moreover, the negative control experimental results were obtained in the absence of PV cell, thiobacillus sp. NAD^+, M, or CO_2, which further confirmed the significant role of each component in this system during PEC catalysis (Figure 14e). A proportionally increased formate yield was observed as a result of an increase in the concentration of lignin (1–5 mg mL^{-1}). Hence, the oxidation of biomass was found to be the rate-determining step which can also influence the reduction of CO_2 on the other side (Figure 14f).

Generally, PEC catalysis could be influenced by many factors. Beyond the intrinsic property of the semiconductor, the electrolyte is one essential factor that greatly contributes to surface catalysis. In broader terms, the composition and pH of electrolyte plays a crucial role in tuning the performance, stability, and selectivity toward the targeted product. Hence, selecting appropriate electrolytes is very important when developing electrolysis

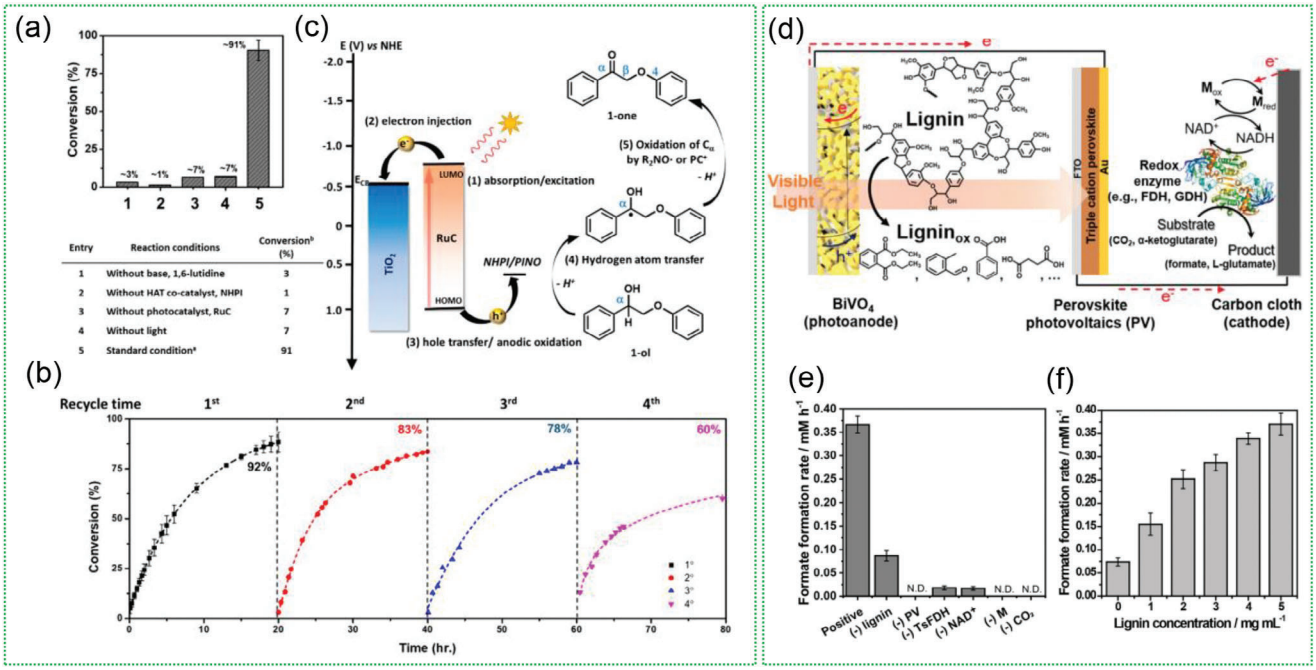

Figure 14. a) Comparison of conversion efficiencies for the PEC oxidation of 1-ol to 1-one under different conditions. The standard conditions for PEC catalysis are 2.5 mM of the feedstocks (1-ol) and 5 mM NHPI/2,6-lutidine in 10 mL of acetonitrile with 0.1 M $TBAPF_6$ under 2 sun illumination (200 mW cm^{-2} white light, AM 1.5G). The applied bias for all PEC tests was 0.75 V versus SCE. b) Stability test for PEC oxidation of 1-ol to 1-one over FTO|TiO_2−RuC photoanode. c) Proposed mechanism for the oxidative conversion of the lignin model. Reproduced with permission.[104] Copyright 2019, American Chemical Society. d) Schematic illustration depicting the transformation of lignin via PEC catalysis over $BiVO_4$ photoanode. e) Control experiment for unassisted PEC catalysis of lignin for formate production. f) Formate production rate under varying initial lignin concentrations. The reaction conditions were as follows: The cathode electrolyte contained NAD^+ (2.0 mM) and M (0.5 mM) in a phosphate buffer solution (100 mM, pH 6.5); the anode electrolyte contained 0–5 mg mL^{-1} lignin in a $KHCO_3$ buffer (10 mM, pH 8.2). Reproduced with permission.[105] Copyright 2020, Royal Society of Chemistry.

conditions in PEC cells. Until now, both aqueous and non-aqueous solutions have been utilized in PEC reactions beyond water splitting. One of the factors that impact an overall PEC process is the pH of the electrolyte solution.[30] A seminal work comparing the PEC glycerol oxidation product, DHA, under different pH led to the understanding of the crucial role of electrolyte pH on the selectivity of products.[30] The DHA appeared as a prominent oxidation product (with selectivity and overall faradaic efficiency reaching ≈50% and ≈30%, respectively) when the electrolyte pH was maintained at 2 (Figure 14). However, with increasing pH (pH = 12), glycerol was completely oxidized to formic acid, exhibiting a nearly 99% FE.

To summarize, solar PEC catalysis targeted at anodic reaction is a feasible strategy to replace the sluggish and industrially less important OER. The last few decades have shown many examples of PEC catalysis for transformative organic synthesis using several organic feedstocks, including alcohols, biomass-based aromatics, aliphatic hydrocarbons, and complex organic molecules. Despite this fact, little is known about the reaction mechanism and kinetics, and detailed theoretical work is still lacking. We suggest that a more comprehensive theoretical work could be helpful for understanding the reaction pathways and enhancing the conversion efficiencies. Moreover, the transformation of biomass-based precursors using a PEC cell would be more attractive yet challenging. Hence, proper optimization of catalyst surface and reaction conditions is still required to design a highly efficient PEC cell that could valorize the targeted biomass-based feedstocks. Therefore, there is still much hope for using PEC technology to produce various chemicals and pharmaceuticals.

4.2. PEC Synthesis at the Cathode

The PEC reduction of various organic and inorganic feedstocks to value-added chemicals is an attractive strategy for obtaining highly valuable chemicals from readily available precursors. This section focuses on the momentous progress of the PEC catalysis at the cathode that produces valuable chemicals from different resources.

4.2.1. Photoelectrochemical N_2 Reduction for NH_3 Synthesis

The industrial production of NH_3 has a century-old story, but its synthesis method still relies on the Haber−Bosch process.[106] This process is currently producing >200 million tons of ammonia, out of which 75–90% is used for fertilizer production.[107] As this NH_3 synthesis is energy-intensive (requires huge fossil fuel consumption) and operated under harsh reaction conditions (high pressure and temperature), there are critical concerns related to both energy and the environment. Hence, many researchers have been devoted to searching for an alternative

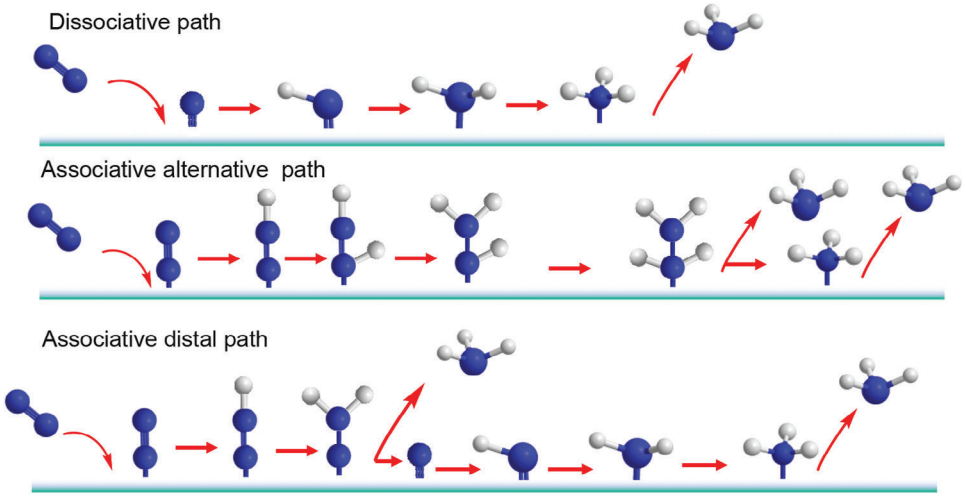

Figure 15. Proposed reaction pathways for NRR. The blue and light gray colors represent nitrogen and hydrogen atoms.

strategy that could be employed for fixing readily available N_2 sources to produce NH_3 via a cleaner route.[16a] In this regard, the PEC reduction of N_2, which combines the sustainable sources (N_2 and solar light) under ambient conditions, is one elegant alternative to upgrading N_2 to value-added and industrially important products (NH_3).[108] Generally, the nitrogen reduction reaction (NRR) is an exothermic reaction that proceeds according to Equation (18). Owing to the high dissociation energy of N≡N bonds (9.80 eV per bond at 298 K) and the high ionization potential (15.0 eV), N_2 owns a characteristic inertness toward chemical reactions. This makes the production of NH_3 from the N_2 source difficult, and the process often requires mild reaction conditions to overcome the high first-bond cleavage energy (410 kJ mol^{-1}).[109] The NRR involves several steps and reaction pathways (**Figure 15**). In the case of the dissociative pathway, the N_2 molecules are firstly adsorbed on the catalyst surface, and the cleavage of the N≡N bonds takes place before the addition of hydrogen atoms. Following the formation of NH_3 through hydrogenation of primarily dissociated N_2, the desorption of NH_3 will take place. In the case of an alternative associative pathway, an adsorbed chemical species can be formed through a transfer of one proton and one electron from the aqueous environment and the catalyst, respectively. Then, the addition of hydrogen and electron on the adsorbed N_2 species will occur, resulting in the production and subsequent desorption of NH_3. Another scenario is the so-called "distal pathway": once the preferential hydrogenation of distal N_2 occurs, the NH_3 is produced simultaneously, leaving the other adsorbed N species on the catalyst surface. This species can undergo hydrogenation and produce the second NH_3 as a product. Unlike the dissociative mechanism, the cleavage of N_2 is not necessary for the associative mechanism, which ultimately reduces the energy required for the overall process.

$$N_2\,(g) + 3H_2\,(g) \rightarrow 2NH_3\,(g) \qquad \Delta H = -92.22\ \text{kJ mol}^{-1} \quad (18)$$

The last few years have seen a surge toward employing various strategies for achieving optimized NH_3 production via PEC catalysis.[110] The construction of composite structures and p-n junctions are among the key strategies employed to improve the NH_3 production rate from N_2.[111] The rational construction of heterojunction could enable optimization, separation, and transportation of charge carriers at the interface.[111a] In 2015, Ali and co-workers reported the PEC reduction of N_2 using plasmon-enhanced black silicon (bSi) decorated with gold nanoparticles (GNPs) and Cr as the reduction catalysis sites and a hole-sink layer, respectively.[112] In particular, the designed architecture was successfully employed to upgrade atmospheric N_2 into NH_3 with a yield reaching 13.3 mg m^{-2} h^{-1} under 2 sun illumination. The authors noted that replacing bSi with pristine silicon caused a decreased NH_3 yield, with its value being only 11% of that obtained from the composite structure. It was pointed out that the bSi had multiple roles in effectively suppressing reflection, enhancing scattering and light absorption, and providing an extremely large surface area for decoration by the GNPs. In another study, Wu's group realized the conversion of N_2 to NH_3 using Ag nanoparticles supported on bSi, and they achieved a FE and NH_3 yield rate of 55.05% (at −0.1 V vs RHE) and 2.82 μmol h^{-1} cm^{-2} (at −0.2 V vs RHE), respectively.[113] A composite photocathode containing $BiVO_4$, $MnCO_3$ amorphous film, and C has been proposed, which showed an eightfold improvement in the NH_3 production compared to the $BiVO_4$ counter component. The authors claimed that $BiVO_4$ plays a prominent role in capturing abundant photons, while $MnCO_3$ amorphous film and C play a significant role in suppressing carriers' recombination and facilitating carrier transport, respectively. Upon illuminating the photoelectrode with light, the photogenerated carriers travel to the $MnCO_3$ amorphous film and interact with the antibonding orbitals of N_2, resulting in a weakening of the N≡N bond.[114] A similar study by Yan et al. has also unveiled the construction of a photocathode composed of MoS_2@TiO_2 nanojunctions, which showed a high NH_3 yield (1.42 μmol h^{-1} cm^{-2}) and an excellent faradaic efficiency (65.52%) under ambient conditions.[111d] Thereafter, the same group utilized hybrid $MoSe_2$@g-C_3N_4 micro/nanostructures catalysts in alkaline media.[32b] The PEC system was shown to be promising, and the FE and NH_3 yield rate reached 28.91% and 7.72 μmol h^{-1} cm^{-2}, respectively.

One of the grand challenges in the PEC N_2 fixation to NH_3 is the adsorption and subsequent activation of N_2 on the

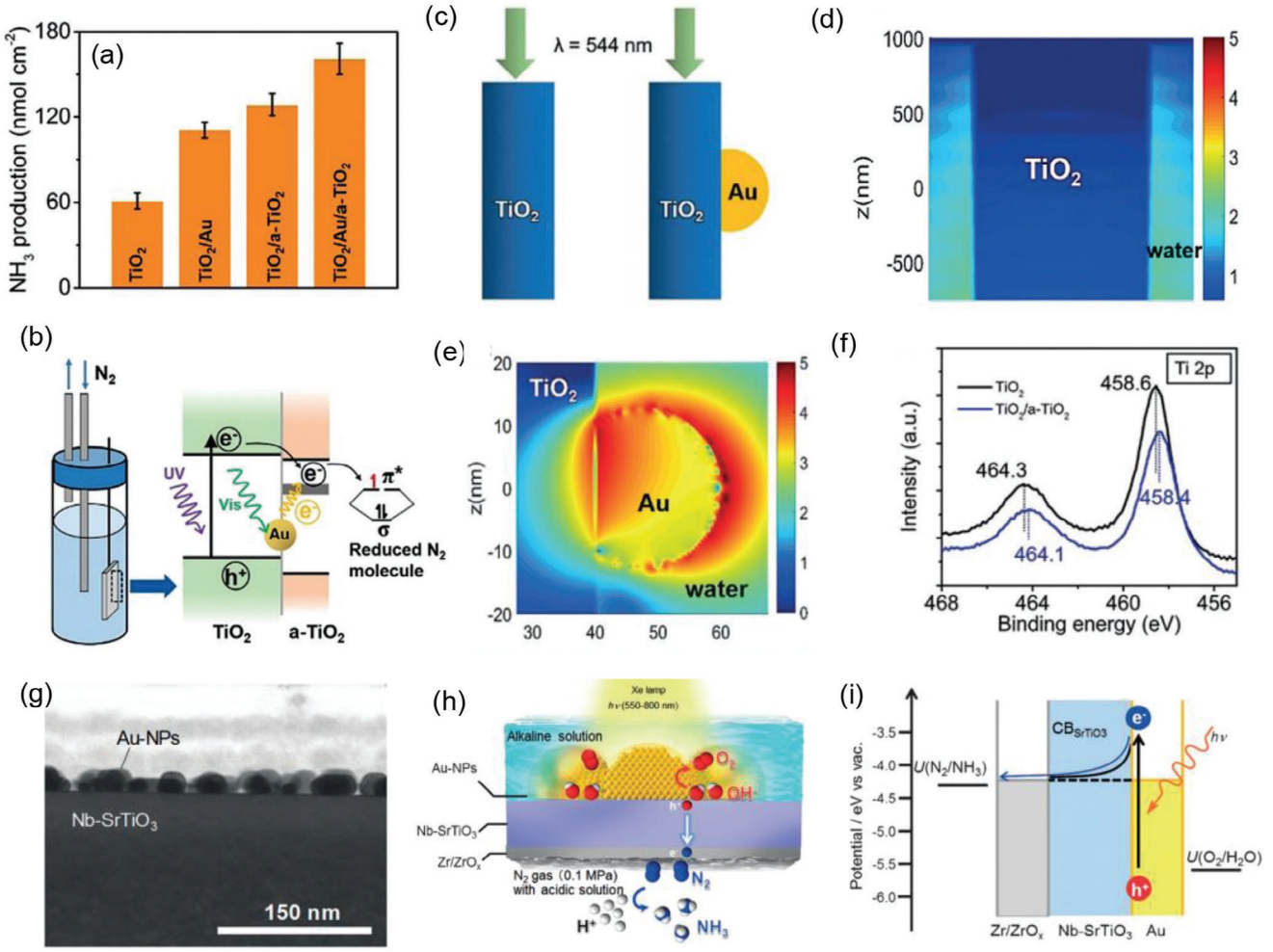

Figure 16. a) Comparison of NH_3 production over different photocathodes after 12 h reaction time. b) Schematic depicting single compartment PEC cell and c) the models of pristine TiO_2 and modified TiO_2/Au structure used in the finite difference time domain (FDTD) simulation work. f) Comparison of Ti 2p XPS spectra of TiO_2 and TiO_2/a-TiO_2. d,e) FDTD simulations depicting the electric field enhancement in TiO_2. Reproduced with permission.[32a] Copyright 2018, Wiley VCH Weinheim. g) Bright-field scanning transmission electron microscopy (BF$^-$STEM) image of the as-fabricated Au-NPs/Nb-$SrTiO_3$ interface. h) Illustration of the NH_3 synthesis device of the Nb-$SrTiO_3$ photoelectrode loaded with Au-NPs and a Zr/ZrO_x thin film. i) Energy-level diagram demonstrating the device for plasmon-induced NH_3 synthesis. CB: conduction band; U: redox potential. Reproduced with permission.[116] Copyright 2016, Wiley VCH Weinheim.

catalyst surface.[111b,115] To address this problem, the Gong group demonstrated the successful integration of surface oxygen vacancy (O_{vac}) and plasmonic Au NPs into TiO_2 photoelectrodes, which showed an enhanced NH_3 production rate exceeding the pristine TiO_2 by 2.6 folds (**Figure 16**a,b).[32a] The spatial distribution of the electric-field intensity calculated from finite difference time domain (FDTD) simulation revealed a tenfold enhancement in the electric field intensity near the Au surface of the Au/TiO_2 sample (Figure 16c–e). Hence, the presence of Au promotes the generation rate of electron–hole pairs within TiO_2, which is supported by the fact that the square of electric field intensity is directly proportional to the rate at which carriers are formed. Moreover, the hot electrons that can be injected from Au to the TiO_2 could directly reduce the adsorbed N_2 species, thereby improving the overall efficiency. In another important example by Misawa et al., the PEC transformation of N_2 into NH_3 was realized using a niobium-strontium titanate (Nb-$SrTiO_3$) photocathode modified with gold nanoparticles (AuNPs) and a zirconium/zirconium oxide (Zr/ZrO_x) thin film (Figure 16g,h). Particularly, localized surface plasmon resonance (LSPR) was employed to excite hot electrons and promote the separation of charge carriers. As a result, abundant electrons and holes could be involved in N_2 reduction and the counter-oxidation reaction, respectively. This PEC system showed a 6.5 nmol h^{-1} cm^{-2} NH_3 production rate using 10% ethanol as a sacrificial electron donor. The authors proposed that the observed NH_3 production was realized through a plasmon-induced charge separation scheme at the photocathode interface.[116] In a recent work by Park et al., α-Fe_2O_3 synthesized under an oxygen-depleted environment demonstrated an improvement of NH_3 production by 1.37-fold.[117] However, the reported performance in these works was quite low for practical application, which further requires careful optimization of

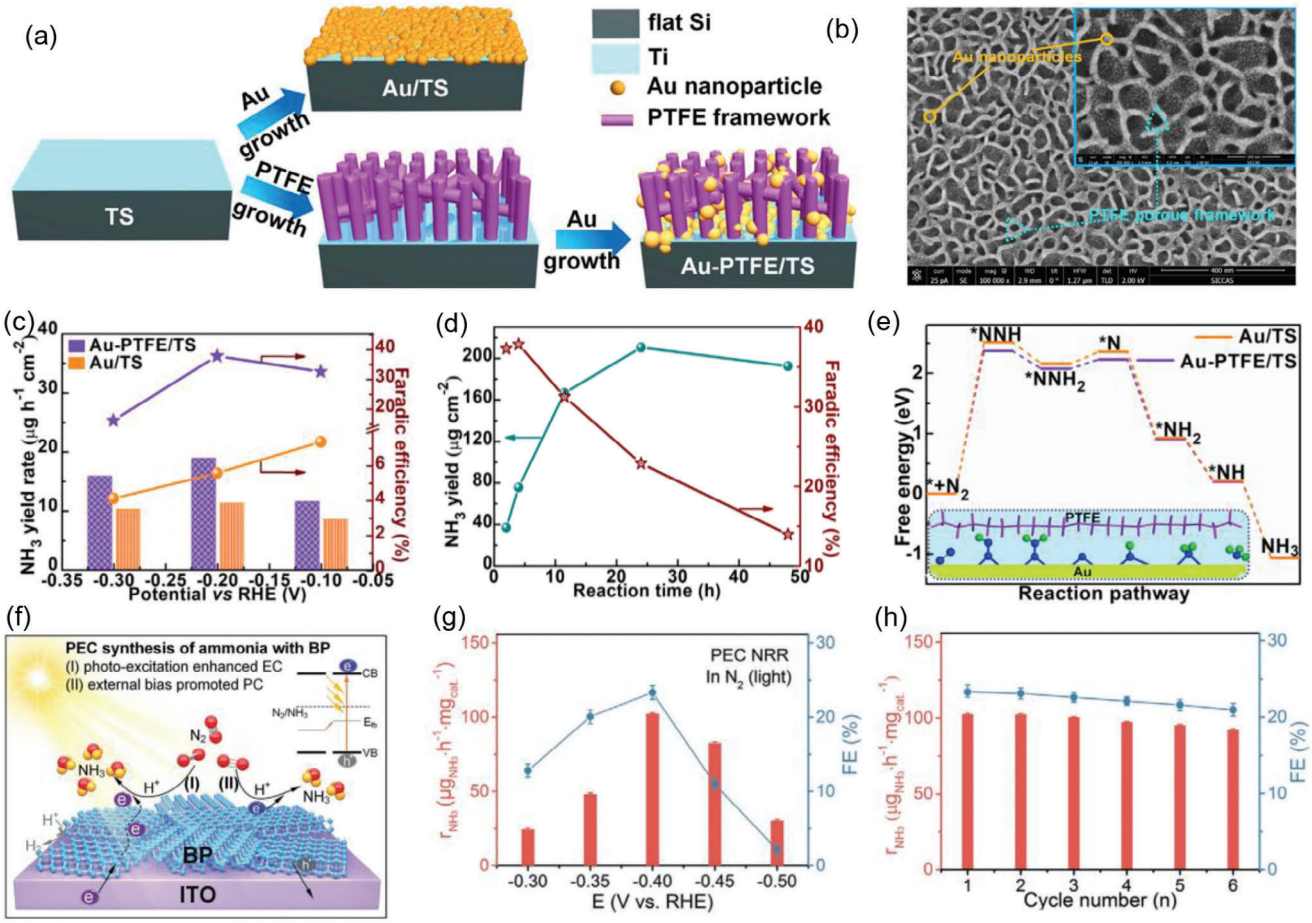

Figure 17. a) Schematics for the fabrication of Au/TS and hydrophobic poly(tetrafluoroethylene) porous framework with Au nanoparticle (Au-PTFE/TS) photocathode. b) The Field emission scanning electron microscopy (FESEM) image of the fabricated electrode. c) The potential-dependent NH_3 production rate (column diagrams) and the corresponding faradic efficiency (point plots) on Au/TS (orange) and Au-PTFE/TS (purple). The test was conducted for 4 h. d) NH_3 yield (green balls) and faradic efficiency (brown stars) over Au-PTFE/TS photoelectrode. e) Free energy diagram depicting the NRR steps on Au/TS and Au-PTFE/TS. The inset is the schematic illustration of distal mechanisms for NRR on the designed Au-PTFE/TS photoelectrode. Reproduced with permission.[118] Copyright 2019, Elsevier BV. f–h) Schematic depicting PEC catalysis over BP photoelectrode to produce NH_3 from N_2 (f) the corresponding potential dependent NH_3 production rate and FE (g) and stability test for 6 consecutive cycles. Reproduced with permission.[40] Copyright 2020, Wiley VCH Weinheim.

catalyst surface area and morphology, and as well as harvesting the proportion of the incident solar energy flux could enhance the energy conversion efficiency.

Apart from the aforementioned challenges, the selectivity and NH_3 production rate in NRR is seriously influenced by the competing HER from the aqueous solution. To tackle this problem, Zheng et al. designed a unique aerophilic-hydrophilic heterostructured photocathode composed of Si, poly(tetrafluoroethylene) (PTFF) porous framework, and Au as a photoabsorber, gas diffusion layer, and active site, respectively (**Figure** 17a,b). The PTFE porous framework plays a vital role in offering an N_2-rich environment on the photocathode surface, while the Au NPs on the PTFE framework efficiently reduce the energy barriers. Consequently, the designed heterostructure exhibited excellent performance with NH_3 yield rate and FE reaching 18.9 μg cm^{-1} h^{-1} and 37.8% at −0.2 V versus RHE (Figure 17c–e).[118] Moreover, research works have also been devoted to designing stable and promising photoelectrodes for efficient NRR. Yu and co-workers have designed a photocathode based on black phosphorus (BP), which efficiently catalyzed NRR under ambient conditions (Figure 17f).[40] Such a PEC system showed an excellent NH_3 production rate (102.4 μg h^{-1} mgcat.$^{-1}$) and Faradaic efficiency (23.3% at −0.4 V) along with auspicious stability for 6 consecutive cycles (Figure 16g,h).

Recent works from the Xiong group have shown that doping B in Bi nanorolls with high curvature surface (BDB NR) could enhance the PEC NRR rate by facilitating the key step in NRR.[119] Specifically, the PEC system composed of BDB NR (cathode) and TiO_2 nanorod arrays (TiO_2/FTO) plate (photoanode) was used to promote NRR. Interestingly, the photoanode employed here played a significant role in harvesting light and providing photogenerated electrons. This PEC system displayed excellent NRR performance with an NH_3 yield rate of 29.2 mg NH_3 gcat.$^{-1}$ h^{-1} and FE of 8.3% at a bias of 0.48 V versus RHE, well exceeding pure Bi nanotubes (10.6 mg NH_3 gcat.$^{-1}$ h^{-1}) and nanosheets (9.1 mgNH_3 gcat.$^{-1}$ h^{-1}). A theoretical study further proved that

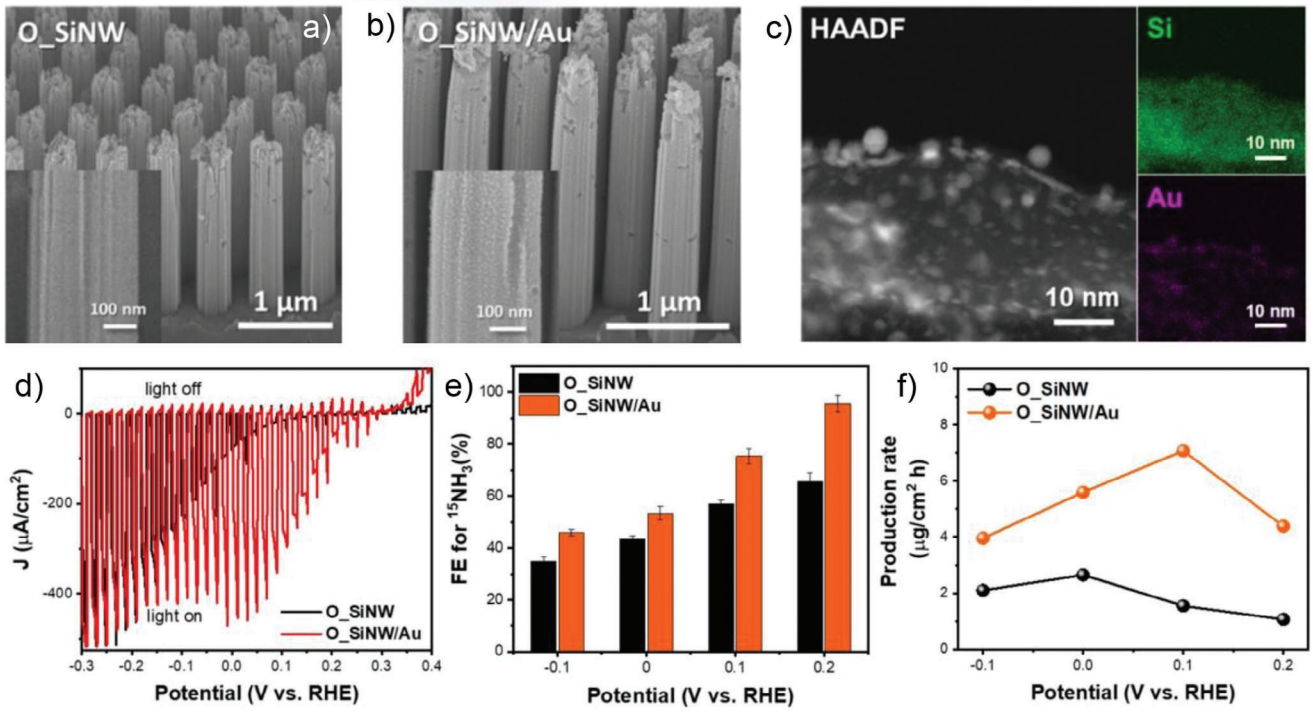

Figure 18. a,b) The SEM images of ordered silicone nanowires (O_SiNW) and gold decorated ordered silicone nanowires (O_SiNW/Au). In sets of (a) and (b) are the magnified images of their respective nanowires. c) The HAADF-STEM and corresponding EDS mapping of O_SiNW/Au sample depicting Au nanoparticles loaded on Si nanowires. d) Comparison of the current density–voltage profile of O_SiNW and O_SiNW/Au samples for nitrate reduction in Ar-saturated electrolyte (pH 3.5) containing 0.5 M K_2SO_4 and 10 mM $K^{15}NO_3$. e) FE and f) production rate of $^{15}NH_3$ using O_SiNW and O_SiNW/Au photoelectrodes under the bias of − 0.1 to 0.2 V versus RHE. Reproduced with permission.[122] Copyright 2022, Wiley VCH Weinheim.

doping with B in Bi matrix significantly reduces the energy barrier of the potential-determining step of NRR (N_2 → *NNH), while the high curvature surface of nanorolls facilitates the N_2 adsorption on the catalyst surface.

4.2.2. Photoelectrochemical Ammonia Synthesis from Nitrate

Nitrates are earth-abundant sources of nitrogen, which can be readily found in industrial wastes, livestock manure, and N-containing fertilizers. As part of the huge effort to develop an environmentally friendly route of NH_3 synthesis, the utilization of electrocatalytic and PEC techniques has attracted enormous research attention as it affords the dual advantage of balancing the global nitrogen cycle by synthesizing ammonia from wastewater and providing an alternative route for NH_3 synthesis to the energy-intensive Haber–Bosh process.[120]

In 2022, the Amal group utilized a metal-organic complex derived, defect-rich TiO_x co-catalyst engineered on a CdS/Cu_2ZnSnS_4 photocathode (TiO_x/CdS/CZTS) for selective transformation of NO_3^- to NH_4^+.[121] The TiO_x was directly covered on CdS/CZTS using a spray-coating method. The ratio of defective Ti^{3+} species in the TiO_x layer was rationally tuned by adjusting the spray-coating temperature, and these species mainly contribute to the adsorption of reactants and intermediates (NO_3^- and $*NO_2$). Under an optimized condition, the overall system exhibits a reduced work function along with an improved carrier lifetime, which further enables photogenerated charge transfer with efficient surface reaction kinetics. The designed photocathode (TiO_x/CdS/CZTS) shows an excellent performance with the FE for NH_3 reaching 89.1% at a bias of 0.1 V versus RHE. In another interesting work by Lee and co-workers, a highly efficient photocathode is designed based on gold nanoparticles decorated on silicon nanowires (O_SiNW/Au) utilizing a metal-assisted chemical etching process (**Figure 18**a–c).[122] The Au deposition presents a greatly improved onset potential and photocurrent density up on 1 sun illumination. This photocathode achieves an average FE and NH_3 production rate of 95.6% and 4.39 μg cm^{-2} h^{-1}, respectively, at 0.2 V versus RHE, which is more positive potential than the thermodynamic requirement.

Understanding the role of heterointerface formation on the PEC NO_3^- reduction performance is essential for future electrode design and optimization.[123] In such attempts, photoelectrodes that possess heterointerface with CeO_2 were employed to enhance the PEC nitrate reduction to NH_3.[123b,c] For instance, Shi et al. designed a copper phthalocyanine/cerium dioxide (CuPc/CeO_2) heterostructure, which showed nearly 33% FE at −0.6 V versus RHE along with robust electrode stability for 5 cycles.[123c] By employing several characterizations, it was found that the presence of oxygen vacancies in CeO_2 improves the carriers' transfer and affords more accessible adsorption and active sites for NO_3^-, thereby improving the PEC NH_3 synthesis performance. More recently, Fan and co-workers constructed frustrated Lewis pair sites in carbon coated $CeO_2/BiVO_4$ (CeO_2−C/$BiVO_4$) for the PEC synthesis of NH_3 from nitrate. The authors demonstrated that the frustrated Lewis pair sites play a key role in

adsorbing and activating NO_3^- while the carbon contributes to enhancing the carrier transport and kinetics.[123b] Though an obvious improvement in PEC performance is seen in the aforementioned works, their FE is still lower, especially when compared with other electrocatalytic processes. Recent works in PEC NO_3^- catalysis utilize the integration of earth-abundant NiFe LDH with graphene/Si to form Schottky junction. The atomically thin layer of graphene deposited between NiFe LDH and Si imparts several advantages to the photoelectrode, including excellent conductivity, inherent chemical stability, and high optical transparency. Consequently, the designed photocathode showed efficient charge separation and large photocurrent density of (-31.9 mA cm^{-2}) along with the highest FE to NH_3 of 92.5% at 0.15 V versus RHE, respectively.[124]

Similar to most of the PEC reduction process at the cathode, the competing HER severely affects the PEC NH_3 synthesis from NO_3^- precursor.[125] Therefore, future catalyst development must take the competing side reactions into account. Apart from this, the design of photoelectrodes that comprise metal sites with optimal adsorption for NO_3^- and strong hydrogenation ability is essential. To fully understand the relationship between the structure and activity of the photoelectrode, detailed in situ and post-mortem electrode characterization is required. In wider dimension, the PEC nitrate reduction could be fully exploited through coupling it with carbon-based organic feedstock to synthesize aliphatic amines, amides, and urea.

4.2.3. Photoelectrochemical H_2O_2 Synthesis

The PEC production of H_2O_2 from both oxygen reduction and water oxidation reactions is among the most active areas of research since H_2O_2 has several applications in wastewater purification, bleaching agent in the paper manufacturing industry, medical disinfection, and organic synthesis.[126] Compared to the energy density of a compressed H_2 gas, which is near 2.8 MJ L^{-1}, aqueous H_2O_2 (60%) could also provide an equivalent energy density (3 MJ L^{-1}). Moreover, the fact that H_2O_2 decomposition only produces water and O_2 in the fuel cell and the ease of transportation endows it to be an economically attractive carbon-neutral clean fuel. Up to now, the commercial manufacturing of H_2O_2 relies on the oxidation of anthraquinone, which involves energy-intensive processes, substantial organic wastes, and expensive Pd hydrogenation catalysts. In this regard, the solar light-assisted PEC process has been regarded as an economically competitive strategy due to the possibility for on-site production with minimized energy consumption.[127] In this section, we highlight the latest development and challenges in developing a PEC cell for the synthesis of H_2O_2.

In 2018, Li et al. developed an unassisted PEC system that integrates water, oxygen, and light to efficiently generate H_2O_2 and electricity.[128] This system successfully realized a two-sided H_2O_2 synthesis (0.48 µmol min^{-1} cm^{-2}) along with an open-circuit voltage and a maximum power density of 0.61 V and 0.194 mW cm^{-2}, respectively. Moreover, as high as 1.09 mA cm^{-2} short circuit current density was also achieved.[129] Alongside developing an efficient PEC system for H_2O_2 synthesis, considerable effort has also been made toward designing a highly efficient photocathode capable of catalyzing O_2 reduction reaction (ORR). Li and collaborators exploited metal-free polyterthiophene photocathode (pTTh) to obtain an H_2O_2 concentration of 110 mM.[130] As shown in **Figure 19a**, the pTTh photocathode and $BiVO_4$ photoanode were parallelly configured which were also separated by the Nafion membrane. Using the pTTh photocathode solely in a three-electrode configuration, as high as 110 mmol L^{-1} H_2O_2 was obtained after 11 h illumination along with >90% FE throughout the course of the reaction (Figure 19b). Further, the authors evaluated an unbiased PEC system for overall H_2O_2 production, and maximum H_2O_2 yield of 90 mmol L^{-1} was achieved after 14 h of illumination (Figure 19c). Interestingly, they conducted a rigorous theoretical investigation, which could help to understand the mechanism of PEC catalysis. The Gibbs free energies were evaluated for a series of ORR steps and transition states (TS) for the C—OOH and CO—OH bond cleavage steps (Figure 19d,e). Accordingly, the selectivity-determining step for the 2e-transfer process was found to be more than 200 times faster than that for the 4e-transfer pathway (Figure 19f). The Ma group recently published a study on using Gd^{3+} doped $CuBi_2O_4$/CuO (CBO/CuO) heterojunction film cathode to catalyze ORR under ambient conditions. The Gd-doped sample showed a nearly 1.3 mM H_2O_2 yield, and this yield was influenced by Gd^{3+} ion concentration and pH of the solution.[131] More recently, Jang and colleagues developed an unassisted PEC cell to efficiently synthesize H_2O_2 from single-step ORR.[132] They used a high-performance hybrid perovskite photocathode and an oxidized buckypaper as the H_2O_2 electrocatalyst and a protection layer to achieve nearly 1.463% STC conversion and 100% selectivity toward H_2O_2.

It is well documented that a complete PEC cell could be constructed to simultaneously derive H_2O_2 production and organic pollutant degradation.[133] In 2019, Quan et al. optimized the H_2O_2 production over a PEC cell consisting of F-doped porous carbon (FPC) cathode and a WO_3 photoanode.[134] This system showed an efficient H_2O_2 production rate and FE of 0.87 mmol L^{-1} h^{-1} and 75%, respectively. Moreover, by introducing Fe^{2+} in the electrolyte system, more •OH could be produced, leading to the rapid degradation of organic pollutants present in the solution.

In an approach different from those discussed earlier, which can be envisaged as an innovative strategy, a number of studies have been communicated on efficient H_2O_2 production from PEC catalysis. For example, Choi and collaborators reported the direct synthesis of concentrated H_2O_2 (80 mM) using an electrolyte free PEC system.[33] This unique PEC system was constructed employing Ru catalyst decorated on TiO_2 as photoanode, anthraquinone-anchored graphite rods as cathode, and solid polymer as electrolyte (SPE). The authors described the working principle as follows: at the anode, H^+ could be produced as a result of water oxidation reaction, and at the cathode HO_2^- could be produced via a 2 electrons oxygen reduction. These two species could be selectively transported through the SPE to form H_2O_2. The designed three-component PEC system achieved promising H_2O_2 production of 80 mM concentration over 100 h, at $E = 0$. However, this system suffered from limitations such as low SPE ionic conductivity and poor membrane stability during long-term operation. Moreover, the utilization of photo-electro-biochemical systems for the synthesis of commodity chemicals has received much research endeavor. In 2019, the Jang group developed a compartmented photo-electro-biochemical system

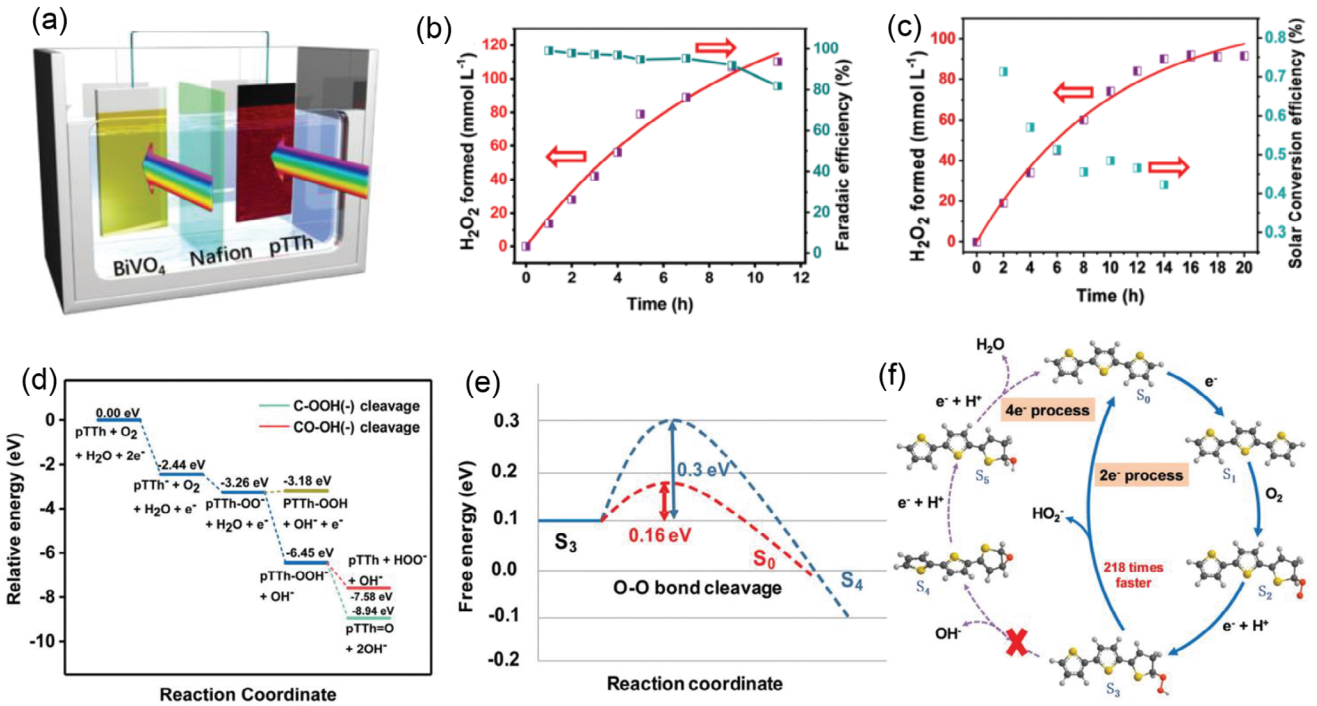

Figure 19. a) Schematics of the unbiased H_2O_2 production cell. The PEC cell consisted of metal-free polyterthiophene photocathode (pTTh) as photocathode and $BiVO_4$-based photoanode in 0.1 M KOH and 1 M borate buffer electrolytes, respectively. b) Time-dependent H_2O_2 production and the corresponding FE using pTTh photocathode (9 cm^2). c) Time-dependent H_2O_2 generation and the corresponding solar to H_2O_2 conversion efficiency. d) Energy profiles depicting the possible ORR pathways on pTTh. e) Free energy diagram of the branching point for $2e^-$ and $4e^-$ process selectivity of the ORR at pH = 13. The blue and red dashed line represents the O—O and C—O bond cleavage pathways, respectively. f) Proposed reaction cycles of PEC H_2O_2 synthesis with the energetically most viable active sites. S_0 is the bare surface, S_x (x = 1, 2, 3, 4, 5) are the structures of the intermediate states involved in the ORR. Reproduced with permission.[130] Copyright 2020, Royal Society of Chemistry.

that integrates a photocatalyst (TiO_2), electrocatalyst (Co-based porphyrins), and biocatalyst (lignin peroxidase isozyme) to derive photovoltage generation, H_2O_2 production, and lignin valorization, respectively (**Figure 20**a,c).[135] Interestingly, the photovoltage generated at the anode in such a system could produce H_2O_2. To alleviate the common stability problem in cobalt-based porphyrins, the authors atomically dispersed Co–N_x sites which were created on carbon nanotubes (Co–N/CNT). Compared to the cobalt porphyrin molecular catalyst simply immobilized on the CNTs (CoTMPP/CNT), the synthesized Co–N/CNT showed a significantly lower overpotential of only 0.04 V (Figure 20d). In addition, the estimated working current obtained using Co–N/CNT in the integrated system was fairly higher (0.62 mA) than Co-based porphyrins, as shown in Figure 20c. Importantly, stable H_2O_2 production could be achieved (Figure 20d,e) in a system that is freely diffused to the biocatalyst compartment to facilitate lignin depolymerization and biopolymer synthesis. Another recent study employed the same electrocatalyst (Co–N/CNT) in PEC cells to facilitate the epoxidation of propylene using an in situ-generated H_2O_2.[136] In the presence of propylene, the H_2O_2 produced remained unchanged, indicating its continuous consumption to produce propylene oxide. This PEC system successfully demonstrated the production of propylene oxide via in situ generated H_2O_2.

To summarize, solar-driven oxygen reduction PEC catalysis has been regarded as an alternative strategy to generate valuable H_2O_2. It has already been pointed out that such a system requires an efficient and integrated platform that could save energy. While there is a potential to design a PEC cell that could simultaneously drive H_2O_2 production and pollutant removal for the complete mineralization of wastewater, a more techno-economical study is required to study the feasibility of this process. In contrast, innovative strategies could be further employed to assess the indirect synthesis of other kinds of organic reactions. For instance, H_2O_2 has many applications in organic synthesis. Hence, some kinds of organic reactions can be carried out with the assistance of an in situ generated H_2O_2, which could also solve one grand problem associated with the stability of H_2O_2 during light illumination. Lastly, the selective reduction of some functional groups in a complex organic molecule could be more attractive to rationally synthesize complex structures, which is helpful in pharmaceutical industries.

Beyond NH_3 and H_2O_2 synthesis, the reductive PEC upgrading of organic chemicals is a promising strategy for synthesizing several industrially relevant chemicals. For instance, the PEC synthesis of aniline from the reduction of nitrobenzene (NB) was reported by Mascaro and co-workers.[137] Similarly, Ohno et al. successfully synthesized aniline using a p-type Cu_2ZnSnS_4 electrode. The authors found that the selective reduction of NB depends on the applied potential, and as high as 99% conversion of NB and >50% production of aniline was recorded.[138] The PEC catalysis targeted at reducing various feedstocks is still

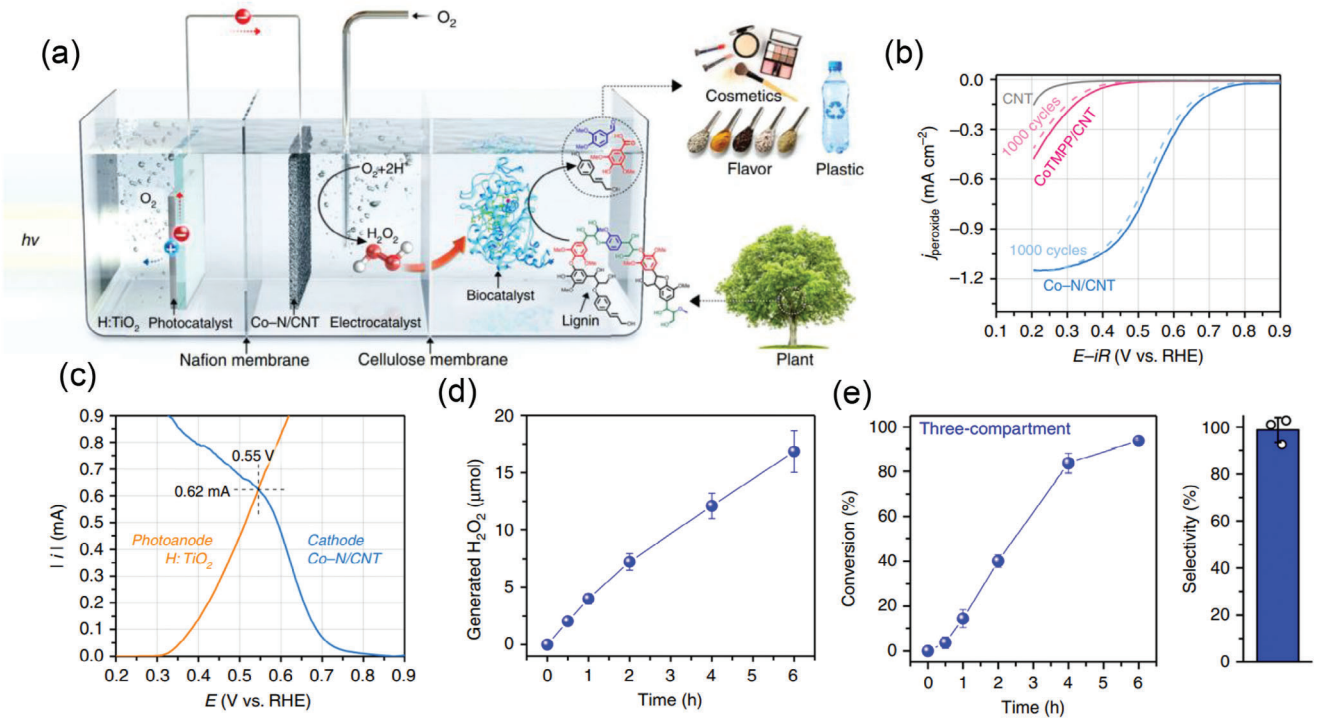

Figure 20. a) Schematic showing a three-compartment photo-electro-biochemical system. b) Comparison of LSV curves of different catalysts. The gray, pink, and sky-blue colors correspond to the scans for photoelectrodes of carbon nanotubes (CNT), cobalt porphyrin molecular catalyst simply immobilized on the CNTs (CoTMPP/CNT), and atomically dispersed Co–N_x sites on carbon nanotubes (Co–N/CNT), respectively. The dashed lines are the corresponding curves after 1000 cycles. c) *J–V* curves of H:TiO_2 photoanode (orange line) and Co–N/CNT cathode (sky blue line). The anode electrolyte is 0.1 M phosphate borate solution (PBS, pH 4.5), and O_2-saturated PBS was used at the cathode. The photoanode was illuminated under simulated 1 sun (AM1.5 G). d) Amount of H_2O_2 produced in a three-compartment integrated cell. e) The conversion and selectivity for H_2O_2 over the course of the reactions in the PEC catalytic system. Reproduced with permission.[135] Copyright 2019, Springer Nature.

underexplored. Considering the availability of biobased precursors, this technology could be further explored to valorize the readily available precursors. An example of a PEC reaction targeted at reducing biomass is the seminal work by the Choi group. The authors used Ag and $BiVO_4$ as a cathode and photoanode in this work, respectively. Upon light illumination, the photogenerated holes at the $BiVO_4$ surface involve water oxidation, whereas the electrons migrate to the counter Ag for an efficient reduction of HMF to BHMF.[35]

4.3. PEC Reactions Involving C—H and C—C Bond Activation and Functionalization

The activation and conversion of C—H and/or C—C bonds is a highly value-added conversion, as it could offer a platform for synthesizing industrially and biologically important pharmaceuticals, natural products, and agrochemicals.[139] In 1980s, metal complexes and salts were used to facilitate the C—H bond activation through the oxidative addition mechanism.[140] However, this strategy suffers from serious limitations since it requires an equimolar amount of organic feedstocks and metal source, and both of these sources were usually consumed at the end. As a result, the feasibility of the process is a major concern, limiting it from being commercialized at a large scale. The past decades have witnessed the development of this reaction via several strategies, including photocatalysis,[141] electrocatalysis,[142] photoelectrocatalysis,[143] electrophotocatalysis,[144] and Hofman–Loffer–Ferytang reactions.[145] The photoelectrochemical activation and conversion of C—H and C—C bonds present several advantages, such as ease of product separation and less energy consumption.

This section highlights the photoelectrochemical activation and conversion of C—H and C—C bonds for the high-valued transformation of organics. We would like to remind the readers that conversion of C—C/C—H bonds to the corresponding oxygenates is already highlighted in Section 4.1, and this section mainly focuses on the functionalization of non-oxygenate organics.

By and large, the selective functionalization of the C—H bond is challenging for organic chemists since the C—H bonds are kinetically inert. The high dissociation energy required to break the C—C bonds makes the process of C—C bond functionalization challenging. Despite all these facts, the activation and functionalization of these bonds have garnered much research interest due to their broad scope of application in manufacturing medicines, dyestuff and agrochemicals. In 2019, Hu and collaborators reported arenes' C–H amination using a hematite photoanode.[146] As shown in **Figure 21a**, upon illumination of the hematite electrode with blue LED light, an early onset potential of 0 V versus Fc/Fc^+ was observed, much lower than the dark (0.9 V vs Fc/Fc^+). The holes generated from photoanode illumination could

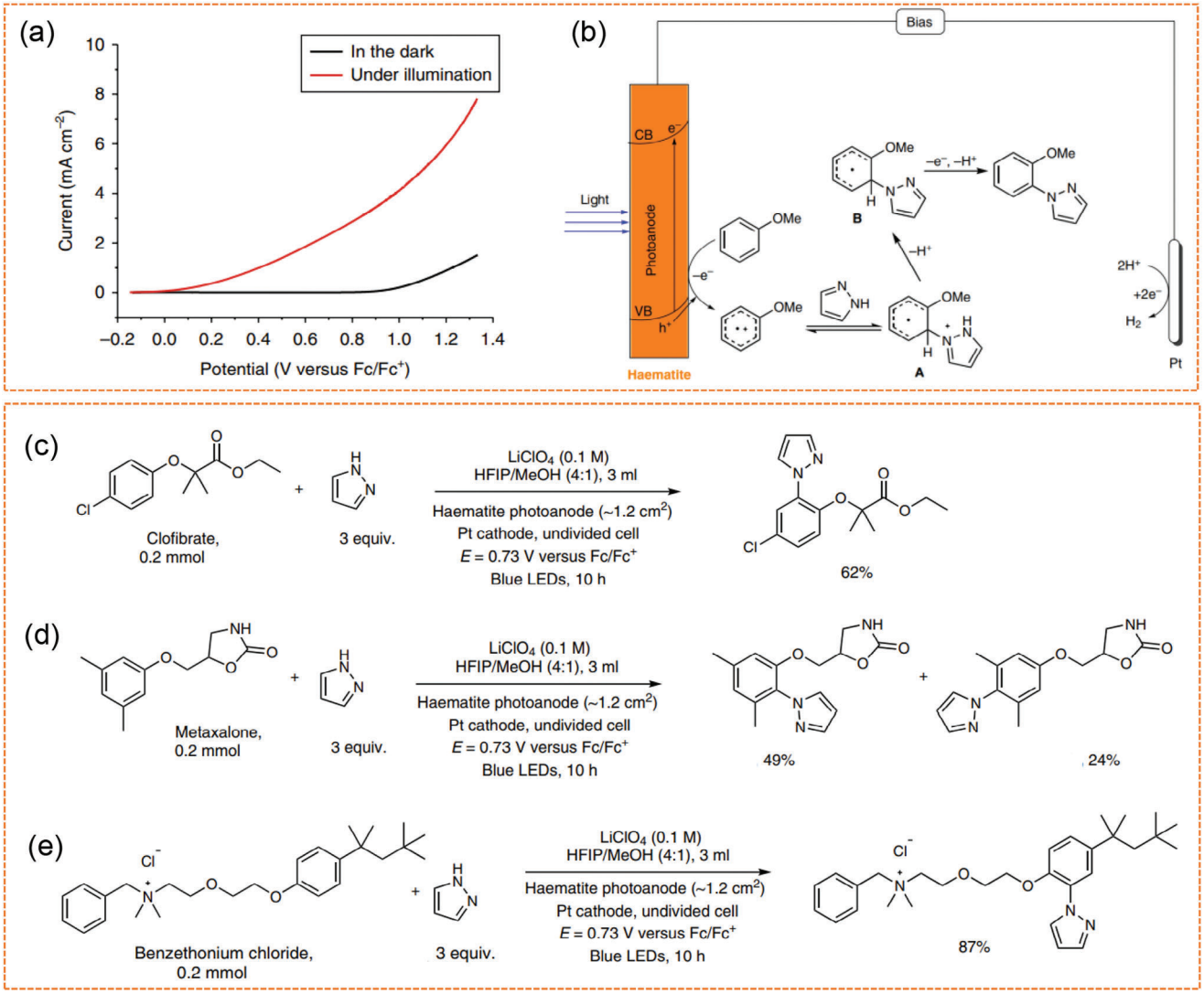

Figure 21. a) *J–V* profile for hematite photoelectrode under LED illumination (red) and in the dark (black). b) Proposed reaction mechanism depicting C—H bond functionalization. c–e) Late-stage functionalization of clofibrate, metaxalone, and benzethonium chloride. Reproduced with permission.[146] Copyright 2019, Springer Nature.

oxidize an electron-rich arene to a radical cation. This radical, which is electrophilic in nature, further reacts with an azole, giving rise to intermediate formation. Next, deprotonation of the as-obtained intermediate and its subsequent oxidation could lead to the resultant amination product (Figure 21b). Interestingly, the authors demonstrated the potential of this process to derive the late-stage functionalization of various pharmaceuticals, including clofibrate, metaxalone, benzethonium chloride, with the product yield reaching 87% (Figure 21c–e). At the same time, the construction of C—P bond via dehydrogenation cross-coupling was reported by Wu et al.[147] The designed PEC system, which utilizes $BiVO_4$ photoanode, displayed good to excellent yield without the aid of metal catalyst and external oxidant. Moreover, this PEC system was compared with the electrocatalytic C—P bond construction system (which utilized glassy carbon anode), and has showed a greatly minimized external energy input by 90%.

More recently, Duan and co-workers have developed a strategy that utilizes oxygen-vacancy-rich TiO_2 photoanode (**Figure 22a**) to yield organic halides through PEC C–H halogenation catalysis.[148] By employing a series of experiments, the authors identified thermally treated TiO_2-Ov at 400 °C as the best photoelectrode to catalyze the efficient synthesis of organic halides (Figure 22b). The authors noted that the photogenerated holes obtained upon irradiation of the photoanode could directly oxidize the halide ions (NaX, where X = Cl^-, Br^-, I^-) to produce the corresponding radical or dihalides (X_2). Importantly, understanding the reaction mechanism was made possible after investigating the EPR spectrum of TiO_2-Ov at different times. After 5 min illumination, both chlorine and carbon center radical were observed. While the carbon-centered radicals remained after 20 min illumination, the chlorine radicals disappeared due to the quenching process after reacting with the C—H bond (Figure 22c). Interestingly, a practical PEC cell containing seawater, where

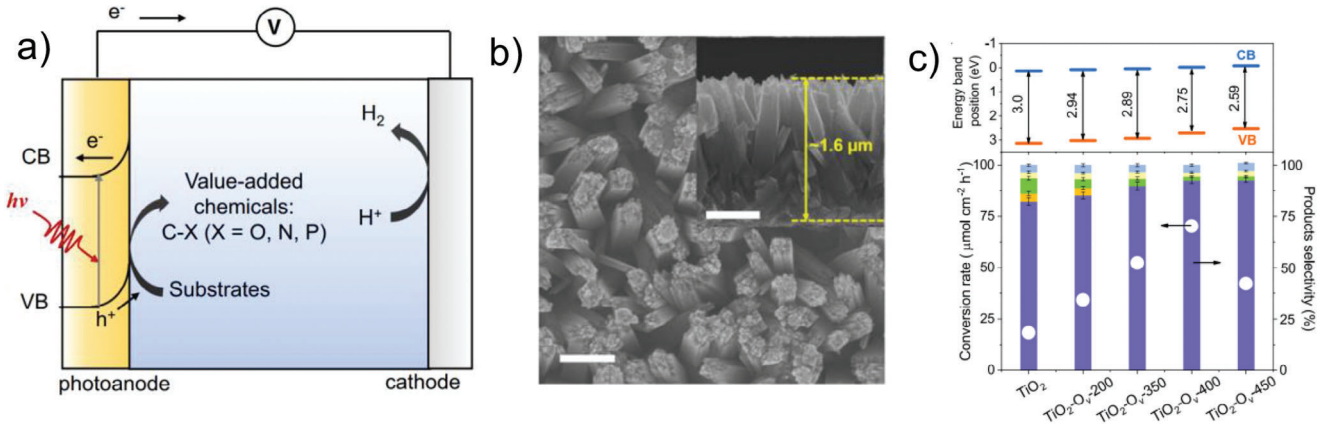

Figure 22. a) PEC C–H halogenation using sodium halide b) SEM images of TiO_2-Ov-400. The scale bar is 200 nm. c) PEC conversion rate and selectivity during C–H halogenation catalysis over TiO_2-Ov treated at different temperature. Reproduced with permission.[148] Copyright 2021, Springer Nature.

halogenation reaction coupled with H_2 could be realized in one pot, was tested and showed a nearly 64.5 μmol cm^{-2} h^{-1} production rate and selectivity of 88.6%. Another PEC C—H bond activation reaction was reported by Sayama and co-workers, where cyclohexanol and cyclohexanone (KA oil) were produced from cyclohexane.[149] In this PEC cell, which employed a porous WO_3 photoanode, the partial oxidation, selectivity, and current utilization ratio were near 99% and 76%, respectively. Moreover, the IPCE at 400 nm was 40% which indicated the potential advantage of this PEC system to produce KA oil from cyclohexane.

Apart from the conversion and activation of C—H bonds through photoelectrochemical technologies, there has recently been a great deal of interest in using light and electricity to derive the activation and functionalization of C—H bonds in a slightly different way. In the process named electrophotocatalysis, the concept of homogeneous photocatalysis is integrated with electrochemistry to bring an intriguing reactivity. It should be noted that the concept employed in electrophotocatalysis is different from photoelectrocatalysis. For a general understanding of this process, we suggest the readers to refer some reviews communicated earlier.[150]

In summary, although at its early stage of infancy, PEC catalysis has been acknowledged to derive several kinds of organic transformations. PEC processes involving the oxidation, reduction, bond activation, and functionalization of various feedstocks (organic and inorganic), such as furan-based feedstocks, waste glycerol, benzyl alcohol, and other readily available precursors (oxygen, nitrogen, water, and nitrate) to high-valued chemicals are discussed in this section. Until recently, the photoelectrode materials that have frequently been used for the oxidation of organic feedstocks are $BiVO_4$, TiO_2, WO_3, and Fe_2O_3. These electrodes always suffer from corrosion when the reaction is carried out in an alkaline aqueous electrolyte. Hence, electrode passivation strategies, incorporation of metal and non-metals in their crystal structure, and heterointerface formation would partly alleviate their potential limitations. Another compelling aspect is the consideration of electrolytes (organic vs aqueous) in the PEC system. Organic electrolytes have been used in PEC reactions for some particular reasons. For instance, they play a critical role in minimizing or even eliminating the competitive HER (in the case of reduction) and OER (in the case of oxidation) processes. Apart from this, an aqueous medium induces high rates of photocorrosion and hence deteriorates the stability of the photoelectrodes.[20] In fact, there are attempts to suppress this photocorrossion by using protective layers such as CoO_x,[151] NiO_x,[152] and FeO_x.[153] However, these layers compromise the rate of oxidation of the organic compound, favoring competitive OER. Overall, the research works described so far focus on unoptimized setups and reaction parameters, which further require future research attention. It appears that the design of flow-based reactors is rarely investigated in PEC organic transformations. Hence, by taking a lesson from the CO_2 PEC catalysis, further studies that focus on the design, cell configuration, and reaction parameter optimization are still required.

5. Conclusion and Future Outlook

Solar-light-driven PEC catalysis for valuable chemical synthesis from various organic and inorganic feedstocks has attracted enormous research endeavors due to its potential to store renewable resources in the form of a chemical bond. In the context of valuable product synthesis, the development of an efficient PEC system relies on several interlinked factors such as electrode preparation, the configuration of the photoelectrodes, the nature and pH of the electrolyte, the stability of photoelectrodes, etc. Moreover, a careful selection of an efficient photoelectrode material, electrode preparation method, and efficiency metrics are detrimental to revolutionizing the development of PEC technology and make the overall PEC system economically competitive. In this review, we have highlighted the emergence of PEC technology as an elegant platform for achieving an efficient chemical transformation under mild experimental conditions.

In general, the PEC oxidation of various feedstocks such as glycerol, HMF, furfural, benzyl alcohol, and lignin-based precursors to valuable oxygenates has been extensively investigated. Studies on the oxidation of biomass-based precursors to value-added aromatics have demonstrated the potential of the PEC tool to efficiently utilize naturally available precursors without posing a huge environmental burden to the globe. Moreover, one or more valuable product has been achieved through PEC

catalysis of various organic feedstocks. For instance, a valuable organic product such as FDCA and DFF could be achieved through the PEC oxidation of HMF. The anodic oxidation of organic precursors has a dual advantage. On the one hand, if a PEC system employing an efficient transformation of organics can be realized, it would be an appealing platform to supplement the energy-intensive thermochemical processes that are widely applied in chemical manufacturing industries. On the other hand, organic oxidation reactions at the anode could be regarded as an alternative reaction to replace the sluggish and industrially less important OER.

Furthermore, cathodic reactions that employ the PEC catalysis are still in progress. The NRR and ORR have shown astounding development, but the performances reported for these two reactions are still far from large-scale practical applications. Particularly, the NRR via PEC catalysis to synthesize NH_3 appears to be challenging due to the inertness of N_2 and its solubility in water. Hence, as an alternative to N_2, nitrate (NO_3^-) and nitrite (NO_2^-) precursors could be tested and optimized via employing PEC catalysis.

To provoke future development in PEC catalysis, we propose the following issues to be considered in the forthcoming research directions. i) Developing an efficient photoelectrode. The type of photoelectrode and its method of preparation not only affect the performance of a PEC system but also determine the overall cost of the process. Until now, only a few photoelectrodes such as $BiVO_4$, Ta_3N_5, WO_3, TiO_2, and Cu_2ZnSnS_4 have been commonly used to derive a number of reactions in their pristine form as well as with other configurations including heterostructures and doped variants. Most of them usually require additional electrode processing procedures to enhance their stability and efficiency. Hence, designing an efficient and stable photoelectrode capable of catalyzing the targeted reactions is still a central challenge that needs to be addressed. Besides, studies related to photoelectrode degradation mechanisms and related strategies for improving their stability are vital. ii) Understanding the reaction mechanism in depth. In this regard, the design of experiment platforms for the real-time analysis of intermediates and products could be helpful to properly assess the reaction path of a particular reaction. Meanwhile, in situ characterization techniques such as X-ray absorption techniques, attenuated-total-reflection, Fourier transform infrared spectroscopy, and dynamic transmission electron microscopy, should also be developed. iii) Novel approaches for an integrated PEC system. In PEC catalysis, an innovative integrated system has been designed to derive some special reactions. In this system, a photoanode can be coupled with an electrode and biocatalytic system to achieve a transformative valuable chemical synthesis. For example, an integrated PEC cell consisting of photoelectrocatalyst, electrocatalysts, and biocatalysts in a three-compartmented system demonstrated efficient biomass valorization. Moreover, recent work has demonstrated the successful integration of a photoelectrocatalyst, electrocatalyst, and photocatalyst systems which efficiently catalyzed propylene epoxidation via an in situ generated H_2O_2. Such kinds of systems with novel reaction routes and PEC cell design could be further developed and optimized. iv) Scope of anodic and cathodic reactions. Taking a lesson from some successful electrochemical synthesis of organics,[154] numerous organic reactions can be tested and optimized. Moreover, only a few cathodic reactions have been frequently investigated, and the scope of the reduction half-reaction beyond water can be taken into account.

PEC catalysis often combines two separate limitations of electrocatalysis (ohmic drop) and photocatalysis (light attenuation), which demand a careful design of PEC cells. Designing a PEC flow reactor should consider several issues, including uniformity of light illumination, mechanism of dissipating the heat generated throughout the reaction, and a separator (usually proton or anion exchange membranes).[10a] Notable examples of PEC CO_2 reduction reactions show that the use of flow-based reactors has great promise for improving overall energy utilization efficiency. For instance, a flow-based PEC cell that utilized silicon PV was able to produce syngas (H_2 + CO) without applying external bias.[155] In recent work by Gong et al. a PEC flow cell that efficiently catalyzes CO_2 reduction reaction to C_{2+} on Cu catalyst is demonstrated, and the cell achieved a FE and STF of nearly 53% and 0.29%, respectively.[24] Driving lessons from the aforementioned works, a PEC cell that integrates electrochemical reduction of some readily available feedstocks with photoelectrochemical oxidation of water could be designed and optimized at high current densities. Meanwhile, integrated research on specific areas of flow chemistry and chemical engineering is urgently required to facilitate the future development of a PEC flow cell device. As such, the utilization of microreactors could lead to the controlled optimization of various parameters, further facilitating its rapid development.

In summary, though at the stage of infancy, employing PEC catalysis for valuable product synthesis could offer a promising avenue to store solar light in the form of chemical bonds. Despite the significant progress seen over the last few years, a number of challenges are still awaiting before applying this tool to real practical application. Along with the development of an efficient PEC system to achieve high efficiency, a techno-economical evaluation of this tool is still required. Finally, it is anticipated that more effort from the diverse field including material science and engineering, theoretical chemistry, and organic chemistry, will be put into action to facilitate the development of PEC tools in the future.

Acknowledgements

M.G.S., F.T.D., B.W., and F.W. acknowledge the support from the National Natural Science Foundation of China (No. 22179029), Fundamental Research Funds for the Central Universities (buctrc202324), and the Young Elite Scientists Sponsorship Program by BAST (BYESS2023093). F.W., M.G.S., and F.T.D. also gratefully acknowledge the support of Youth Innovation Promotion Association CAS and the CAS-TWAS president's fellowship. T.A.S. acknowledge the MSCA Fellowship. A.V. acknowledges the Kempe Foundation, the Knut & Alice Wallenberg Foundation, and the Ca' Foscari University of Venice (SPIN project) for financial support. A.V. also acknowledges the National Recovery and Resilience Plan (NRRP), Mission 4 Component 2 Investment 1.3, Project NEST. K.B.I. acknowledges the PNRR RTD A.

Conflict of Interest

The authors declare no conflict of interest.

Keywords

photoelectrochemical catalysis, photoelectrode fabrication, value-added chemicals

Received: August 10, 2023
Revised: January 19, 2024
Published online:

[1] X. Wu, N. Luo, S. Xie, H. Zhang, Q. Zhang, F. Wang, Y. Wang, *Chem. Soc. Rev.* **2020**, *49*, 6198.
[2] a) F. W. Lucas, R. G. Grim, S. A. Tacey, C. A. Downes, J. Hasse, A. M. Roman, C. A. Farberow, J. A. Schaidle, A. Holewinski, *ACS Energy Lett.* **2021**, *6*, 1205; b) S. Jin, *ACS Publications* **2018**, *3*, 2610.
[3] a) G. Dodekatos, S. Schünemann, H. Tüysüz, *ACS Catal.* **2018**, *8*, 6301; b) M.-Y. Qi, M. Conte, M. Anpo, Z.-R. Tang, Y.-J. Xu, *Chem. Rev.* **2021**, *121*, 13051.
[4] a) Z. Sun, G. Bottari, A. Afanasenko, M. C. Stuart, P. J. Deuss, B. Fridrich, K. Barta, *Nat. Catal.* **2018**, *1*, 82; b) Z. Zhang, J. Song, B. Han, *Chem. Rev.* **2017**, *117*, 6834; c) L. Song, R. Wang, L. Che, Y. Jiang, M. Zhou, Y. Zhao, J. Pang, M. Jiang, G. Zhou, M. Zheng, *ACS Catal.* **2021**, *11*, 11588; d) D. S. Achilleos, W. Yang, H. Kasap, A. Savateev, Y. Markushyna, J. R. Durrant, E. Reisner, *Angew. Chem., Int. Ed.* **2020**, *59*, 18184; e) D. W. Wakerley, M. F. Kuehnel, K. L. Orchard, K. H. Ly, T. E. Rosser, E. Reisner, *Nat. Energy* **2017**, *2*, 17021; f) J. Yu, F. Dappozze, J. Martín-Gomez, J. Hidalgo-Carrillo, A. Marinas, P. Vernoux, A. Caravaca, C. Guillard, *Appl. Catal., B* **2021**, *299*, 120616; g) X. Yu, E. C. Dos Santos, J. White, G. Salazar-Alvarez, L. G. Pettersson, A. Cornell, M. Johnsson, *Small* **2021**, *17*, 2104288; h) D. M. Morales, D. Jambrec, M. A. Kazakova, M. Braun, N. Sikdar, A. Koul, A. C. Brix, S. Seisel, C. Andronescu, W. Schuhmann, *ACS Catal.* **2022**, *12*, 982; i) Z. Zhang, G. W. Huber, *Chem. Soc. Rev.* **2018**, *47*, 1351; j) H. G. Cha, K.-S. Choi, *Nat. Chem.* **2015**, *7*, 328; k) X. Pang, H. Bai, H. Zhao, W. Fan, W. Shi, *ACS Catal.* **2022**, *12*, 1545; l) M. Park, M. Gu, B.-S. Kim, *ACS Nano* **2020**, *14*, 6812.
[5] a) M. Dong, J. Zhou, J. Zhong, H. T. Li, C. Y. Sun, Y. D. Han, J. N. Kou, Z. H. Kang, X. L. Wang, Z. M. Su, *Adv. Funct. Mater.* **2022**, *32*, 2110136; b) Y. Wang, S. Furukawa, S. Song, Q. He, H. Asakura, N. Yan, *Angew. Chem.* **2020**, *132*, 2309.
[6] A. Yazdani, G. G. Botte, *Curr. Opin. Chem. Eng.* **2020**, *29*, 89.
[7] G. G. Botte, *Electrochem. Soc. Interface* **2014**, *23*, 49.
[8] a) L. Xiong, J. Tang, *Adv. Energy Mater.* **2021**, *11*, 2003216; b) L. Marzo, S. K. Pagire, O. Reiser, B. König, *Angew. Chem., Int. Ed.* **2018**, *57*, 10034.
[9] G. Segev, J. W. Beeman, J. B. Greenblatt, I. D. Sharp, *Nat. Mater.* **2018**, *17*, 1115.
[10] a) L. Buglioni, F. Raymenants, A. Slattery, S. D. Zondag, T. Noël, *Chem. Rev.* **2021**, *122*, 2752; b) E. Kalamaras, M. M. Maroto-Valer, M. Shao, J. Xuan, H. Wang, *Catal. Today* **2018**, *317*, 56.
[11] P. Chatterjee, M. S. K. Ambati, A. K. Chakraborty, S. Chakrabortty, S. Biring, S. Ramakrishna, T. K. S. Wong, A. Kumar, R. Lawaniya, G. K. Dalapati, *Energy Convers. Manage.* **2022**, *261*, 115648.
[12] Z. Tian, Y. Da, M. Wang, X. Dou, X. Cui, J. Chen, R. Jiang, S. Xi, B. Cui, Y. Luo, *Nat. Commun.* **2023**, *14*, 142.
[13] a) Q. Shi, H. Duan, *Chem. Catal.* **2022**, *2*, 3471; b) Y. Zhao, Z. Niu, J. Zhao, L. Xue, X. Fu, J. Long, *Electrochem. Energy Rev.* **2023**, *6*, 14; c) Y. Miao, M. Shao, *Chin. J. Catal.* **2022**, *43*, 595.
[14] a) B. Liu, S. Wang, G. Zhang, Z. Gong, B. Wu, T. Wang, J. Gong, *Chem. Soc. Rev.* **2023**, *52*, 4644; b) M. Kumar, B. Meena, P. Subramanyam, D. Suryakala, C. Subrahmanyam, *NPG Asia Mater.* **2022**, *14*, 88.
[15] a) D. Li, K. Yang, J. Lian, J. Yan, S. Liu, *Adv. Energy Mater.* **2022**, *12*, 2201070; b) N. Nandal, S. L. Jain, *Coord. Chem. Rev.* **2022**, *451*, 214271; c) L. K. Putri, B. J. Ng, W. J. Ong, S. P. Chai, A. R. Mohamed, *Adv. Energy Mater.* **2022**, *12*, 2201093; d) W. Zhang, Z. Jin, Z. Chen, *Adv. Sci.* **2022**, *9*, 2105204; e) B. Tang, F.-X. Xiao, *ACS Catal.* **2022**, *12*, 9023; f) E. Zhao, K. Du, P. F. Yin, J. Ran, J. Mao, T. Ling, S. Z. Qiao, *Adv. Sci.* **2022**, *9*, 2104363.
[16] a) D. Zhu, L. Zhang, R. E. Ruther, R. J. Hamers, *Nat. Mater.* **2013**, *12*, 836; b) H. Lu, J. Zhao, L. Li, L. Gong, J. Zheng, L. Zhang, Z. Wang, J. Zhang, Z. Zhu, *Energy Environ. Sci.* **2011**, *4*, 3384; c) M. Zhang, C. Chen, W. Ma, J. Zhao, *Angew. Chem., Int. Ed.* **2008**, *47*, 9730.
[17] a) X. Liu, Z. Chen, S. Xu, G. Liu, Y. Zhu, X. Yu, L. Sun, F. Li, *J. Am. Chem. Soc.* **2022**, *144*, 19770; b) D. Tang, K. Dang, J. Wang, C. Chen, J. Zhao, Y. Zhang, *Sci. China: Chem.* **2023**, *66*, 3415.
[18] H. Tateno, Y. Miseki, K. Sayama, *Chem. Commun.* **2017**, *53*, 4378.
[19] B. D. Terry, J. L. DiMeglio, J. P. Cousineau, B. M. Bartlett, *ChemElectroChem* **2020**, *7*, 3776.
[20] T. Li, T. Kasahara, J. He, K. E. Dettelbach, G. M. Sammis, C. P. Berlinguette, *Nat. Commun.* **2017**, *8*, 390.
[21] W. Shao, B. Lu, J. Cao, J. Zhang, H. Cao, F. Zhang, C. Zhang, *Chem. - Asian J.* **2023**, *18*, e202201093.
[22] a) D. Bae, T. Pedersen, B. Seger, M. Malizia, A. Kuznetsov, O. Hansen, I. Chorkendorff, P. C. Vesborg, *Energy Environ. Sci.* **2015**, *8*, 650; b) Z. Lin, J. Hu, B. Zhang, L. Wu, J. Wang, *Appl. Catal., A* **2023**, *652*, 119024.
[23] R. Mazzaro, S. B. Bibi, M. Natali, G. Bergamini, V. Morandi, P. Ceroni, A. Vomiero, *Nano Energy* **2019**, *61*, 36.
[24] B. Liu, T. Wang, S. Wang, G. Zhang, D. Zhong, T. Yuan, H. Dong, B. Wu, J. Gong, *Nat. Commun.* **2022**, *13*, 7111.
[25] S. Giménez, J. Bisquert, *From Basic Principle to Advanced Devices*, Springer, Cham, Switzerland **2016**.
[26] R. A. Pala, A. J. Leenheer, M. Lichterman, H. A. Atwater, N. S. Lewis, *Energy Environ. Sci.* **2014**, *7*, 3424.
[27] Z. Chen, T. F. Jaramillo, T. G. Deutsch, A. Kleiman-Shwarsctein, A. J. Forman, N. Gaillard, R. Garland, K. Takanabe, C. Heske, M. Sunkara, *J. Mater. Res.* **2010**, *25*, 3.
[28] K. Sivula, R. Van De Krol, *Nat. Rev. Mater.* **2016**, *1*, 15010.
[29] a) P. Hauke, T. Merzdorf, M. Klingenhof, P. Strasser, *Nat. Commun.* **2023**, *14*, 4708; b) F. Ye, S. Zhang, Q. Cheng, Y. Long, D. Liu, R. Paul, Y. Fang, Y. Su, L. Qu, L. Dai, *Nat. Commun.* **2023**, *14*, 2040; c) X. Zhang, H. Su, P. Cui, Y. Cao, Z. Teng, Q. Zhang, Y. Wang, Y. Feng, R. Feng, J. Hou, *Nat. Commun.* **2023**, *14*, 7115; d) M. Yan, Z. Wei, Z. Gong, B. Johannessen, G. Ye, G. He, J. Liu, S. Zhao, C. Cui, H. Fei, *Nat. Commun.* **2023**, *14*, 368; e) K. Fan, W. Xie, J. Li, Y. Sun, P. Xu, Y. Tang, Z. Li, M. Shao, *Nat. Commun.* **2022**, *13*, 7958; f) Z.-Y. Wu, M. Karamad, X. Yong, Q. Huang, D. A. Cullen, P. Zhu, C. Xia, Q. Xiao, M. Shakouri, F.-Y. Chen, *Nat. Commun.* **2021**, *12*, 2870.
[30] D. Liu, J.-C. Liu, W. Cai, J. Ma, H. B. Yang, H. Xiao, J. Li, Y. Xiong, Y. Huang, B. Liu, *Nat. Commun.* **2019**, *10*, 1779.
[31] D. K. Bora, M. Nadjafi, A. Armutlulu, D. Hosseini, P. Castro-Fernández, R. Toth, *Energy Adv.* **2022**, *1*, 715.
[32] a) C. Li, T. Wang, Z. J. Zhao, W. Yang, J. F. Li, A. Li, Z. Yang, G. A. Ozin, J. Gong, *Angew. Chem., Int. Ed.* **2018**, *57*, 5278; b) M. A. Mushtaq, M. Arif, X. Fang, G. Yasin, W. Ye, M. Basharat, B. Zhou, S. Yang, S. Ji, D. Yan, *J. Mater. Chem. A* **2021**, *9*, 2742.
[33] T. H. Jeon, B. Kim, C. Kim, C. Xia, H. Wang, P. J. Alvarez, W. Choi, *Energy Environ. Sci.* **2021**, *14*, 3110.
[34] a) Y. Song, Y. Wu, S. Cao, Y. Zhang, D. Luo, J. Gao, Z. Li, L. Sun, J. Hou, *Adv. Energy Mater.* **2022**, *12*, 2201782; b) X. M. C. Ta, R. Daiyan, T. K. A. Nguyen, R. Amal, T. Tran-Phu, A. Tricoli, *Adv. Energy Mater.* **2022**, *12*, 2201358.
[35] J. J. Roylance, T. W. Kim, K.-S. Choi, *ACS Catal.* **2016**, *6*, 1840.
[36] J. Ma, K. Mao, J. Low, Z. Wang, D. Xi, W. Zhang, H. Ju, Z. Qi, R. Long, X. Wu, *Angew. Chem.* **2021**, *133*, 9443.
[37] C. Acar, I. Dincer, *Int. J. Hydrogen Energy* **2016**, *41*, 7950.
[38] a) M. G. Sendeku, F. Wang, Z. Cheng, P. Yu, N. Gao, X. Zhan, Z. Wang, J. He, *ACS Appl. Mater. Interfaces* **2021**, *13*, 13392; b) W. Gao, C. Ran, J. Xi, B. Jiao, W. Zhang, M. Wu, X. Hou, Z. Wu, *ChemPhysChem* **2018**, *19*, 1696.

[39] C. Zuo, A. D. Scully, M. Gao, *ACS Appl. Mater. Interfaces* **2021**, *13*, 56217.
[40] D. Liu, J. Wang, S. Bian, Q. Liu, Y. Gao, X. Wang, P. K. Chu, X. F. Yu, *Adv. Funct. Mater.* **2020**, *30*, 2002731.
[41] J. Xia, N. Karjule, L. Abisdris, M. Volokh, M. Shalom, *Chem. Mater.* **2020**, *32*, 5845.
[42] a) N. Karjule, J. Barrio, L. Xing, M. Volokh, M. Shalom, *Nano Lett.* **2020**, *20*, 4618; b) M. Volokh, G. Peng, J. Barrio, M. Shalom, *Angew. Chem., Int. Ed.* **2019**, *58*, 6138.
[43] a) J. Y. Zheng, G. Song, J. Hong, T. K. Van, A. U. Pawar, D. Y. Kim, C. W. Kim, Z. Haider, Y. S. Kang, *Cryst. Growth Des.* **2014**, *14*, 6057; b) J. Y. Zheng, G. Song, C. W. Kim, Y. S. Kang, *Nanoscale* **2013**, *5*, 5279.
[44] J. S. Lee, J. H. Kim, Y. J. Lee, N. C. Jeong, K. B. Yoon, *Angew. Chem., Int. Ed.* **2007**, *46*, 3087.
[45] T. Minegishi, N. Nishimura, J. Kubota, K. Domen, *Chem. Sci.* **2013**, *4*, 1120.
[46] Z. Sun, T. Liao, W. Li, Y. Qiao, K. Ostrikov, *Adv. Funct. Mater.* **2019**, *29*, 1901460.
[47] H. Chen, H. K. Mulmudi, A. Tricoli, *Chin. Chem. Lett.* **2020**, *31*, 601.
[48] F. Wang, A. Chemseddine, F. F. Abdi, R. van de Krol, S. P. Berglund, *J. Mater. Chem. A* **2017**, *5*, 12838.
[49] J. A. Seabold, K.-S. Choi, *J. Am. Chem. Soc.* **2012**, *134*, 2186.
[50] Y. Park, D. Kang, K.-S. Choi, *Phys. Chem. Chem. Phys.* **2014**, *16*, 1238.
[51] D. Kang, T. W. Kim, S. R. Kubota, A. C. Cardiel, H. G. Cha, K.-S. Choi, *Chem. Rev.* **2015**, *115*, 12839.
[52] C. Feng, F. Wang, Z. Liu, M. Nakabayashi, Y. Xiao, Q. Zeng, J. Fu, Q. Wu, C. Cui, Y. Han, *Nat. Commun.* **2021**, *12*, 5980.
[53] S. H. Gebre, M. G. Sendeku, *J. Energy Chem.* **2022**, *65*, 329.
[54] B. Chaudhary, Y. K. Kshetri, D. R. Dhakal, S. W. Lee, T.-H. Kim, *Prog. Nat. Sci.: Mater. Int.* **2022**, *32*, 594.
[55] a) G. Wang, H. Wang, Y. Ling, Y. Tang, X. Yang, R. C. Fitzmorris, C. Wang, J. Z. Zhang, Y. Li, *Nano Lett.* **2011**, *11*, 3026; b) Z. Bai, X. Yan, Z. Kang, Y. Hu, X. Zhang, Y. Zhang, *Nano Energy* **2015**, *14*, 392; c) C. W. Kim, Y. S. Son, M. J. Kang, D. Y. Kim, Y. S. Kang, *Adv. Energy Mater.* **2016**, *6*, 1501754.
[56] W.-Q. Wu, B.-X. Lei, H.-S. Rao, Y.-F. Xu, Y.-F. Wang, C.-Y. Su, D.-B. Kuang, *Sci. Rep.* **2013**, *3*, 1352.
[57] J. Y. Kim, G. Magesh, D. H. Youn, J.-W. Jang, J. Kubota, K. Domen, J. S. Lee, *Sci. Rep.* **2013**, *3*, 2681.
[58] L. E. Greene, M. Law, D. H. Tan, M. Montano, J. Goldberger, G. Somorjai, P. Yang, *Nano Lett.* **2005**, *5*, 1231.
[59] Z. Jiao, J. Wang, L. Ke, X. W. Sun, H. V. Demir, *ACS Appl. Mater. Interfaces* **2011**, *3*, 229.
[60] B. Liu, E. S. Aydil, *J. Am. Chem. Soc.* **2009**, *131*, 3985.
[61] S. Feng, J. Yang, H. Zhu, M. Liu, J. Zhang, J. Wu, J. Wan, *J. Am. Ceram. Soc.* **2011**, *94*, 310.
[62] a) Y. Zhang, Y. Yao, M. G. Sendeku, L. Yin, X. Zhan, F. Wang, Z. Wang, J. He, *Adv. Mater.* **2019**, *31*, 1901694; b) M. Bahri, S. H. Gebre, M. A. Elaguech, F. T. Dajan, M. G. Sendeku, C. Tlili, D. Wang, *Coord. Chem. Rev.* **2023**, *475*, 214910.
[63] M. A. Ehsan, S. S. Shah, S. I. Basha, A. S. Hakeem, M. A. Aziz, *Chem. Rec.* **2022**, *22*, 202100278.
[64] S. Ariffin, H. Lim, Z. Talib, A. Pandikumar, N. Huang, *Int. J. Hydrogen Energy* **2015**, *40*, 2115.
[65] a) G. Liu, Z. Li, T. Hasan, X. Chen, W. Zheng, W. Feng, D. Jia, Y. Zhou, P. Hu, *J. Mater. Chem. A* **2017**, *5*, 1989; b) Y. Liu, C. Lu, M. Luo, T. Han, Y. Ge, W. Dong, X. Xue, Y. Zhou, X. Xu, *Nanoscale Horiz.* **2022**, *7*, 1217.
[66] J. Qin, J. Barrio, G. Peng, J. Tzadikov, L. Abisdris, M. Volokh, M. Shalom, *Nat. Commun.* **2020**, *11*, 4701.
[67] R. R. Katzbaer, M. J. Theibault, N. E. Kirchner-Hall, Z. Mao, I. Dabo, H. D. Abruña, R. E. Schaak, *Adv. Energy Mater.* **2022**, *12*, 2201869.
[68] a) G. H. Han, J. Bang, G. Park, S. Choe, Y. J. Jang, H. W. Jang, S. Y. Kim, S. H. Ahn, *Small* **2023**, *19*, 2205765; b) S. Verma, A. Yadav, *Energy Fuels* **2023**, *37*, 5712.
[69] A. D. da Silva Ruy, A. L. F. Ferreira, A. É. Bresciani, R. M. de Brito Alves, L. A. M. Pontes, **2020**, available at: https://doi.org/10.5772/intechopen.96935.
[70] H. Tateno, S.-Y. Chen, Y. Miseki, T. Nakajima, T. Mochizuki, K. Sayama, *ACS Sustainable Chem. Eng.* **2022**, *10*, 7586.
[71] R. Ciriminna, C. D. Pina, M. Rossi, M. Pagliaro, *Eur. J. Lipid Sci. Technol.* **2014**, *116*, 1432.
[72] L. Fan, Y. Ji, G. Wang, J. Chen, K. Chen, X. Liu, Z. Wen, *J. Am. Chem. Soc.* **2022**, *144*, 7224.
[73] J. Yu, J. González-Cobos, F. Dappozze, N. Grimaldos-Osorio, P. Vernoux, A. Caravaca, C. Guillard, *Appl. Catal., B* **2023**, *327*, 122465.
[74] J.-A. Lin, I. Roh, P. Yang, *J. Am. Chem. Soc.* **2023**, *145*, 12987.
[75] J. Ouyang, X. Liu, B.-H. Wang, J.-B. Pan, S. Shen, L. Chen, C.-T. Au, S.-F. Yin, *ACS Appl. Mater. Interfaces* **2022**, *14*, 23536.
[76] S. Çetinkaya, G. Khamidov, L. Özcan, L. Palmisano, S. Yurdakal, *J. Environ. Chem. Eng.* **2022**, *10*, 107210.
[77] a) Z. Gu, X. An, R. Liu, L. Xiong, J. Tang, C. Hu, H. Liu, J. Qu, *Appl. Catal., B* **2021**, *282*, 119541; b) Y. Lee, S. Kim, S. Y. Jeong, S. Seo, C. Kim, H. Yoon, H. W. Jang, S. Lee, *Catal. Today* **2021**, *359*, 43.
[78] a) Y.-H. Wu, D. A. Kuznetsov, N. C. Pflug, A. Fedorov, C. R. Müller, *J. Mater. Chem. A* **2021**, *9*, 6252; b) L. L. Nascimento, J. Z. Marinho, A. L. R. dos Santos, A. M. de Faria, R. A. Souza, C. Wang, A. O. T. Patrocinio, *Appl. Catal., A* **2022**, *646*, 118867.
[79] R. Tang, L. Wang, Z. Zhang, W. Yang, H. Xu, A. Kheradmand, Y. Jiang, R. Zheng, J. Huang, *Appl. Catal., B* **2021**, *296*, 120382.
[80] L. Luo, W. Chen, S.-M. Xu, J. Yang, M. Li, H. Zhou, M. Xu, M. Shao, X. Kong, Z. Li, *J. Am. Chem. Soc.* **2022**, *144*, 7720.
[81] a) F. J. Mancilla, S. F. Rojas, A. F. Gualdrón-Reyes, M. I. Carreño-Lizcano, L. J. Duarte, M. Niño-Gómez, *RSC Adv.* **2016**, *6*, 46668; b) Y. Miao, Z. Li, Y. Song, K. Fan, J. Guo, R. Li, M. Shao, *Appl. Catal., B* **2023**, *323*, 122147.
[82] T.-G. Vo, C.-C. Kao, J.-L. Kuo, C.-C. Chiu, C.-Y. Chiang, *Appl. Catal., B* **2020**, *278*, 119303.
[83] Y. Sun, G. Han, L. Du, C. Du, X. Zhou, Q. Sun, Y. Gao, G. Yin, Y. Li, Y. Wang, *Chem. Catal.* **2021**, *1*, 1260.
[84] Y. Liu, M. Wang, B. Zhang, D. Yan, X. Xiang, *ACS Catal.* **2022**, *12*, 6946.
[85] a) C. Xu, E. Paone, D. Rodríguez-Padrón, R. Luque, F. Mauriello, *Chem. Soc. Rev.* **2020**, *49*, 4273; b) H. Zhao, J. E. Holladay, H. Brown, Z. C. Zhang, *Science* **2007**, *316*, 1597; c) S. De, S. Dutta, B. Saha, *Green Chem.* **2011**, *13*, 2859.
[86] G. Marcì, E. García-López, F. Pomilla, L. Palmisano, A. Zaffora, M. Santamaria, I. Krivtsov, M. Ilkaeva, Z. Barbieriková, V. Brezová, *Catal. Today* **2019**, *328*, 21.
[87] D. J. Chadderdon, I. Wu, M. G. Panthani, W. Li, *Chemelectrochem* **2019**, *6*, 3387.
[88] C. R. Lhermitte, N. Plainpan, P. Canjura, F. Boudoire, K. Sivula, *RSC Adv.* **2021**, *11*, 198.
[89] Y. Kwon, K. J. P. Schouten, J. C. van der Waal, E. de Jong, M. T. Koper, *ACS Catal.* **2016**, *6*, 6704.
[90] X.-D. Wang, Y.-H. Huang, J.-F. Liao, Z.-F. Wei, W.-G. Li, Y.-F. Xu, H.-Y. Chen, D.-B. Kuang, *Nat. Commun.* **2021**, *12*, 1202.
[91] a) Z. Zhou, Y.-N. Xie, W. Zhu, H. Zhao, N. Yang, G. Zhao, *Appl. Catal., B* **2021**, *286*, 119868; b) W. Fang, D. Yan, R. Tao, Z. Sun, F. Li, L. Xu, *Dalton Trans.* **2020**, *49*, 10084; c) R. Zhang, M. Shao, Z. Li, F. Ning, M. Wei, D. G. Evans, X. Duan, *Chem. - Eur. J.* **2017**, *23*, 8142; d) D. Bruggeman, S. Mathew, R. Detz, J. Reek, *Sustainable Energy Fuels* **2021**, *5*, 5707.
[92] M. T. Bender, X. Yuan, K.-S. Choi, *Nat. Commun.* **2020**, *11*, 4594.
[93] C. Lin, Z. Shan, C. Dong, Y. Lu, W. Meng, G. Zhang, B. Cai, G. Su, J. H. Park, K. Zhang, *Sci. Adv.* **2023**, *9*, 9442.

[94] E. Nikoloudakis, P. B. Pati, G. Charalambidis, D. S. Budkina, S. Diring, A. Planchat, D. Jacquemin, E. Vauthey, A. G. Coutsolelos, F. Odobel, *ACS Catal.* **2021**, *11*, 12075.
[95] a) J. L. DiMeglio, A. G. Breuhaus-Alvarez, S. Li, B. M. Bartlett, *ACS Catal.* **2019**, *9*, 5732; b) J. L. DiMeglio, B. D. Terry, A. G. Breuhaus-Alvarez, M. J. Whalen, B. M. Bartlett, *J. Phys. Chem. C* **2021**, *125*, 8148.
[96] R. Arcas, E. Peris, E. Mas-Marzá, F. Fabregat-Santiago, *Sustainable Energy Fuels* **2021**, *5*, 956.
[97] a) A. Navaee, A. Salimi, *Electrochim. Acta* **2013**, *105*, 230; b) L. Jin, F. Cheng, H. Li, K. Xie, *Angew. Chem., Int. Ed.* **2020**, *59*, 8891; c) D. S. Choi, J. Kim, F. Hollmann, C. B. Park, *Angew. Chem.* **2020**, *132*, 16020; d) L. M. Reid, T. Li, Y. Cao, C. P. Berlinguette, *Sustainable Energy Fuels* **2018**, *2*, 1905; e) N. P. Martínez, M. Isaacs, K. K. Nanda, *New J. Chem.* **2020**, *44*, 5617; f) C. A. Mesa, A. Kafizas, L. Francàs, S. R. Pendlebury, E. Pastor, Y. Ma, F. L.e Formal, M. T. Mayer, M. Grätzel, J. R. Durrant, *J. Am. Chem. Soc.* **2017**, *139*, 11537; g) R. Wadhwa, K. K. Yadav, T. Goswami, Ankush, S. K. G., Sunaina, S. N., H. N. Ghosh, M. Jha, *ACS Appl. Mater. Interfaces* **2021**, *13*, 9942; h) S. Yurdakal, S. Çetinkaya, M. B. Şarlak, L. Özcan, V. Loddo, L. Palmisano, *Catal. Sci. Technol.* **2020**, *10*, 124; i) H. Shi, Y. Wang, C. Tang, W. Wang, M. Liu, G. Zhao, *Appl. Catal., B* **2019**, *246*, 50; j) H. He, J. Du, B. Wu, X. Duan, Y. Zhou, G. Ke, T. Huo, Q. Ren, L. Bian, F. Dong, *Green Chem.* **2018**, *20*, 3722.
[98] a) M. S. A. Sher Shah, C. Oh, H. Park, Y. J. Hwang, M. Ma, J. H. Park, *Adv. Sci.* **2020**, *7*, 2001946; b) J. Ding, R. Ran, J. Jia, D. Weng, Z. Yang, *Prog. Nat. Sci.: Mater. Int.* **2021**, *31*, 373.
[99] J. Zhang, H. Sun, *Solar-to-Chemical Conversion: Photocatalytic and Photoelectrochemcial Processes*, Wiley-VCH, Weinheim, Germany **2021**.
[100] W. Li, D. He, G. Hu, X. Li, G. Banerjee, J. Li, S. H. Lee, Q. Dong, T. Gao, G. W. Brudvig, *ACS Cent. Sci.* **2018**, *4*, 631.
[101] F. Amano, A. Shintani, K. Tsurui, H. Mukohara, T. Ohno, S. Takenaka, *ACS Energy Lett.* **2019**, *4*, 502.
[102] H. Tateno, Y. Miseki, K. Sayama, *Chem. Commun.* **2019**, *55*, 9339.
[103] J. King, S. S. Chuang, *Catal. Commun.* **2021**, *149*, 106219.
[104] S. Li, Z.-J. Li, H. Yu, M. R. Sytu, Y. Wang, D. Beeri, W. Zheng, B. D. Sherman, C. G. Yoo, G. Leem, *ACS Energy Lett.* **2019**, *5*, 777.
[105] D. Wang, S. H. Lee, S. Han, J. Kim, N. V. T. Trang, K. Kim, E.-G. Choi, P. Boonmongkolras, Y. W. Lee, B. Shin, *Green Chem.* **2020**, *22*, 5151.
[106] T. Travis, *Chem. Ind.* **1993**, *15*, 581.
[107] X. Han, S. Yang, M. Schröder, *J. Am. Chem. Soc.* **2023**, *145*, 1998.
[108] a) P. Li, Y. Liu, M. A. Mushtaq, D. Yan, *Inorg. Chem. Front.* **2023**, *10*, 4650; b) G. Bharath, C. Liu, F. Banat, A. Kumar, A. Hai, A. K. Nadda, V. K. Gupta, M. A. Haija, J. Balamurugan, *Chem. Eng. J.* **2023**, *465*, 143040; c) C. Guo, J. Ran, A. Vasileff, S.-Z. Qiao, *Energy Environ. Sci.* **2018**, *11*, 45.
[109] L. Shi, Y. Yin, S. Wang, H. Sun, *ACS Catal.* **2020**, *10*, 6870.
[110] a) S. Ajmal, A. Rasheed, N. Q. Tran, X. Shao, Y. Hwang, V. Q. Bui, Y. D. Kim, J. Kim, H. Lee, *Appl. Catal., B* **2023**, *321*, 122070; b) Y. Mao, H. Zhang, W. Jiang, R. Zhao, Y. Liu, Z. Wang, P. Wang, Z. Zheng, K. Song, W. Wei, *Nano Energy* **2022**, *102*, 107639.
[111] a) Y. Jia, J. Gao, Z. Xiao, Z. Tian, Y. Xia, C. Wang, *ACS Appl. Mater. Interfaces* **2023**, *15*, 26111; b) S. Lin, J.-B. Ma, J.-J. Fu, L. Sun, H. Zhang, J. Cheng, J.-F. Li, *J. Phys. Chem. C* **2023**, *127*, 1345; c) S. F. Blaskievicz, I. Freitas Teixeira, L. H. Mascaro, J. Ferreira de Brito, *ChemCatChem* **2023**, *15*, 202201610; d) W. Ye, M. Arif, X. Fang, M. A. Mushtaq, X. Chen, D. Yan, *ACS Appl. Mater. Interfaces* **2019**, *11*, 28809.
[112] M. Ali, F. Zhou, K. Chen, C. Kotzur, C. Xiao, L. Bourgeois, X. Zhang, D. R. MacFarlane, *Nat. Commun.* **2016**, *7*, 11335.
[113] B. Wang, L. Yao, G. Xu, X. Zhang, D. Wang, X. Shu, J. Lv, Y.-C. Wu, *ACS Appl. Mater. Interfaces* **2020**, *12*, 20376.
[114] D. Sun, H. Bai, Y. Zhao, Q. Zhang, Y. Bai, Y. Liu, X. Pang, F. Wang, J. Ding, D. Xu, *ACS Appl. Mater. Interfaces* **2020**, *12*, 52763.
[115] C. Sun, Z. Shao, Y. Hu, Y. Peng, Q. Xie, *ACS Appl. Mater. Interfaces* **2023**, *15*, 23085.
[116] T. Oshikiri, K. Ueno, H. Misawa, *Angew. Chem., Int. Ed.* **2016**, *55*, 3942.
[117] C. H. Kim, J. Kim, F. Hollmann, C. B. Park, *Appl. Catal., B* **2023**, 122925.
[118] J. Zheng, Y. Lyu, M. Qiao, R. Wang, Y. Zhou, H. Li, C. Chen, Y. Li, H. Zhou, S. Wang, *Chem* **2019**, *5*, 617.
[119] F. Xu, F. Wu, K. Zhu, Z. Fang, D. Jia, Y. Wang, G. Jia, J. Low, W. Ye, Z. Sun, *Appl. Catal., B* **2021**, *284*, 119689.
[120] a) Y. Zhang, Y. Wang, L. Han, S. Wang, T. Cui, Y. Yan, M. Xu, H. Duan, Y. Kuang, X. Sun, *Angew. Chem., Int. Ed.* **2023**, *62*, 202213711; b) Y. Xiong, Y. Wang, J. Zhou, F. Liu, F. Hao, Z. Fan, *Adv. Mater. 35*, 2304021; c) Y. Wang, A. Xu, Z. Wang, L. Huang, J. Li, F. Li, J. Wicks, M. Luo, D.-H. Nam, C.-S. Tan, *J. Am. Chem. Soc.* **2020**, *142*, 5702.
[121] S. Zhou, K. Sun, C. Y. Toe, J. Yin, J. Huang, Y. Zeng, D. Zhang, W. Chen, O. F. Mohammed, X. Hao, *Adv. Mater.* **2022**, *34*, 2201670.
[122] H. E. Kim, J. Kim, E. C. Ra, H. Zhang, Y. J. Jang, J. S. Lee, *Angew. Chem.* **2022**, *134*, 202204117.
[123] a) Y. Liu, J. Lu, Q. Zhang, Y. Bai, X. Pang, S. Wang, H. Bai, W. Fan, *Chem. Commun.* **2021**, *57*, 8031; b) H. Bai, F. Wang, Q. Ding, W. Xie, H. Li, G. Zheng, W. Fan, *Inorg. Chem.* **2023**, *62*, 2394; c) X. Li, W. Fan, Y. Bai, Y. Liu, F. Wang, H. Bai, W. Shi, *Chem. Eng. J.* **2022**, *433*, 133225.
[124] C.-H. Chiang, Y.-T. Kao, P.-H. Wu, T.-R. Liu, J.-W. Lin, P.-T. Chen, J.-W. Lin, S.-C. Yang, H.-L. Chen, S. B. Patil, *J. Mater. Chem. A* **2023**, *11*, 11179.
[125] V. R. Silveira, R. Bericat-Vadell, J. Sá, *J. Phys. Chem. C* **2023**, *127*, 5425.
[126] J. H. Kim, D. Hansora, P. Sharma, J.-W. Jang, J. S. Lee, *Chem. Soc. Rev.* **2019**, *48*, 1908.
[127] a) K. Zhang, J. Liu, L. Wang, B. Jin, X. Yang, S. Zhang, J. H. Park, *J. Am. Chem. Soc.* **2020**, *142*, 8641; b) X. Shi, S. Siahrostami, G.-L. Li, Y. Zhang, P. Chakthranont, F. Studt, T. F. Jaramillo, X. Zheng, J. K. Nørskov, *Nat. Commun.* **2017**, *8*, 701.
[128] B. Zhang, L. He, T. Yao, W. Fan, X. Zhang, S. Wen, J. Shi, C. Li, *ChemSusChem* **2019**, *12*, 1026.
[129] X. Shi, Y. Zhang, S. Siahrostami, X. Zheng, *Adv. Energy Mater.* **2018**, *8*, 1801158.
[130] W. Fan, B. Zhang, X. Wang, W. Ma, D. Li, Z. Wang, M. Dupuis, J. Shi, S. Liao, C. Li, *Energy Environ. Sci.* **2020**, *13*, 238.
[131] Z. Li, Q. Xu, F. Gou, B. He, W. Chen, W. Zheng, X. Jiang, K. Chen, C. Qi, D. Ma, *Nano Res.* **2021**, *14*, 3439.
[132] R. Mehrotra, D. Oh, J.-W. Jang, *Nat. Commun.* **2021**, *12*, 6644.
[133] a) W. Chen, S. Liu, Y. Fu, H. Yan, L. Qin, C. Lai, C. Zhang, H. Ye, W. Chen, F. Qin, *Coord. Chem. Rev.* **2022**, *454*, 214341; b) W. Leng, W. Zhu, J. Ni, Z. Zhang, J. Zhang, C. Cao, *Appl. Catal., A* **2006**, *300*, 24; c) T. H. Jeon, M. S. Koo, H. Kim, W. Choi, *ACS Catal.* **2018**, *8*, 11542.
[134] F. Ye, T. Wang, X. Quan, H. Yu, S. Chen, *Chem. Eng. J.* **2020**, *389*, 123427.
[135] M. Ko, L. T. M. Pham, Y. J. Sa, J. Woo, T. V. T. Nguyen, J. H. Kim, D. Oh, P. Sharma, J. Ryu, T. J. Shin, *Nat. Commun.* **2019**, *10*, 5123.
[136] M. Ko, Y. Kim, J. Woo, B. Lee, R. Mehrotra, P. Sharma, J. Kim, S. W. Hwang, H. Y. Jeong, H. Lim, *Nat. Catal.* **2022**, *5*, 37.
[137] M. A. Andrade Jr., L. H. Mascaro, *Chemosphere* **2018**, *212*, 79.
[138] S. Kamimura, Y. Kubo, T. Tsubota, T. Ohno, *Appl. Catal., B* **2018**, *225*, 445.
[139] L. Guillemard, N. Kaplaneris, L. Ackermann, M. J. Johansson, *Nat. Rev. Chem.* **2021**, *5*, 522.
[140] R. G. Bergman, *Nature* **2007**, *446*, 391.
[141] a) Á. Velasco-Rubio, P. Martínez-Balart, A. M. M. Á. Constantino, M. Fañanás-Mastral, *Chem. Commun.* **2023**, *59*, 9424; b) F. Li, B. Wang,

X. Chen, W. Zeng, R. Sun, X. Liu, Z. Ren, X. Yang, H. Fan, Q. Guo, *J. Phys. Chem. C* **2022**, *126*, 11963; c) S. Cao, W. Hong, Z. Ye, L. Gong, *Nat. Commun.* **2021**, *12*, 2377; d) M.-J. Luo, Q. Xiao, J.-H. Li, *Chem. Soc. Rev.* **2022**, *51*, 7206; e) P. Bellotti, H.-M. Huang, T. Faber, F. Glorius, *Chem. Rev.* **2023**, *123*, 4237.

[142] a) P. K. Baroliya, M. Dhaker, S. Panja, S. A. Al-Thabaiti, S. M. Albukhari, Q. A. Alsulami, A. Dutta, D. Maiti, *ChemSusChem* **2023**, *16*, 202202201; b) L. F. Novaes, J. Liu, Y. Shen, L. Lu, J. M. Meinhardt, S. Lin, *Chem. Soc. Rev.* **2021**, *50*, 7941.

[143] a) K. Sun, F. Xiao, B. Yu, W.-M. He, *Chin. J. Catal.* **2021**, *42*, 1921; b) D. Shrestha, K. Dhakal, T. Pokhrel, A. Adhikari, T. Hardwick, B. Shirinfar, N. Ahmed, *Solar Fuels*, **2023**, pp. 185–203; c) S. Li, K. Huang, Z. Tang, J. Wang, *J. Mater. Chem. A* **2023**, *11*, 3281.

[144] a) T. Shen, T. H. Lambert, *Science* **2021**, *371*, 620; b) H. Huang, K. A. Steiniger, T. H. Lambert, *J. Am. Chem. Soc.* **2022**, *144*, 12567; c) H. Huang, T. H. Lambert, *Angew. Chem., Int. Ed.* **2021**, *60*, 11163.

[145] a) F. W. Friese, C. Mück-Lichtenfeld, A. Studer, *Nat. Commun.* **2018**, *9*, 2808; b) G. J. Choi, Q. Zhu, D. C. Miller, C. J. Gu, R. R. Knowles, *Nature* **2016**, *539*, 268.

[146] L. Zhang, L. Liardet, J. Luo, D. Ren, M. Grätzel, X. Hu, *Nat. Catal.* **2019**, *2*, 366.

[147] J.-H. Wang, X.-B. Li, J. Li, T. Lei, H.-L. Wu, X.-L. Nan, C.-H. Tung, L.-Z. Wu, *Chem. Commun.* **2019**, *55*, 10376.

[148] Z. Li, L. Luo, M. Li, W. Chen, Y. Liu, J. Yang, S.-M. Xu, H. Zhou, L. Ma, M. Xu, X. Kong, H. Duan, *Nat. Commun.* **2021**, *12*, 6698.

[149] H. Tateno, S. Iguchi, Y. Miseki, K. Sayama, *Angew. Chem.* **2018**, *130*, 11408.

[150] J. Liu, L. Lu, D. Wood, S. Lin, *ACS Cent. Sci.* **2020**, *6*, 1317.

[151] a) J. A. Seabold, K.-S. Choi, *Chem. Mater.* **2011**, *23*, 1105; b) Q. Jia, K. Iwashina, A. Kudo, *Proc. Natl. Acad. Sci. U. S. A.* **2012**, *109*, 11564.

[152] M. Zhang, R. P. Antony, S. Y. Chiam, F. F. Abdi, L. H. Wong, *ChemSusChem* **2019**, *12*, 2022.

[153] T. W. Kim, K.-S. Choi, *J. Phys. Chem. Lett.* **2016**, *7*, 447.

[154] S. A. Akhade, N. Singh, O. Y. Gutiérrez, J. Lopez-Ruiz, H. Wang, J. D. Holladay, Y. Liu, A. Karkamkar, R. S. Weber, A. B. Padmaperuma, *Chem. Rev.* **2020**, *120*, 11370.

[155] F. Urbain, P. Tang, N. M. Carretero, T. Andreu, L. G. Gerling, C. Voz, J. Arbiol, J. R. Morante, *Energy Environ. Sci.* **2017**, *10*, 2256.

Marshet Getaye Sendeku obtained his M.Sc. degree in physical chemistry (2011) from Haramaya University, Ethiopia. He worked as a lecturer and researcher at Jigjiga University and the Ethiopian Biotechnology Institute for 6 years. He then obtained his Ph.D. at the University of Chinese Academy of Sciences, National Center for Nanoscience and Technology in 2022. Currently, he is a postdoc fellow at Ocean Hydrogen Energy R&D Center, Research Institute of Tsinghua University, Shenzhen. His research interest focuses on the rational design of 2D materials for photo(electro)catalytic synthesis of valuable chemicals and fuel.

Tofik Ahmed Shifa received his PhD from University of Chinese Academy of Sciences in 2018. Subsequently, he worked as a postdoctoral researcher at the Luleå University of Technology for 2 years. Currently, he holds the positions of associate professor and Marie Skłodowska-Curie Fellow at Ca'Foscari University of Venice. He leads funded projects including *Progetti di Ricerca Scientifica di Rilevante Interesse Nazional*. Additionally, he serves as an ambassador in EUTOPIA and holds membership in GYA. He received several awards including the Chinese government outstanding international student award. His research focuses on controllable synthesis and development of novel materials for green energy.

Elisa Moretti (Ph.D. in Chemistry, 2005) is Associate Professor of Inorganic Chemistry at DSMN, Ca' Foscari University of Venice (Italy). She leads a multidisciplinary team focused on the development of 0–2D inorganic nanomaterials for environmental and energy-related applications. She is co-author of more than 70 papers, patents, and more than 30 keynote/invited talks. She is Chair-holder of a UNESCO Chair on Technologies and Materials for Green and Energy Applications (AID4GEA). She is leading industrial research project funded for 1 M€ in the last 3 years. Her Spinoff ChEERS—Circular Economy for Energy Recycling Solutions received several awards at national level, among which the Italian "Innovation Business Award" ANGI 2021 in the category "Energy & Environment."

Alberto Vomiero (Ph.D. in Electronic Engineering, 2003) holds the chair of experimental physics at the Luleå University of Technology, Sweden and the chair of industrial engineering at Ca' Foscari University of Venice. He is leading two research groups working on composite nanomaterials for environmental applications. He published more than 250 papers and 6 book chapters. He is former Marie Curie international outgoing fellow of the European Commission, and fellow of several Societies. He is associate editor of Nano Energy (Elsevier) and editorial board member of Small (Wiley), Scientific Reports (Nature Publishing Group), and other journals. Since 2024 he is co-Chair-holder of a UNESCO Chair on Technologies and Materials for Green and Energy Applications (AID4GEA).

Fengmei Wang received her B.S. degree in applied chemistry from Hunan University, China, in 2012. Then she received her Ph.D. degree in physical chemistry from the University of Chinese Academy of Sciences at the National Center for Nanoscience and Technology (NCNST), China, in 2017. From 2017 to 2022 she worked in NCNST. In 2022, she joined college of Chemistry, Beijing University of Chemical Technology (BUCT). Her major research interests include synthesis and development of novel 2D materials, such as transition metal chalcogenides, metal phosphorous trichalcogenides, etc., for (photo)electrochemical synthesis.